MPHIL

Heterogeneous Catalysts for Sustainable Chemistry

Keir, Callum

Award date:
2010

Awarding institution:
University of Bath

Heterogeneous Catalysts for Sustainable Chemistry

Callum Gregory Keir

A thesis submitted for the degree of Master of Philosophy

University of Bath

Department of Chemistry

April 2010

PREFACE

The research presented in this thesis was conducted by the author in the Department of Chemistry at the University of Bath, between October 2007 and January 2010. It is original work except where specific reference is made to the contrary, and none of this work has been submitted in whole or in part for another degree.

Contents

Chapter 3: Results and Discussion of Biodiesel Catalysts

Chapter 4: Results and Discussion on the use of Silsesquioxanes as Homogeneous Model Compounds

Chapter 5: Appendix

Acknowledgements

First and foremost I wish to thank Dr. Matthew Jones for his excellent supervision over the past 2 and half years, and his advice, enthusiasm, patience and understanding, over what has been at times a bumpy ride. I would also like to thank Dr. Andrew Johnson for his limited role as a co-supervisor. I would like to show my gratitude to Cliff Williams, Ruth Robertson, and Ian Little of Ineos Technologies for their contribution towards the direction of the project, as well as provision of the GC. Ineos and the EPSRC are gratefully acknowledged for the financial support of this work.

All members of the Jones group are thanked for their friendship, guidance, and simply contributing towards a thoroughly enjoyable working environment. Thanks too to David Cousins and Christopher Hawkins for admirably putting up with me as their lone office-mate.

The following staff at Bath are all thanked for their contributions to this work; Drs. Mary Mahon and Gabriele Kociok-Köhn for help with crystallographic studies, Dr. John Lowe for his assistance with NMR spectroscopy, Dr. Alexi Lapkin for use of the catalyst rig and his lab, and Alan Carver for the Elemental Analyses.

Finally I would like to extend my deepest thanks to my parents and my girlfriend Helen, who have fully supported me at every point, and I know will continue to do so in whatever I plan to do next.

List of Papers Published

Explanatory Notes:

The following is a list of the author's publications in chronological order. Those that relate to work contained in this thesis are numbered 2-4. 1 is a result of work carried out during undergraduate studies.

1. Synthesis and structure of a molecular barium aminebis(phenolate) and its application as an initiator for ring-opening polymerization of cyclic esters.
   M. G. Davidson, C. T. O'Hara, M. D. Jones, C. G. Keir, M. F. Mahon and G. Kociok-Kohn, *Inorganic Chemistry*, 2007, **46**, 7686-7688.

2. Heterogeneous catalysts for the controlled ring-opening polymerisation of rac-lactide and homogeneous silsesquioxane model complexes.
   M. D. Jones, M. G. Davidson, C. G. Keir, A. J. Wooles, M. F. Mahon and D. C. Apperley, *Dalton Trans.*, 2008, 3655-3657.

3. Zinc(II) Homogeneous and Heterogeneous Species and Their Application for the Ring-Opening Polymerisation of rac-Lactide.
   M. D. Jones, M. G. Davidson, C. G. Keir, L. M. Hughes, M. F. Mahon and D. C. Apperley, *Eur. J. Inorg. Chem.*, 2009, 635-642.

4. Crystallographic characterisation of novel Zn(II) silsesquioxane complexes and their application as initiators for the production of polylactide.
   M. D. Jones, C. G. Keir, A. L. Johnson and M. F. Mahon, *Polyhedron*, **29**, 312-316.

Abstract

In recent years there has been considerable interest in 'green' chemistry in order to reduce our dependence on oil and finite natural resources. One industrial processes that currently relies on oil is the production of 1,3-butadiene (1,3-BD). It is possible to convert ethanol, a sustainable source, in to 1,3-BD. Previously reported catalysts for this process do not possess the desirable conversion or selectivity for 1,3-BD to be able to compete with the petroleum based process. A number of heterogeneous catalysts have been prepared and tested on a fixed-bed, continous-flow reactor. The reaction products were analysed by gas chromatography and ^{1}H NMR. Catalysts were initially based upon the naturally occurring mineral sepiolite, which was impregnated with a range of divalent metal ions, however results were poor due to structural degradation of the materials during the calcination process, confirmed by powder X-ray diffraction. Greater success was achieved with a range of bi- and tri-metallic catalysts where a combination of zinc, zirconium, and copper are supported on silica. 1,3-BD selectivity and conversions were shown to be related to the pore diameter of the silica. Silica with a larger pore diameter was shown by ^{29}Si solid-state NMR to possess fewer Brønsted acidic sites on the catalyst. Reduction of these sites suppressed the production of ethylene from the alcohol feed. A trimetallic catalyst of Cu/Zn/Zr on 150 Å pore diameter silica, containing 1 wt% of each metal, gave the most impressive results (44 % conversion, 67 % 1,3-BD selectivity over a 3-hour run) with a purely ethanolic feed. The yield of 1,3-BD for bimetallic Zn/Zr catalysts can be improved by the addition of acetaldehyde, an intermediate in the conversion process, to the ethanol feed. The trimetallic catalyst did not show any considerable improvement with added acetaldehyde, as copper is a well known alcohol dehydrogenation catalyst, implying the catalyst struggles elsewhere.

Biodiesel production is another area of sustainable chemistry that has been investigated. Biodiesel is produced from the transesterification of oils with methanol. A series of Schiff-base ligands were produced from various cyclic aldehydes and anilines. Eight Zn(II) Schiff-base complexes have been characterised by single crystal X-ray diffraction, and shown to be active as homogenous catalysts for the transesterification of vegetable oil.

Aluminium, titanium, and zinc silsesquioxane complexes have also been synthesised and fully characterised by single crystal X-ray diffraction for use as soluble models for silica supported heterogeneous catalysts. Two distinct Zn(II)-silsesquioxane complexes were produced, with only one previously reported in the literature.

Chapter 1: Introduction and Literature Review

1.1 An Introduction to 1,3-Butadiene

The simple alcohol ethanol has a huge number of applications, from alcoholic drinks, to use as a solvent, fuel, or feedstock for the production of more useful chemicals. It is produced by the petroleum industry by the acid-catalysed hydration of ethylene, most commonly employing phosphoric acid as the catalyst, or it can be produced from microbial fermentation of sugars and starch from a range of crops, such as sugar cane, wheat, barley, and potatoes. The latter process gives so-called "bio-ethanol", considered a sustainable resource as the agricultural feedstock is renewable. Of course it is not always this simple, as fuel is required for the machines that harvest the crops, and fertilisers are needed to enable growth, but overall the net energy gain is significant. As well as being considered as an alternative to petroleum fuel, a possible use of bio-ethanol would be used as a sustainable chemical feedstock for the production of higher value chemicals such as 1,3-butadiene.[1]

1,3-butadiene (1,3-BD) is a colourless gas at room temperature, and has many uses, the largest being as the starting monomer for the production of polymeric rubbers and plastics. Polymerisation of 1,3-BD itself to yield polybutadiene accounts for 26% of the world's 1,3-BD usage. This soft and elastic rubber is largely used as a component in vehicle tyres. 1,3-BD is also copolymerised with other olefins to give products with substantially different properties. The largest single end use for 1,3-BD is in the production of styrene-butadiene-rubber (SBR), which accounts for 28% of use. SBR is the major component of car tyres as it has superior abrasion resistance, and it is also used in adhesives and sealants. Other well known polymers that contain 1,3-BD are acrylonitrile-butadiene-styrene (ABS) resins, which are used for automotive parts, and make up the tough plastic cases of appliances such as computers, printers etc. Nitrile rubber also contains 1,3-BD, and is used for manufacturing gloves amongst other things.

1,3-BD may be a component of footwear, children's toys, plastic plates and cups, drinks bottles, food packaging, and even carpets and clothing.[2] It is an extremely useful and well utilised chemical and as such it is important we are able to continue to produce it well in to the future.

1.2 Current Industrial Production Methods for 1,3-Butadiene

Most 1,3-BD is currently a product of the petrochemical industry, and the most important process is steam cracking of saturated hydrocarbons to give olefins of varying size. 1,3-BD is usually a co-product of the ethylene industry and this accounts for over 95% of globally produced 1,3-BD. The other two commonly employed industrial processes involve dehydrogenation of other hydrocarbons. In the steam cracking process, the feedstock, which can be liquid or gaseous hydrocarbons, is fed to a reactor where they are mixed with steam, and "cracked" by being heated to temperatures between 790-830 °C for a very brief period. Modern furnaces need only heat the feedstock for milliseconds, and the gas is quickly quenched to stop the reaction and retain good yields of the desired products. This quenching also immediately removes any high-boiling point components from the mixture of gases. Compression of the remainder removes any C5 or larger hydrocarbons, and the C1-C4 molecules that are left, usually methane, ethylene, propylene, butenes and also hydrogen, can be separated via a series of distillation steps. 1,3-BD can be separated from other C4 products by absorption into a polar aprotic solvent, which can then be evaporated.[2]

The actual yield of 1,3-BD can be dependent on the nature of the chemical feedstock. Usually, olefin plants can be separated into those that utilise gas feedstock (light crackers), and those which use a liquid hydrocarbon feedstock (heavy crackers). Plants which use light gases such as ethane and propane produce product feeds which will mostly contain shorter-chained alkenes, such as ethylene or propylene. For example, an ethane cracker will produce only 2kg of 1,3-BD for every 100kg of ethylene. Similarly, a

feedstock of heavy naphtha (a liquid mixture of hydrocarbons containing 7-9 carbon atoms) will again give some 1,3-BD and lighter olefins, but the product mixture will be rich in aromatics and long chain alkenes which may be suitable for use in petroleum. Using light naphtha, which contains a greater percentage of shorter chain alkanes, as a feedstock, can give much better yields of 1,3-BD, in the region of 16kg per 100kg of ethylene produced. The temperature of the reactor can also have an effect on the yield – lower temperature favours C1-C4 olefins.

1.3 Ethanol to 1,3-Butadiene and Reported Catalysts

The earth's natural supply of fossil fuels is being used at a remarkable rate and it is vital that we develop sustainable, 'green' chemistry to enable us to continue with the life we are accustomed to when these reserves have been used up. The ability to produce 1,3-BD from ethanol in high yields and selectivity, and at low temperatures, would be extremely beneficial. The sugar cane industry in Brazil currently produces 45 million litres of ethanol every single day, and this is only set to increase. However, to supply only one-tenth of the worlds motoring fuel, the country would have to step-up its output by a factor of 40.[1] A better use for this ethanol would be as a sustainable chemical feedstock. In 2004, the global demand for 1,3-BD was 9 million metric tons, and is predicted to increase by up to 3% year upon year. An efficient process for ethanol conversion would be able to compete with petroleum derived 1,3-BD, and the vast quantity of ethanol produced in one country alone should be able to supply the demand for 1,3-BD, enabling us to decrease our dependence on finite resources. Bio-ethanol as a feedstock is advantageous because the carbon present in the 1,3-BD was captured from the atmosphere only a few years prior by photosynthetic plants, rather than millions of years as in the case of fossil fuels.

The idea of converting ethanol to 1,3-BD is in itself not a new one, though literature on the subject is scarce. Catalytic processes were developed in the 1940s, and are still

prevalent in some European, Asian, and African countries. The technology was utilised during World War II by both Russia and the United States for their synthetic rubber supplies, though different processes were used. Alcohol-based production was unable to compete with its petroleum based counterpart on a large scale, which is why it is still fairly underutilised today. Ethanol prices in the past were significantly higher, where as today production from sugar cane costs as little as 25 pence a litre. However, the higher prices more than half a century ago meant that commercialisation of the process was not cost effective. For it to compete with other processes, catalysts with high alcohol conversion and 1,3-BD yields were needed, and this was not achieved.

There exist two different approaches for converting ethanol into 1,3-BD – the one-step and the two-step process. In the two-step process, ethanol is oxidised (or dehydrogenated) to acetaldehyde, which is then fed in to a separate reactor, where it is combined with more ethanol and passed over a dehydration catalyst to form 1,3-BD. The one-step process is exactly as it sounds – both dehydrogenation and dehydration reactions occur in the same furnace, in the presence of a catalyst capable of performing both tasks, which is often binary metal oxide systems, with each metal contributing in a different way. The one-step process was invented by the Soviet chemist Sergei Lebedev, and utilised by the Russians during the Second World War and beyond. The two-step process was also pioneered by a Russian, yet was popular in the United States, where it was used to make government rubber during the same conflict.

American scientists claim the two-step process gives higher degrees of ethanol conversion and leads to a pure product. The one-step process is of course simpler in operation if not chemistry, as less capital would be required to build the plant as separate reactors would not be needed. Given the technology and knowledge we have today in terms of catalyst development, supports, and the ability to fine-tune conditions to a greater degree, there is no reason why a single-step process should be inferior. Given this, the one-step process is the focus of the work described herein.

It was known for many years that 1,3-BD could be synthesised in very low yields, simply by passing ethanol over powdered aluminium. Using alumina (aluminium oxide, Al_2O_3) and a mixture of ethanol and acetaldehyde as the feedstock was shown to give improved yields, though they were still low and the 1,3-BD impure.[3] One of the catalytic systems that first garnered significant attention were silica/magnesia (SiO_2/MgO) catalysts, and a number of patents were filed in the US during the 1940s that utilised this type of catalyst for 1,3-BD production.

One such patent filed in 1948 describes how SiO_2/MgO, including those where other substances are also added to the catalyst in small quantities to act as promoters, can be used for direct production of 1,3-BD from ethanol, or a mixture of ethanol and acetaldehyde in what is essentially the second step of a two-step reaction.[4] Powdered celite was actually used as the source of SiO_2, as it contains approximately 86% SiO_2 by mass. The celite, or indeed SiO_2 on its own, were found to be catalytically inactive at the temperatures employed. MgO was prepared by precipitation from soluble salts, or combustion of the nitrates. The two oxides were mixed and then heated to between 90-100°C in an aqueous solution of strong alkali (0.1 – 8% by volume), giving rise to magnesium silicates as well as the individual oxides. A change in the composition of the catalyst, and the production of Si-O-Mg linkages as the active species is a possible explanation as to why these alkali-digested catalysts gave much higher yields than simple mixtures of the two materials. The actual ratios of SiO_2 to MgO used vary quite considerably, but the preferred proportions are roughly 3-4:1. After digestion, the catalysts were washed, and dried at 100°C.

Catalysts were tested with varying compositions, including small amounts of cobalt and copper oxide. Only two are really worthy of any mention. The catalysis tests were carried out using 100 cm^3 of each catalyst which was heated in an electric furnace, and 125cm^3 of ethanol was passed over the catalyst at a constant rate. Using a catalyst composed of 21% MgO and 79% celite, by mass, ran at 435°C for over 3 hours gave a

1,3-BD yield of 48.1%. This yield is given as a percentage of the theoretical based on the quantity of ethanol consumed, however the patent was not forthcoming with ethanol conversion data. A ternary catalyst SiO_2/MgO/CuO with composition 76.2%, 20.3% and 3.5% respectively gave a similar yield in a third of the time. Again, there is no conversion data, and the yields as a whole are not overly impressive. Also, the catalysts only retained their activity for a few days, after which a build up of coke reduced their catalytic ability. Burning off the deposit at very high temperatures restored activity. Coking is a problem that will be difficult to overcome in the majority of catalysts, and it is not unlikely that a regenerative step may have to be incorporated in to a catalytic cycle. One point to mention is that water present in the ethanol did little to reduce the 1,3-BD yield, though rates were reduced. The crude product of the sugar cane industry contains approximately 85% water, and the less refinement that has to be done to the catalytic feedstock, the cheaper the whole process will become.[4]

1.4 Mechanism of the Conversion of Ethanol to 1,3-Butadiene

The mechanism of the one-step conversion has been widely debated in the literature. Some that have been suggested were very improbable and quickly discounted, such as that by Lebedev, who pioneered the one-step reaction. He and his associates hypothesised that it was two C2 radicals coming together to form a four-carbon radical, which then goes on to lose water. However, if this were the case, one would predict much more ethylene as co-product than is actually seen. The theory also ignores acetaldehyde, which is formed by dehydrogenation of ethanol, and is much more susceptible to dehydration than an ethanol radical. Other more complicated theories with a huge number of intermediate species have been published, but the most widely accepted are those of Quattlebaum,[5] and Gorin, who suggested a very similar mechanism, with the addition of one more intermediate species.[6] The mechanism is summarised in the following diagram (**Figure 1.4.1**).

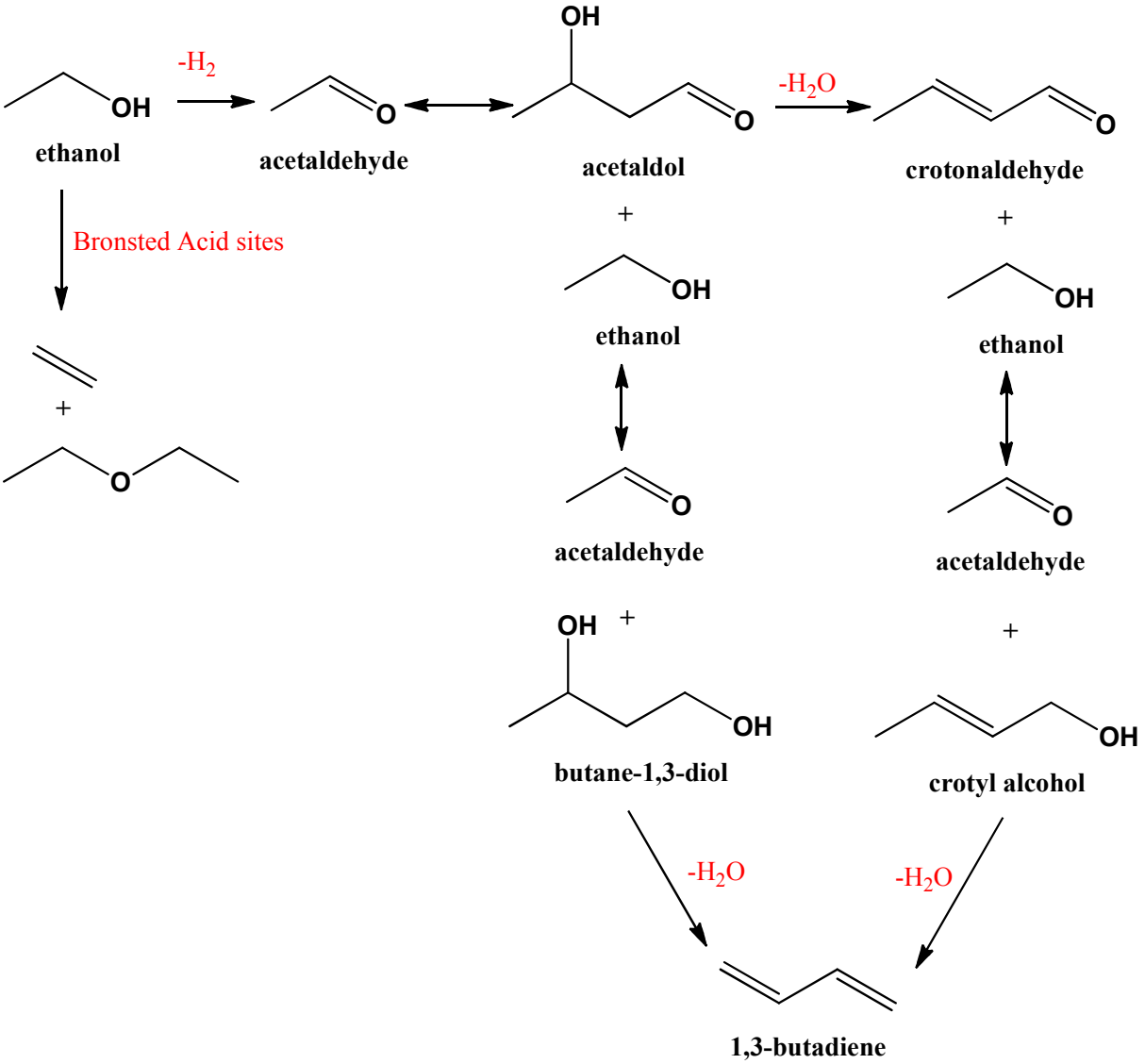

Figure 1.4.1: Mechanistic Scheme for the conversion of ethanol to 1,3-butadiene

The first step in the process is the dehydrogenation of ethanol to acetaldehyde, followed by a condensation reaction between two molecules of acetaldehyde to form acetaldol, which may possibly undergo rapid dehydration to crotonaldehyde. Whether this dehydration occurs or not a proton transfer then occurs. Both crotyl alcohol and butane-1,3-diol are readily dehydratable. It is important to note that acetaldehyde is regenerated. The main byproduct of this reaction is ethylene, as a result of ethanol dehydration. It is imperative that this be kept to a minimum, as various production

methods already exist for ethylene so the recovery of small volumes economically viable. Ethanol dehydration to ethylene has been shown to be directly related to the Brønsted acidity of catalysts, so this must also be kept to a minimum, although some acidity may be required to drive later steps.[7]

Quattlebaum possessed quite conclusive evidence for his theories, conducting a number of experiments with simple silica gel, and promoted silica gel catalyst. When a mixture of crotonaldehyde and ethanol was passed over a purified silica gel catalyst, 1,3-BD was formed in reasonable yield, and gave a 1,3-BD fraction of 98% purity. Substituting acetaldehyde for crotonaldehyde in the process gave a significant reduced amount of the desired product. This is a good indication that the mechanism involves crotonaldehyde as an intermediate, and the poor yield when using acetaldehyde in the feed simply implies the catalyst does not adequately promote the aldol condensation reaction.[5]

Quattlebaum investigated impregnating the silica gel with tantalum oxide, and this was found to give higher 1,3-BD yields under the same conditions, and also less acetaldehyde. When a stream of only acetaldehyde was passed over the Ta_2O_5/SiO_2 catalyst, crotonaldehyde was produced, meaning that as well as promoting the conversion of crotonaldehyde to 1,3-BD, this particular catalyst was also accelerating the condensation step.[5]

This catalyst was fairly successful at performing the dehydration and proceeding reactions in the one-step process, so it was hypothesised that adding a metal oxide known to promote dehydrogenation would produce a catalyst capable of creating 1,3-BD from ethanol alone. Zirconium oxide was found to be nearly as active as tantalum. A SiO_2 gel catalyst containing 1.5% ZrO_2 and 0.5% CdO by mass was able to do the complete one-step reaction in the same tube, with an efficiency of 44%. The efficiency was described as the yield based upon the consumed ethanol, and the conversion was

in no way complete. The purity of the C4 fraction was however in excess of 94% which means the catalyst produced only very small amounts of other butylenes. Preparation of this catalyst is simple, as the nitrates of the metals can simply be stirred into a slurry of silica gel, the water allowed to evaporate, and then the catalyst calcined at high temperature to decompose the nitrates to the respective oxides.[5]

Gorin *et al* had suggested that crotyl alcohol existed as an intermediate between the crotonaldehyde and 1,3-BD, whereas Quattlebaum chose to overlook it.[6] H.E. Jones *et al* carried out investigation into the mechanism of the catalytic conversion of an ethanol/acetaldehyde feed into 1,3-BD, and found that crotyl alcohol was found in large amounts in the product stream. However it was determined that even if it was an intermediate, production of crotyl alcohol was not rate controlling.[8] As American scientists, they were interested at the time in the two-step process. Using a 2% Ta_2O_5 – 98% SiO_2 catalyst, a variety of feed mixtures were tested. A mixture of crotyl alcohol and a much smaller quantity of acetaldehyde were passed over the catalyst and gave a 60% yield of 1,3-BD, indicating dehydration of crotyl alcohol is one possible route to 1,3-BD. Crotyl alcohol had also been suggested as a potential source material for 1,3-BD, however when utilised in runs at 350 °C, after only one hour significant amounts of carbon were deposited on the catalyst, and raising the temperature yielded more by-products and less 1,3-BD. One point of interest is the functions assigned by the researchers to the different components of their catalyst. Jones *et* al found that silica on its own was more effective than the Ta promoted silica for the condensation of two acetaldehyde molecules, and the primary function of the Ta was to promote the proton transfer and subsequent chemistry.[8] This is not in agreement with Quattlebaum.[5] Through a series of different catalysis runs and rate data, Jones *et* al were able to determine that the rate-limiting process in the second-step of the commercially utilised two-step process is the condensation of acetaldehyde, which is second order at atmospheric pressure, though it becomes first order above 4 atmospheres.[8]

1.5 The Meerwein-Podondorf-Verley and Oppenauer Reactions and Reported Catalysts

The plausibility of the suggested mechanism can also be investigated by seeing if there exists accepted mechanisms for each individual step, and particularly whether catalysts exist for the process. The most difficult concept when looking at the mechanism is the proton transfer that occurs to produce the dehydratable C4 species that can dissociate and decompose to form 1,3-BD and water. This can be rationalised using a pair of very well known reactions, the Meerwein-Pondondorf-Verley (MPV) reduction of aldehydes and ketones, and Oppenauer's (O) oxidation of alcohol. The reactions, though discovered separately, are actually the same, just in a different direction as the reaction exists as an equilibrium. Together they are denoted MPVO reactions, are highly selective, and can account for the conversion of ethanol to acetaldehyde and crotonaldehyde to but-2-en-1-ol in the penultimate step of the production of 1,3-BD from ethanol. It is generally accepted that MPVO reactions proceed via a transition state complex where both the alcohol and aldehyde are coordinated to a Lewis acidic metal centre, and the hydride transfer occurs as shown below, utilising the reagents we are interested in (**Figure 1.5.1**).

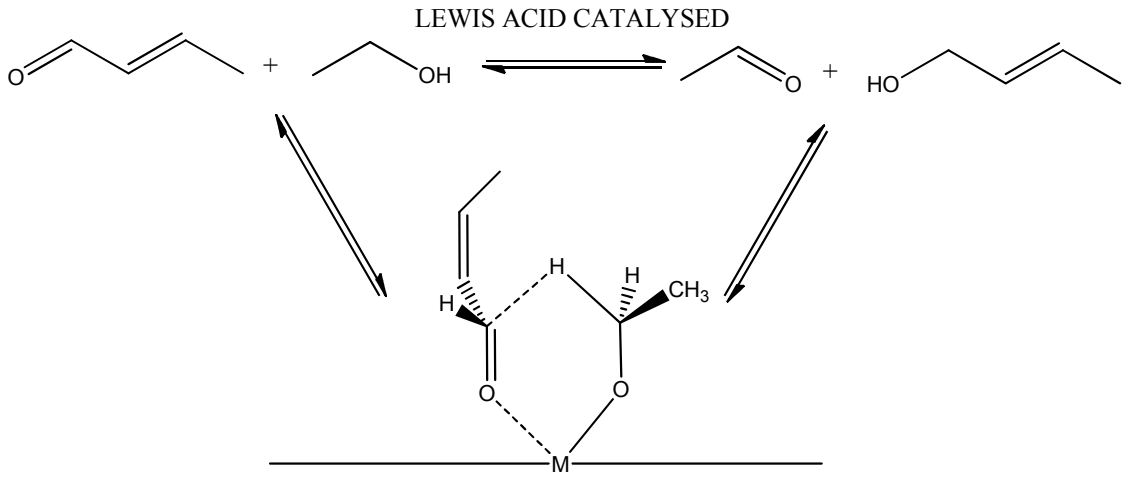

Figure 1.5.2: Mechanism of Lewis acid catalysts in the MPVO reaction, where M is a Lewis acidic metal centre

MPVO reactions have traditionally been catalysed by homogeneous aluminium species such as alkoxides, in particular $Al(O^iPr)_3$.[9] This catalyst is extremely inefficient however, as problems with dissociation of the products means stoichiometric quantities rather than catalytic amounts of $Al(O^iPr)_3$ must be used. In recent years other homogeneous systems have been published in the literature, such as bidentate bis(dialkoxyaluminium) complexes, and alkoxides of other metals.[10, 11] Heterogeneous catalysts for this reaction are now being investigated, and it is these which are most interesting to this work, and which can be implemented in to the design of the catalysts described herein.

Many have investigated the use of β-zeolite as catalysts for MPVO reactions.[12] β-zeolite is a 12-ring aperture aluminosilicate zeolite that possesses both Brønsted and Lewis acidity. The Lewis acidity is believed to be as a result of surplus aluminium atoms that are not contained within the framework, as well as framework Al that is not in a tetrahedral environment, with the number of these sites depending on the method of preparation and water content.[13,14] It has been shown that partially hydrolysed framework aluminium is the active site. Extra framework cations were shown not to be catalytically active, but can have an effect on the selectivity of the catalyst with regards to geometric isomers of the product alcohol.[12] A titanium-containing β-zeolite that is completely free of aluminium has also been synthesised, and reported as an excellent catalyst for MPVO reactions. Dealuminated tin β-zeolite has recently been reported as being more active than its Al or Ti analogues.[15] This is rationalised by Sn being more electronegative than Ti, inducing more polarisation in the carbonyl bond, yet also is more capable of coordinating both the aldehyde/ketone and the alcohol than framework aluminium. All three materials were prepared by Corma *et al* and compared for catalytic activity alongside numerous other heterogeneous and homogeneous catalysts.[15] The quantity and strength of Lewis acidic sites was measured by infrared (IR) spectroscopy of pyridine absorbed and desorbed on the materials. It found that Ti- β-zeolite and Sn-β-zeolite catalysts showed the same, relatively weak Lewis acidity when

compared to Al-β-zeolite, which also exhibits strong Brønsted acidity. This is surprising when comparing the catalytic activity of the materials. Sn-β-zeolite that contained 2 wt% SnO_2 gave a 91% conversion of cyclohexanone to cyclohexanol using 2-propanol as the reductant, with 100% selectivity. For comparison, Ti-β-zeolite gave only 3% conversion and optimised Al-β-zeolite nearly half as much conversion as well as significant amounts of unwanted products. The performance of Sn-β-zeolite was not far short of homogeneous $Al(O^iPr)_3$. One of the limitations of the latter is its complete and irreversible deactivation by water. Hydrophobic zeolites can be prepared, meaning less water will be absorbed by the catalyst, which can retain some activity. In fact, even with 4 wt% H_2O in the reaction mixture, Sn-β-zeolite gives higher turnover than the titanium and aluminium systems when there is no water present. If these materials, or derivatives thereof, are found to be active for the conversion of ethanol to 1,3-BD, this resistance to water content is a valuable asset, as it means that crude bio-ethanol can be utilised as a feedstock.[15]

MPVO reactions have also been reported as being base catalysed, and it was found that the activity of MgO/SiO_2 materials increased with their surface basicity.[16] Basic metal oxides such as MgO were investigated as catalysts, and it was found to be much more active for the reduction of acetone with ethanol than Lewis acidic catalysts such as ZrO_2 and Al_2O_3, and did not form any secondary products, only the expected acetaldehyde and isopropanol.[17] The mechanism of MgO catalysis is unlikely to include coordination of ethanol to Mg sites, but rather hydrogen bonding to basic O^{2-} sites. It was proposed that the mechanism involved the alcohol absorbed on these basic sites, and the aldehyde/ketone on Brønsted OH groups, as shown.[18]

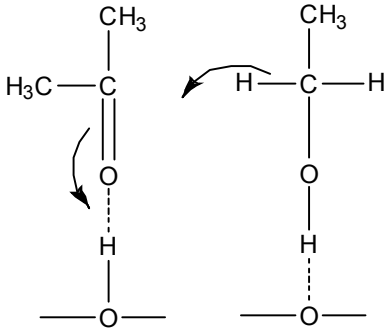

However, for this to be the case, both types of adsorption site must be in very close proximity so that the proton transfer can take place, and it also relies on a degree of acidity in the OH group. IR spectroscopy of the MgO after ethanol adsorption shows an ethoxy group coordinated to Mg as a result of O-H bond cleavage of the ethanol, suggesting the active OH groups are a result of ethanol dissociation on the catalyst surface. The proton of these newly formed OH groups was shown to remain close to the ethoxy group, favouring the interaction shown below.

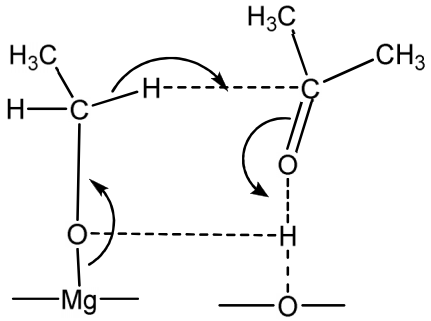

The reaction is favourable due to the weak interaction between the Mg cations and ethoxy group, as Mg is not particularly electronegative, and this accounts for why basic metal oxides are active catalysts for MPVO reactions.[17]

The final MPVO catalyst of note is a three-dimensional, mesoporous silicate containing zirconium. Drawbacks of the β-zeolite based materials mentioned previously are their limited pore size, and complex synthesis. In the synthesis of TUD-1, the templating agent that the mesopores form around also acts as a metal complexing agent, depositing the metal on the surface of the mesopores, aiding its incorporation in to the metal framework.[19] Zirconium (IV) isopropoxide was used as the Zr source for this simple synthesis under hydrothermal conditions, to give Zr-TUD-1, with a Si/Zr ratio of 25:1. The material is highly Lewis acidic, and in combination with its high surface area and simple preparation, possesses all the characteristics required for a good MPVO catalyst. Activity was good for the reduction of simple molecules such as 4-*tert*-butyl cyclohexanone with isopropanol (95% conversion), though *cis/trans* selectivity was not as good as other catalysts, in particular H-beta zeolite, which is selective due to its

smaller pore size favouring one isomer. It is however able to reduce bulky steroid molecules that other mesoporous catalysts could not, with surprising efficiency.[20]

1.6 Catalysts based upon Silica and other Metal Oxides for 1,3-Butadiene Production

The most widely studied catalysts for the conversion of ethanol to 1,3-BD are those based on MgO/SiO_2, sometimes impregnated with other metals. Though much work has been done, the optimum ratio of the components is still not entirely clear. Common to all of the catalysts is that they contain both basic and acidic sites. In 1971, Niiyama described both the dehydration and dehydrogenation of alcohols over acid-base bifunctional catalysts. He theorised that as 1,3-BD production involved the same two processes, acid/base properties of catalysts may be significant.[18] He found that maximum acidity was reached when MgO made up 50 mol% of the catalyst, and basicity increased with MgO, as did 1,3-BD yields, up to 85 mol%. Pure MgO however was hardly catalytically active. Niiyama had shown in previous papers that it was basic sites that catalysed the dehydrogenation of ethanol. However, the run with solely MgO gave crotonaldehyde as a product, which hints that that the MgO has a role in the condensation reaction, and tells us that there is more to investigate than simply the acid/base properties of a catalyst.[18]

A paper published in the 1980's concluded that an MgO/SiO_2 catalyst prepared by wet-kneading of the individual oxides introduces $MgO\text{-}SiO_2$ interactions, which are what gives it favourable catalytic properties in the production of 1,3-BD when compared to a mechanical mixture of the two, or the individual oxides.[21] X-ray analysis of the catalyst confirmed that crystalline MgO was present, but they were very poor examples when compared to MgO on its own or in a mechanical mixture. The variations in the crystals were attributed to crystal defects brought about by interaction with the SiO_2. It could

not be confirmed whether the enhanced catalytic activity is due to structural defects in the MgO, or an actual Si-O-Mg interaction.[21]

A single-step process was patented in the US in 1957 that used a SiO_2/MgO catalyst impregnated with a minor weight percentage of calcium phosphate, the two most preferable being $CaHPO_4$ and tricalcium phosphate, $Ca_3(PO_4)_2$.[22] Results showed that it was preferable to have a greater mass of MgO than SiO_2. The catalysts were prepared in a simple fashion, with mixing of the required amounts of each dry component, and the addition of a large volume of water to form a hydration mass which was then stirred until it became a paste, which could be formed into a cake, which was dried for 18 hours and could then be cut and pressed into pellets. The $Ca_3(PO_4)_2$ catalyst was shown to give a high degree of catalytic activity, with good selectivity and yields when the feedstock was fairly concentrated ethanol solutions. However, the activity was noticeably reduced when more dilute solutions are used, such as a feed of 70 wt% ethanol, 10 wt% acetaldehyde and 20 wt% water. It was concluded that this catalyst would only be commercially viable when the price of concentrated ethanol was much lower. The catalyst utilising $CaHPO_4$ as the promoter did not have this problem, and hence was a much more preferred choice for an industrial process at the time of invention. It was found that the more dilute the solution was, the greater the selectivity for 1,3-BD over other olefins. A feed mixture of 44 wt% ethanol, 6 wt% acetaldehyde and 50 wt% water gave the optimum yields. Though ethanol is now much cheaper, a catalyst able to deal with bio-ethanol which has undergone very little purification is helpful.

Using a dilute solution such as the one detailed above has its drawbacks, with the feed conversion being most obviously affected, as only half of it is able to form product. However this can be can be compensated for by the increased selectivity, and a high feed rate of the relatively cheap solution can still give good quantities of 1,3-BD. The optimum conditions were a temperature between 390-400°C, and atmospheric

pressure. Some of the most active catalyst compositions are summarised in the table below (**Table 1.6.1**).

Catalyst composition in weight percent	**Feed rate, ml. of feed / litres of catalyst / hr**	**Reaction temp, degrees Celsius**	**Wt.% conversion of feed**	**Wt.% 1,3-butadiene yield**	**Wt.% ethylene yield**
67.9 MgO, 20.1 SiO_2 12 $CaHPO_4$	600	390	23	41	2.5
66.6 MgO, 22 SiO_2 11.4 $CaHPO_4$	600	390	25	40	4

Table 1.6.1: Conversion and yield data for $MgO/SiO_2/CaHPO_4$ catalysts

The catalyst containing $Ca_3(PO_4)_2$ gave a 46 % conversion and a 30 % yield at using a fairly pure ethanol feedstock at 410°C.

Ohnishi *et al* have developed a SiO_2/MgO catalyst containing trace amounts of sodium oxide that has a very high selectivity for 1,3-BD production.[23] The catalysts were based on an equimolar SiO_2/MgO with a small amount of basic oxide, either sodium or potassium. The catalysts were prepared via a number of different methods, which had a great effect on the catalytic activity. The most active was prepared as by firstly forming the MgO by hydrolysis of a solution of $Mg(NO_3)_2.6H_2O$ with aqueous ammonia, whereby the MgO precipitate can be filtered. The silica was formed from hydrolysis of an aqueous solution of tetraethyl orthosilicate, nitric acid, and ethanol with ammonia, again followed by filtration. The MgO and SiO_2 were then kneaded together, dried and calcined at 500 °C in nitrogen for 3 hours. This on its own had provided a 50 % conversion at 350 °C, with 84 % selectivity for 1,3-BD, giving a respectable 40 % yield. Other methods of preparing the catalyst proceeded via chlorides, and these were found to be much less selective for 1,3-BD. Although one provided 98 % conversion of the

ethanol, 49 % formed C2 hydrocarbons, as well as vast amounts of ethyl chloride, giving only a 2 % 1,3-BD yield. Addition of 0.1 wt% Na_2O to the most active SiO_2/MgO catalyst proved to be highly effective. A 100 % conversion of ethanol at 350 °C, fairly low by some standards, gave a 1,3-BD selectivity, and thus a yield, of 87 %.[23]

Another groups of catalysts patented in the 1940s, submitted by Toussaint and Dunn of the Carbide and Carbon Chemicals Corporation, consists of ZrO_2, Ta_2O_5, NbO_2, and combinations and mixtures of these with SiO_2.[24] These were tested as catalysts for the dehydration step of the two-step process, passing a mixture of ethanol and a variety of different C4 or higher aldehydes over the catalysts. A patent submitted a year later is of slightly more interest as the catalysts were tested on a purely ethanolic feed as well as mixtures of ethanol with acetaldehyde, crotonaldehyde, and acetaldol.[25] The mixed feeds gave greater yields of 1,3-BD which is to be expected from the accepted mechanism. As described in the previous patent, catalysts were prepared from alkali-digested mixtures of zirconium or thorium oxide with silica, be it in pure precipitated form or present in finely powdered celite. The metal oxides were prepared by precipitation from a soluble salt or decomposition of the nitrates. All of the given results were for a one-step catalytic process at temperatures between 375 and 525 °C. There are three catalysts that particularly stand out. A mixture of 79 % celite and 21 % ZrO_2, by mass, gave a yield of 44.1 % 1,3-BD in under an hour at 455 °C. A catalyst with 44.5 % ZrO_2 and the remainder celite gave a yield in the low-40's, after a run of one and three-quarter hours at the same temperature. Finally, a yield of 40 % occurred for a catalyst consisting of 44.3 % ZrO_2, 55.3 % celite, and 0.4 % Cu. The run lasted only 40 minutes however, and the production rate was roughly 50% higher than that of a catalyst without the copper promoter, but otherwise an extremely similar composition. CuO is a well known dehydrogenation catalyst, and it is the production of acetaldehyde from ethanol that is regarded by some as the rate determining step.[25]

1.7 Alumina based and Single Metal Oxides for 1,3-Butadiene Production

Other catalysts have been invented that utilise alumina as a support. Alumina itself is able to catalyse the reaction of ethanol to 1,3-BD, and a number of binary and ternary catalysts on Al_2O_3 have been studied by Bhattacharyya, as well as single oxide systems of other metals.[26] Finding many that were catalytically active, they set about testing them all again on a fluidised bed, and carrying out an exhaustive number of runs to find the optimum conditions for each. A fluidised bed is when the solid catalyst, contained within a vessel, is forced to behave like a liquid by the forced introduction of a gas. In this case a sintered disk sits below the bed of the catalyst, and it is the vaporised ethanol feedstock that is introduced at a certain velocity so that the force of the vapour is able to balance the weight of the catalyst – if the feed rate is increased further the solid will be agitated, and swirl and flow like a liquid. A fluidised bed is good for catalysis as it provides better ethanol/catalyst contact, hopefully increasing conversion, while also providing a uniform temperature gradient within the catalyst bed.

As well as Al_2O_3, other single oxide catalysts tested were Fe_2O_3, ZrO_2, and ThO_2. All runs were carried out at 425 °C, with feed rates, catalyst bed height and ethanol concentration varied, so all data given was at the optimum conditions for each individual catalyst.[26] All the single oxides provided near 100 % ethanol conversion; however the yields were not exemplary, ranging from 17 % for the Al_2O_3 to 30 % for the ZrO_2. The activity of all the catalysts degraded after multiple uses owing to carbonaceous deposits most likely formed from the cracking of ethanol as well as other by-products. Though 1,3-BD yields decreased, there was no change in the amount of aldehydes formed from the deactivated catalyst.

It was known many years before this extensive study that for an oxide catalyst to be efficient at converting ethanol, it needs to be able to promote both dehydrogenation, and dehydration. Thus, to further increase yields, binary catalysts were made in which

both oxides were known to possess both properties. Owing to its impressive performance as a catalyst in its own right, Al_2O_3 was combined with ZnO, MgO, CaO, and Cr_2O_3, in various different catalyst compositions. It was found that for all but the Al_2O_3/MgO catalyst the optimum composition was when the Al_2O_3:metal oxide ratio was 60:40. For the MgO derivative it was 80:20. All catalysts converted 100 % of the ethanol feed, however the only one that gave a particularly impressive 1,3-BD yield was Al_2O_3/ZnO_2 (60:40), with 72.8 %. The other systems had yields in the 20 and 30 % range. The optimum temperature for all the catalysts was again found to be 425°C. Raising the temperature above this reduced 1,3-BD yields considerably, and larger volumes of gas were produced, indicating decomposition of the products. All the catalysts were again deactivated, even after the first 20 minute run. The Al_2O_3/ZnO oxide catalyst proved most resistant, still performing admirably after 60 minutes of continuous use. Passing air over the catalyst at 425 °C removed the carbon deposits as carbon dioxide, reactivating the catalyst.

Comparisons were made for all catalysts between the efficiency on fixed and fluidised beds. Some seemed to perform better in the fixed bed, possibly because the high feed rates required to fluidise the catalyst did not allow enough contact time for the required reactions to occur. The best performer in both cases was Al_2O_3/ZnO_2, and the fluidised bed improves 1,3-BD yield by 17% compared to the fixed bed. A simple explanation for this is that the optimum catalyst mass for the fluidised bed was nearly three times greater, and this obviously gives a much larger surface area of catalyst, and improves contact time. It was also noted that the fixed bed system was able to cope with considerably more water in the ethanol feed, with only slight reduction of catalytic activity.[26]

1.8 Catalysts based on Metal-doped Sepiolite for 1,3-Butadiene Production

Sepiolite is a complex magnesium silicate that has itself been shown to dehydrogenate ethanol. Fibrous sepiolite contains infinite and regular zeolite-like channels running the length of the fibres, however its use as a catalyst or even as a support is limited by its low thermal stability and cation exchange capacity (CEC). Alumination of the material using $KAlO_2$ replaces some of the Mg and Si at specific sites, and improves thermal stability as well as CEC, and also gives the material some Lewis acidity.[27] Calcination of the solid at 300 °C opens up the pore size slightly, which also increases the CEC, and enables the introduction of silver ions by cation exchange. Many other ions could be introduced, so aluminated sepiolites could prove very useful as catalysts.

Both the aluminated sepiolite and the Ag containing catalyst (approximately 6 wt% Ag) were tested for their activity towards the conversion of ethanol, with runs performed at 280 °C, and the products evolved analysed by GC-MS. Both have relatively long induction periods before any 1,3-BD was observed forming. The catalyst that didn't contain Ag produced significantly lower yields of 1,3-BD, with ethylene being the major product, though there is significant selectivity for acetaldehyde. Lewis acidic sites were found on the catalyst surface, where it is suspected the dehydrogenation reaction occurs, as normal sepiolite, which does not contain these sites, is only able to dehydrate ethanol to ether or ethylene.

The Ag containing aluminated sepiolite gives an increased selectivity towards 1,3-BD. At around 65 % conversion the selectivity was just below 10 %, with ethylene remaining the major product. Though the results are not exceptional, impregnation of these aluminated sepiolites with other metal ions may yield much more active catalysts.[28]

The Mg ions in sepiolite can be exchanged with a number of metals of similar steric and coordination requirements. Kitayama *et al* reported that manganese supported on sepiolite is an effective catalyst for conversion of ethanol to 1,3-BD.[29] Catalysts were synthesised containing Mn(II) ions, by stirring as-bought sepiolite in aqueous solutions of $MnCl_2.4H_2O$ or $Mn(CH_3COO_2).2H_2O$, followed by calcination in air at 500 °C. Mn exchanged sepiolite prepared using manganese acetate proved to be more active than that made with the chloride or ordinary sepiolite, and 1,3-BD yield was found to increase with Mn loading. With a 79 mol% Mn loading and a reaction temperature of 300 °C, ethanol conversion was complete after 7 h, and 1,3-BD yield was 33 %, with ethylene being the major product (41%).[29] A catalyst featuring Mn grafted to a number of supports, but preferably sepiolite, was also patented by the Takeda Pharmaceutical Company.[30] A variety of preparation methods were investigated, and the most effective catalyst was produced by having the Mn salt dissolved in a mixed ethanol/water solvent, and then burning the ethanol to dry the sample, followed by calcination at 500 °C. Ethanol vapour circulating in a reactor at 300 °C, containing 1g of the catalyst, gave 90.5% conversion after 11 hours, and 70.8% yield of 1,3-BD. Other preparation methods that involving more complex washing steps did not yield more active catalysts, nor did the introduction of a second metal (Zn or Cu) to the Mn-sepiolite material.[30] In a separate patent from the same company, vanadium was also supported on sepiolite.[31] Various amounts of vanadium were loaded on to the sepiolite by stirring it with an aqueous solution of vanadium(V) oxalate of the desired concentration, followed by drying and calcinations (500 °C). Some of their findings are summarised in the following table, and as found for the Mn-sepiolite, lower reaction temperatures raise the selectivity for 1,3-BD (**Table 1.8.1**).[31]

V content of catalyst (mmol/g of support)	1	2	3	4	2
Reaction Temperature (°C)	300	300	300	300	280
Reaction Time (minutes)	20	140	120	100	80
Amount of 1,3-butadiene Produced (wt% of product stream)	35.51	41.33	26.11	29.57	42.06

Table 1.8.1: The effect of molar Vanadium concentration on catalytic activity

The addition of further metals was also detailed in the patent. Tungsten, sodium, and silver ions were also impregnated in to the V-sepiolite to produce three new catalysts, the activities of which are summarised below, with all catalytic runs taking place at 300 °C (**Table 1.8.2**).[31]

Metal composition of catalysts (mmol/g of support)	Yield of 1,3-Butadiene (wt% of products)
V 1.5; W 0.9; Ag 0.02	40.2
V 1.5; W 0.9; Na 0.02	39.9
V 1.5; W 0.9	39.2

Table 1.8.2: Catalytic activity of mixed-metal materials

1.9 Calcium Phosphate Catalysts for 1,3-Butadiene Production

The final catalyst system to be discussed is a fairly recent invention, which was submitted for patenting in 1999 and followed up with a publication in 2008. [32,33] Tsuchida *et al* aimed to provide an efficient production method for 1,3-BD as well as ethylene, diethyl ether, butanol, and a high-octane fuel, using a catalyst made from different calcium phosphates, either singly or in a mixture.[32,33] One such phosphate is hydroxyapatite, which has the formula $Ca_{10}(PO_4)_6(OH)_2$, however even when the

stoichiometery of the mineral is not exactly correct, it still forms the same hexagonal crystal structure, meaning the calcium/phosphate molar ratio can be adjusted. This can also be achieved by preparing the catalyst using a mixture of different calcium phosphates. When this value of Ca/P for the catalyst is between 1.4 and 1.8, all the potential products named earlier are prepared in good yields. The Ca/P ratio controls the acid/base properties of the catalyst surface, but this can also be achieved by the addition of metals. For example, addition of dehydrogenation promoting metal such as Ni, Cu or Zn will increase the basicity of the catalyst surface, the same as increasing the Ca/P ratio. Addition of a dehydration accelerating metal such as Al will increase the acidity, as would lowering the Ca/P molar ratio. The metals can be quite easily added by taking a solution of calcium phosphate(s) and adding in soluble salts of the metals. The water can then be removed by evaporation to form the solid mixture. Two different solid catalyst materials, one acidic and the other basic, can be mixed in a solvent which is then removed to form a catalyst capable of both dehydrogenation and dehydration. All of the catalysts did not respond favourably to the existence of water in the feed, hence crude ethanol cannot be used as the raw material. The best performing catalysts were those that had a (Ca + metal)/P molar ratio of between 1.6 -1.7, when mixed with small amounts of Al, Zr or W. A sample with a (Ca + Al)/P ratio of 1.65 which contained 0.1 mol% Al had by far the highest activity. At 500°C, ethanol conversion was near complete (93.6%), and the catalyst was highly selective for the production of 1,3-BD giving a space time yield of 1111. Space time yield (STY) was defined by the authors as the yield in grams of 1,3-BD per litre of catalyst per hour, and is useful when making comparisons between catalysts. All the runs were performed with a 20% ethanol feed, and a flow rate of 100 ml min^{-1}. The most active catalysts, based upon the STY, and their characteristics are summarised below. Others may have had a higher selectivity but a poor conversion value (**Table 1.9.1**).[32,33]

(Ca + M)/P	Metal	Amount of substituted metal (mole %)	Specific surface area (m^2/g)	Temperature (°C)	Ethanol conversion (%)	Selectivity for 1,3-Butadiene (%)	Space time yield
1.62	Zr	1	42.1	500	95.2	38.6	917
1.65	Al	0.1	37.2	500	93.6	47.6	1111
1.65	W	3	54.4	500	96.2	38.6	926
1.65	Zr	3	52.9	500	86.9	43.7	977

Table 1.9.1: Performance of hydroxylapatite catalysts[32, 33]

1.10 An Introduction to Biodiesel

Biodiesel is a non-petroleum based fuel that is produced by the transesterification of triglycerides present in vegetable oils or animal fats. It can be used as a substitute for regular diesel fuel in internal combustion engines, either alone or as a blend, with little if any modification to the engine.

Conventional petrodiesel is produced by the catalytic cracking of petroleum, and it boils in the mid-range of the cracking products, hence it is often also referred to as "middle distillates". It can be broken down into further classes based on the temperature range at which it comes off. The fraction that is commonly used as a fuel for cars and other transportation methods is denoted No. 2 DF (diesel fuel) in the United States, and occurs within the 180-340 °C boiling range. Other fractions may be required where the engine is operating at considerably low temperatures, high-speeds, or where the load on the engine varies frequently. No.2 DF consists mainly of saturated hydrocarbons, particularly alkanes and cycloalkanes, and approximately 25 % aromatic compounds such as alkyl benzenes.[34] There are many reasons to look for alternative sources of energy, not just the depletion of the world's oil reserves, though this is obviously a major factor. A review by BP in 2009 revealed that there remains 1,258 billion barrels of oil that are accessible for drilling with current extraction technology.[35] If fuel consumption continues as the rate it is now, oil reserves will be fully depleted within 40 years. Of course another huge problem we are facing is the damage to our environment that occurs from the combustion of these fuels, with climate change being the major concern. Human health is also at risk from pollution due to petrol and diesel emissions. Biodiesel is not a complete replacement for petroleum derived diesel, it is likely a combination of technologies will be required to keep the worlds transportation moving, but the lower emissions of most pollutants, including CO_2, and the possibility of being a completely renewable source of energy means biodiesel, and a more efficient way of producing it, is still of interest.[36]

The main component of animal and vegetable fats is triacylglycerols, commonly known as triglycerides. Triacylglycerols consist of a single molecule of glycerol, a trihydric alcohol that is esterified with three fatty acids. A fatty acid is simply a carboxylic acid with a long, unbranched carbon tail, which may be saturated or unsaturated. The three fatty acids in the triacylglycerol need not be the same, and an example of an unsaturated triacylglycerol is shown below (**Figure 1.10.1**).

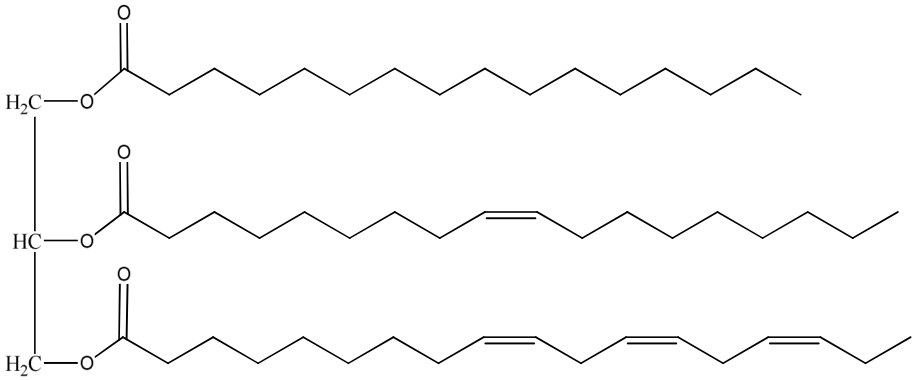

Figure 1.10.1: An unsaturated triacylglycerol fat

In the production of biodiesel, the vegetable or animal fat undergoes a transesterification reaction. In the presence of a catalyst, the fat reacts with an alcohol to give the corresponding alkyl esters of the three fatty acid chains, and free glycerol. It is these alkyl esters that make up biodiesel.

The alcohol that is most commonly used for producing biodiesel is methanol, because it is the cheapest available in most parts of the world. This gives rise to the term FAME (fatty acid methyl esters) as an alternative name to biodiesel. This is not to say that other alcohols (such as ethanol) cannot be used, indeed in some cases they may yield better performing fuels. Biodiesel produced in Brazil uses ethanol as it is less expensive than methanol, due to the country's extensive ethanol industry. Methanolysis of a triacylglycerol molecule is shown below (**Figure 1.10.2**).

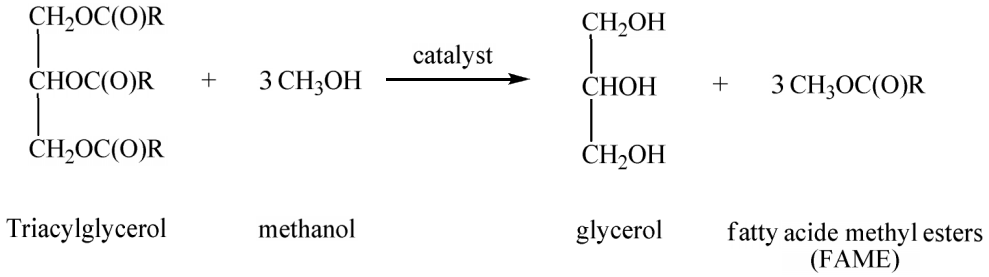

Figure 1.10.2: Transesterification of triacylglycerols with methanol to produce FAME

The benefits of biodiesel are numerous. Exhaust emissions is a global problem that needs to be tackled by both behavioral changes and the development of greener fuels. Biodiesel is non-toxic, and free of sulfurous compounds, aromatics, and other substances present in petrodiesel that are potentially harmful to human health and the environment. A number of reports have been carried out in the United States by the Environmental Protection Agency, Department of Agriculture (USDA), and Department of Energy (US DOE), comparing biodiesel to petrodiesel. Some of the more interesting results of these studies are noted below.[37]

- Carbon monoxide emissions from biodiesel are 50 % lower.
- Fine particle emissions, which are a major cause of lung cancer and other respiratory diseases, are approximately 30 % lower.
- Emission of sulfur containing compounds, such as SO_2, a major cause of acid rain, are completely eliminated.
- Emission of PAH (polycyclic aromatic hydrocarbons), many of which are known carcinogens, were reduced by 75-80 %, with the exception of 1,2-benzanthracene, which was only reduced by 50 %. Nitrated PAH compounds were reduced by at least 90 %, and most were only detectable in minute levels. Overall hydrocarbon emissions are reduced by 95 % or higher.
- Emissions of carbon dioxide over the entire life cycle of the fuel were 78 % lower.

The only pollutants that are not reduced are nitrogen oxides, and these have been shown to be increase slightly, particularly when using pure biodiesel (B100). Nitrogen oxides also contribute to acid rain, however there are a number of technologies designed to reduce their emission. Some cars manufactured in the last few years have come equipped with NO_x absorbers, which consist of a zeolite material designed to act like a molecular sponge. The technology is however experimental and therefore very expensive, with more affordable solutions being fuel additives.[36]

Biodiesel can also be more efficiently produced than petrodiesel, though this depends on numerous factors. For example, biodiesel which is produced domestically will be more energy efficient, and therefore more sustainable, than that produced from imported palm oil. The efficiency also depends upon the nature of the feedstock, as some crops require less energy to process than others. It was calculated by the US DOE that the life cycle fossil energy for petrodiesel is 0.83:1, meaning the potential energy of the fuel is less than the energy it takes to produce. An example of biodiesel being produced using locally collected waste oils, and utilised in nearby vehicles, therefore limiting transportation costs, has been estimated to have an efficiency ratio of 7.8:1. As well as being a renewable source of energy, because biodiesel is derived from plants it is almost carbon neutral. Carbon dioxide emissions for biodiesel are not that much lower than conventional diesel, however because it is made from plants which seize carbon dioxide from the atmosphere, there is no net CO_2 increase from biodiesel combustion. This is not to say that this recycling of carbon dioxide is 100 % efficient, as petrodiesel or other fossil fuels will most likely be used for power during the manufacturing process. Still, it was calculated in the report mentioned above that the petrodiesel life cycle emits 178 % more CO_2 than that associated with vegetable oil derived biodiesel.

An additional benefit is that for most applications biodiesel is able to replace petrodiesel with no modifications to the equipment. Rudolf Diesel designed the diesel engine to run on peanut oil, however the viscosity of pure vegetable oils poses a problem, particularly

at low temperatures, hence the need for the transesterification reaction to produce FAME. The only modification that needs to be made to older diesel powered vehicles is replacement of rubber hoses and gaskets with synthetic parts. This is due to the excellent solvent abilities of FAME, which can degrade rubber over time, particularly if the vehicle is being run on pure biodiesel or a high-blend. The fact that it is a good solvent also means it keeps the fuel lines and engine clean.

1.11 Biodiesel Production and Catalysts Employed

Biodiesel production also enables the recycling of waste fats, oils, and grease from a multitude of sources. The downside to this is that these feedstocks may have a high free fatty acid (FFA) content compared to virgin oils, and this means additional processes are required for separation, as many of the catalysts employed industrially are intolerant to high FFA levels, as well as water. The transesterification reaction can proceed by either acid or base catalysis, however in the homogeneous catalysis usually utilised in industry, a basic catalyst such as NaOH, KOH, or the corresponding alkoxides, are much more rapid and therefore advantageous for high-volume output. The parameters of the transesterification reaction have also been intensely studied, to find the optimum ratio of methanol to oil, temperature of reaction, and effects of the quality of oil and the presence of water. It was found that for optimum FAME yield when using base catalysis, the methanol should be completely moisture-free, and FFA content kept to below 0.5 %.[38] The absence of water is particularly important, as hydrolysis of the methyl ester products and the starting triacylglycerols can occur, producing FFA. With homogeneous Brønsted catalysts such as NaOH, the catalytic species forms by reaction with the methanol, to produce the corresponding alkoxide, as shown.[39]

$$NaOH + MeOH \rightarrow H_2O + MeO^-Na^+$$

This species then attacks the carbonyl group of the triacylglycerol. This is why alkoxides are often used directly as a catalyst, as the reaction remains as moisture free as

possible. A study using NaOH and NaOMe catalysts showed that at temperatures in excess of 60 °C, with a methanol:oil molar ratio of at least 6:1, and using pure oils, reaction had reached completion within 1 hour. These parameters soon became the standard for producing FAME in industry. Below is a schematic of the processes involved in industrial biodiesel production (**Figure 1.11.1)**.[34]

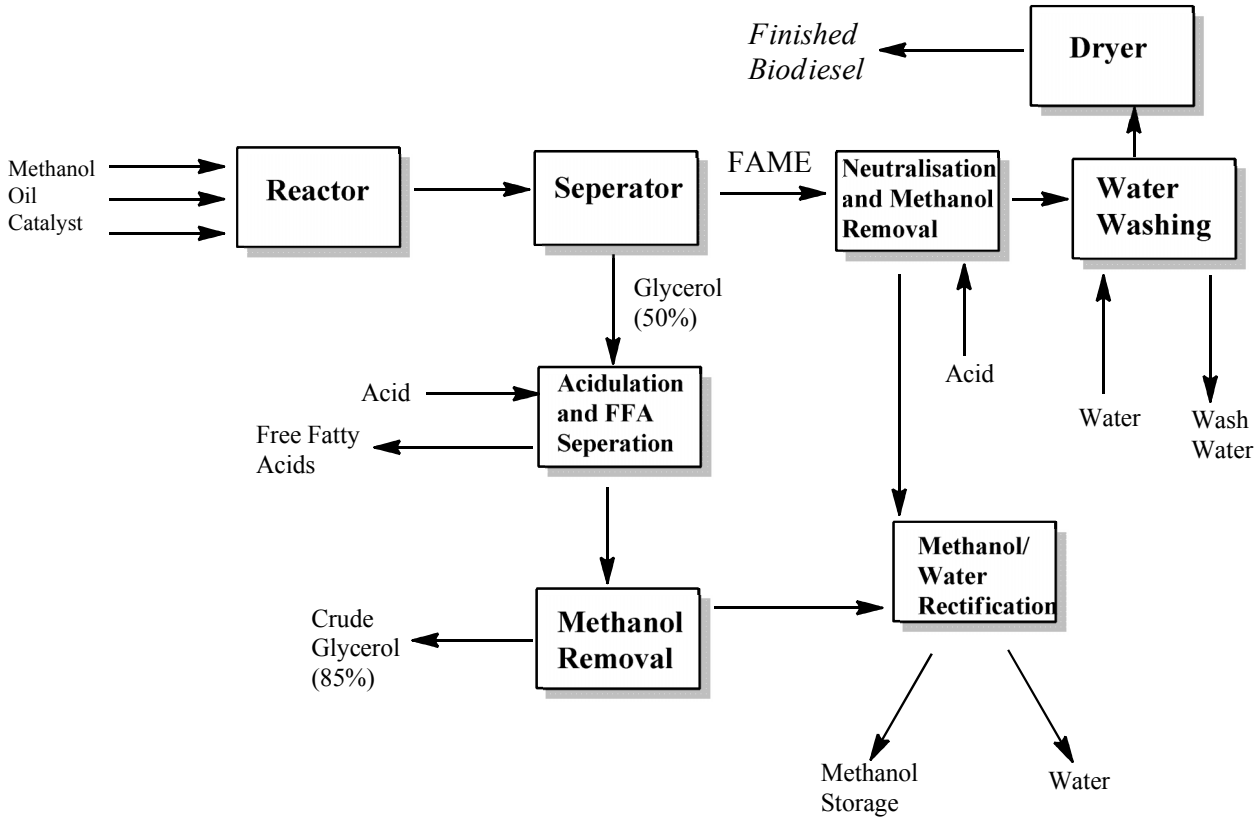

Figure 1.11.1: Process flow scheme for commercial biodiesel production

Most large scale operations use a continuous flow reactor. After the transesterification reaction has occurred, glycerol is separated from the FAME by use of a settling tank or centrifuge, as glycerol is only sparingly soluble in the esters. The glycerol stream is fairly impure, containing excess methanol, catalyst, and any soaps that have formed, and requires further separation to produce crude glycerol of some value, which can then be sold on to a refinery. Methanol is removed from the desired product, usually by

evaporation. Acid is then added, to neutralise any remaining catalyst and to break down any soaps that have formed in the reaction, according to the equation below.

R-COONa + HAc → R-COOH + NaAc

The water-soluble salts are easily removed during the washing step, and any residual water remaining after this step is removed under vacuum. The FFA however remains in the finished product.

If the feedstock contains more than 5% FFA, then pre-treatment is required. If it is not treated, then the alkaline catalyst will react with FFA to produce soaps and water. The excess of soap not only means that more catalyst is needed, but it also inhibits separation of the FAME from glycerol. The fix for these kinds of feedstock is pre-treatment with an acid catalyst such as H_2SO_4. This converts the FFA to FAME via an esterification reaction, and the treated oil can then undergo the base catalysed reaction as usual.

It is quite obvious that this process could do with some simplification. The large degree of processing means that manufacturing costs of biodiesel are still relatively high when compared to petrodiesel. High purity oil feedstocks are expensive, low quality ones add extra steps to the production process.[39] A possible solution to the complexity of the process is using supercritical methanol with no catalyst present. This has been proven to work well, as complete conversion occurs within 5 minutes, and subsequent steps are greatly reduced due to a lack of catalyst to separate. The reaction conditions are unfortunately very harsh, with temperatures in the range of 350-450 °C, and pressures of 100-150 bar. Reaching these conditions requires a lot of energy and vessels capable of withstanding such high pressure, so as far as commercialisation is concerned this process does little to reduce the cost of production.[40]

Concerning the use of waste oils, steps have been taken to produce catalysts capable of both the transesterification reaction and esterification of FFA in the oil, in one single

step, using an acid catalyst. Zhang *et al* have recently shown that homogeneous H_2SO_4 catalysis fulfils this obligation, however there are problems concerning large quantities of unwanted byproducts, and the corrosive nature of the acid catalyst.[41]

In recent years, focus has shifted to heterogeneous catalysts in order to ease separation from the products. The amount of research in this area is vast, as such this report will briefly detail some of the work that has taken place in the past few years. Acid and base catalysts can be classified as Brønsted or Lewis catalysts, but in some examples both types of site may be present. It is useful to perform a general overview of the mechanism of the transesterification reaction with each type of catalyst, to aid design of our own. Heterogeneous Brønsted base catalysts often act in a similar manor to homogeneous catalysis, which was described previously. For example, a zeolite in which there are surface bound metal ions leads to production of a homogeneous alkoxide species.

$$O^-Na^+ + MeOH \rightarrow O\text{-}H + MeO^-Na^+$$

If the positive counterion is bonded directly and strongly to the support material, then the catalytic methanol anions are retained on the catalyst surface, where they react with the triacylglycerols. Heterogeneous Lewis basic catalysts, such as MgO, also rely upon alkoxide formation on the catalyst surface, as the methanol is absorbed on to free basic Mg sites.

Concerning acid catalysts, both Brønsted acids (e.g. H_2SO_4) and Lewis acids (complexes of a variety of metals) have been used as homogeneous catalysts for both the esterification of FFA, and transesterification of triacylglycerols. It has been found however that Brønsted acids are more active for the esterification reaction, and Lewis acids more suitable for FAME production. This can be seen in the following data, where *p*-toluenesulfonic (PTSA) acid and lead acetate were tested for biodiesel production from soybean oil, with a molecule simulating FFA added for some of the runs (**Table 1.11.1**).[42]

Catalyst	Initial FFA conc /%	Temp /°C	Reaction Time /min	Amount of Catalyst /mol	FAME Yield /%	Final FFA conc /%
None	-	180	40	-	2	-
None	20.5	180	60	-	22	10.7
$Pb(OAc)_2$	-	180	40	5.47×10^{-5}	92	-
PTSA	-	180	40	5.35×10^{-5}	29	-
$Pb(OAc)_2$	20.5	180	60	5.38×10^{-5}	57	6.8
PTSA	20.5	180	60	6.40×10^{-5}	48	1.1

Table 1.11.1: Comparison of catalysts using 8g of soybean oil, and a methanol/oil molar ratio of 12:1

Brønsted acid catalysts work by simple protonation of the carbonyl group, which makes it more susceptible to attack by the nucleophilic methanol molecule. This is true of both homogeneous and heterogeneous catalysts. Homogeneous and heterogeneous Lewis acid catalysts also work in a similar manner, as coordination of the oxygen of the carbonyl group to a metal site renders the carbon more electrophilic, and it then undergoes attack by the alcohol. It has been found that it is desorption of the FAME from the Lewis acid sites that is the rate determining step of the reaction. Metals which are highly Lewis acidic will disfavour desorption of the product, thus rendering them ineffective catalysts. There exists an optimal range for the strength of Lewis acidic sites when used for transesterification catalysis.[43,44]

1.12 Basic Catalysts for Biodiesel Production

Oxides, hydroxides and alkoxides of the alkaline earth metals have been thoroughly investigated for basic heterogeneous catalysis. Gryglewicz *et al* showed through a number of tests that sodium and barium hydroxides were the most active species, however it is the oxides of magnesium and calcium which have garnered the most

interest and research.[45] The reaction rates using CaO as a catalyst were found by Gryglewicz to be quite slow, however biodiesel yield has been shown to increase with increasing temperature and raising the methanol to oil ratio.[46] For example a run using a methanol to sunflower oil ratio of 6:1 gave only a 65 % FAME yield after 15 minutes at 252 °C, however under the same conditions, a ration of 41.1:1 gave a 99 % yield.[47] Various other methods have been employed to raise the activity of CaO. Use of nanocrystalline material (crystals 20 nm in size) provided 100 % conversion of soybean oil at room temperature after 12 hours. The commercially available material had crystals on average 42 nm in size, and the substantial loss of catalyst surface area lead to a FAME yield of only 2 % after the same time.[48]

Magnesium oxide has also been shown to perform strongly. 5 wt% of MgO gave a yield of 90 % after 1 hour at 180 °C using a methanol to soybean oil ration of 12:1.44. Slightly higher yields have been reported by others using supercritical conditions (300 °C), though a higher methanol/oil ratio was also employed, and the full range of calcium compounds (CaO, $Ca(OH)_2$, $CaCO_3$) gave higher yields under the same conditions.[49] Nanocrystalline MgO has also been found to have improved performance over the microcrystalline form. A paper by Parvalescu *et al* studied a number of different forms of nanocrystalline MgO for their catalytic activity.[50] Different approaches to the production of these materials can lead to different particle sizes, and more importantly, different surface morphologies, which can make a great degree of difference in their chemistry. Parvalescu *et al* prepared sheet-like MgO, in which the primary surface is composed of alternating monolayers of magnesium cations and oxygen anions, creating a strong electrostatic field perpendicular to the catalytic surface.[51] This is advantageous due to the manner in which the methanol is adsorbed on to the MgO surface. Preparation of the material was by the addition of 4-methoxy-benzyl alcohol to a 10 wt% methanolic solution of $Mg(OCH_3)_2$, followed by the addition of water/methanol and supercritical treatment and calcination in air at 500 °C. It was then tested against microcrystalline MgO and two other forms of nanocrystalline MgO prepared from

previously known methods, in which the surface atomic arrangement and coordination was different. At autoclave conditions (100 °C), their material performed better than the others tested, however the transesterification of sunflower oil under microwave conditions was outstanding. As is typical with performing the reaction under these conditions, the conversion of methanol occurred to a greater degree and in a much shorter time. Using 23 ml of sunflower oil, 5 ml of methanol (1:4 molar ratio), 300 mg of MgO, at 70 °C for 40 minutes and under microwave conditions, conversion of methanol and yields of FAME were over 95 %, and recycling of the catalyst for subsequent runs showed no deterioration of performance over the course of at least 7 runs. There was also very little leaching of Mg into the FAME or glycerol as a soap, as analysis of both phases showed Mg ion concentrations of less than 10 ppm. This would imply that further purification of the biodiesel would not be required, reducing production costs. Rapeseed oil was also used as a triacylglycerol source; however, even under microwave conditions, yields did not exceed 70 %.[50]

Many oils, fats, and alcohols contain water, and this is of some concern when using a number of catalysts, however it was found that even with a high water concentration (10,000 ppm), the catalytic activity of various MgO catalysts was not compromised.[52] This is important when considering industrially implementing these technologies, as it makes it possible to use unrefined bioethanol as a feedstock, which inherently contains some moisture. This is just another step to reducing the cost of biodiesel so that it may be competitive with petrodiesel.

Several catalysts have also been reported where the MgO is attached to silica based supports. Rudolph *et al* recently tried functionalising mesoporous silicate materials such as MCM-41, SBA-15, and KIT-6.[53] Preparation of the materials was to take the freshly calcined SiO_2 support and stir it in methanol with either $Mg(CH_3COO)_2.2H_2O$ or $Mg(NO_3)_2.6H_2O$ to give an Mg^{2+}/Si ratio of 1:1, and these materials were calcined at 450 °C. In-situ synthesis of MgO doped SBA-15 was also attempted. The catalysts (1 g) were

tested for their activity towards the transesterification of blended vegetable oil (50 g, purchased from a supermarket) with ethanol (17 g), at 200 °C for 5 hours. The mesoporous materials were themselves tested, but showed very little activity as expected. Loading of MgO gave higher yields for all materials, though it was the impregnated SBA-15 material that gave the highest yield of ethyl esters with 96%. The in-situ synthesised MgO-SBA-15 catalyst, though possessing a larger surface area and pore size due to the inclusion of Mg in to the framework, only gave a 78% yield. The impregnated material was shown by X-ray photoelectron spectroscopy (XPS) to have a greater surface concentration of Mg ions available for catalysis, resulting in the higher conversions. Both of these results were achieved using the acetate as the Mg source, and both types of SBA-15 catalysts synthesised using the nitrate gave slightly lower yields. When comparing the 3 different support types used there was little correlation between any properties (surface area, porosity, and Mg concentration) and catalytic activity. Basicity of the materials was also determined by CO_2 chemisorption as an indication of the number of basic sites. The MgO-KIT-6 material had the strongest basic sites, yet did not perform as admirably, indicating the activity of a basic catalyst cannot be attributed to its basicity alone, nor any other isolated feature, and that it is likely to be a combination of these attributes.[53]

Hydrotalcites are layered double oxides of the general formula $Mg_{1-x}Al_x(OH)_2(CO_3)_{x/2}.nH_2O$. Commercially available hydrotalcites were tested for transesterification of rapeseed oil but were found to be significantly less active than pure MgO. Calcination of the materials gives amorphous porous metal oxides upon evolution of water and carbon dioxide, are much more active. They were tested for the transesterification of soybean oil with methanol at 60 °C, and it was found that the rate of the reaction increases steadily with the Mg content, with a catalyst of the atomic ratio Al/(Mg+Al) = 0.25 being the most active (66% yield of FAME after 9 hours, using 7.5 wt% catalyst and a 15:1 methanol/oil ratio).[54] Others have tested calcined hydrotalcites for the transesterification of glycerol tributyrate with methanol, and came to the same

conclusion on the optimum catalyst composition.[55] Higher reaction temperatures have also been investigated with hydrotalcites of the same composition, and a 96 % yield of FAME has been reported after 1 hour at 180 °C, using soybean oil, a 12:1 methanol/oil ratio and 5 wt% of catalyst.[52]

Hydrotalcites have also been doped with other metals to enhance their activity. One example is the substitution of a fraction of the Al^{3+} ions with Fe^{3+}, in order to tune the basicity of the catalyst.[56] Hydrotalcite materials with a molar ratio Mg/(Al+Fe) of approximately 3 were prepared by the common method used for undoped materials, except the addition of the third metal salt in the reaction mixture. Catalysts containing 10 and 20 mol% of iron respectively were tested for transesterification of soybean oil at 80 °C, with a 6:1 methanol/oil ratio, and using 1 wt% of catalyst. The 10 mol% Fe doped material gave a yield of 38 % after 60 minutes. Other trivalent cations such as Ga and Cr were also inserted in to hydrotalcite, however activity was only comparable to that of undoped materials. Regeneration of the catalysts after centrifuge separation from the FAME and washing with methanol consisted of calcining the spent catalyst at the same temperature employed for the initial synthesis (460 °C), however the regenerated catalyst was approximately half as active. A second regeneration process however showed no degradation of the catalyst performance.[56]

ZnO is fairly widely used as a catalyst support, and attempts have been made to dope the material with alkaline earth metals, which have already been discussed and recognised as suitable catalysts. A number were synthesised by Yang *et al*, with the most promising being the incorporation of strontium.[57] This was prepared by stirring the ZnO with $Sr(NO_3)$ in water, and then calcining the material at 600 °C for 5 hours to decompose the nitrate and form SrO, which is likely the main active species in the material. Using refluxing methanol (65 °C), a 12:1 methanol/soybean oil ratio, and 5 wt% of catalyst gave a FAME yield of 94.7 % after 5 hours. Regeneration of the spent catalyst by washing at heating at a moderate temperature proved ineffective, as use of the

recovered catalyst provided only a 14% FAME yield under the same conditions, suggesting significant deactivation. Regeneration by stirring the catalyst in a fresh solution of $Sr(NO_3)_2$ proved more fruitful; however this would add considerable expense to an industrial process. They also investigated the effect of a co-solvent in the transesterification reaction, and noted that a small volume of THF most effectively increased the rate of transesterification by merging of the methanol and oil phases.[57]

Others have loaded ZnO with alkali metals such as Li, Na and K.[58] This was achieved simply by stirring commercially available zinc oxide powder with an aqueous solution of alkali-metal nitrate, followed by drying at 120 °C and calcinations at 600 °C in air for 5 hours, to give the corresponding alkali-metal oxide. The metals were loaded at a dosage of 3 mmol g^{-1} of support material, based on the concentration of the solution used. Among the catalysts screened, Li/ZnO was the most active, and the Na and K materials gave very poor conversion. Though different activities were observed, the strength of the basic sites for all catalysts was determined to be the same, thus it was concluded that the quantity of basic sites is of the up most importance to activity. The effect of calcination temperature, Li loading, methanol/oil ratio, and catalyst loading were investigated. It was found that the optimal values for transesterification were calcination at 600 °C, 3 mmol g^{-1} Li loading (above which conversion of methanol decreased), 12:1 methanol/oil ratio, and 5 wt% catalyst loading. This catalyst gave a FAME yield of 96.3 % after 5 hours at 65 °C. As with the previous catalyst, leaching of the dopant when the catalyst is washed after use dramatically reduced the activity, and impregnation of further Li via a fresh solution of nitrate is required to reactive the catalyst, though only a yield of 83.6 % was achived.[58]

KF loaded on to ZnO has also been reported to be an efficient solid base catalyst for transesterification reactions.[59] Other potassium compounds were also investigated but did not give as good results. The catalyst can be prepared by stirring ZnO in aqueous KF solution, followed by drying and calcination at the required temperature, the optimum

for FAME yield being 600 °C. KF and ZnO themselves were tested as catalysts and showed no activity, suggesting that the active sites are produced by reaction of the potassium fluoride with the surface of the support. Activity increased with KF loading, reaching an optimum of 1.47 mmol/g of ZnO. Beyond 15 wt% KF loading, yields fell, possibly due to agglomeration of the active phase, or blocking of the active basic sites by superfluous KF. With the optimum reaction conditions of a 10:1 methanol/soybean oil ratio, 3 wt% catalyst loading, and at methanol reflux temperature, a maximum FAME yield of 87 % was achieved over the catalyst after a 9 hour run. No information was given by the authors as to whether the catalyst remained fully active for more than 1 run.[59] KF has also been loaded on to other supports such as alumina.[60] KF/Al_2O_3 is a well known and extremely versatile basic catalyst that has been found to promote a number of chemical reactions, such as the Michael addition, aldol condensation, and alkene isomerisation amongst others. Despite its applications in organic synthesis, very little literature exists on its use as a transesterification catalyst. Powder X-ray diffraction of the uncalcined material shows peaks which can be assigned to KF and Al_2O_3, however after calcination at 600 °C for 3 hours, the KF peak is no longer seen in the diffraction pattern. A new peak is observed, thought to correspond to a new K_3AlF_6 phase which forms at the high calcination temperature. It is this species to which the catalyst owes its basic activity.[61] The peak for this material was shown to grow stronger when more KF had been loaded on to the alumina support, also illustrating that it is a result of a reaction between the two compounds. The pXRD of the spent catalyst shows a diminished peak for the K_3AlF_6 phase, indicating that the interaction between KF and Al_2O_3 has been weakened. Regeneration of the catalyst would therefore be required before further catalytic runs. The optimal conditions for the transesterification of palm oil with methanol were a KF/Al_2O_3 ratio of 0.331 (wt/wt), a 12:1 methanol/oil ratio, a catalyst load of 4 wt%, and a temperature of 65 °C. Under these conditions, a FAME yield of 91 % was achieved in under 3 hours.[60]

1.13 Acid Catalysts for Biodiesel Production

Despite the fact that acid catalysis promotes esterification and transesterification reactions, therefore enabling use of lower quality feedstocks containing substantial amounts of FFA, most of the literature is focused upon the esterification reaction. Lopez *et al* tested a number of acid catalysts for the transesterification of triacetin with methanol at 60 °C.[62] Triacetin is arguably the simplest triacylglycerol, as the R group of each ester is a methyl group, so it is often used for catalytic testing rather than commercially obtained oils which may have impurities. Some homogeneous systems were also tested for comparison, and a homogeneous H_2SO_4 catalyst was deemed to be the most active on a wt/wt basis. Next in the order of activity was Amberlyst-15, a polystyrene sulfonic acid ion-exchange resin, which is highly acidic, and gave a conversion of 79 % after 8 hours. Sulfated zirconia (SZ) yielded a conversion of 57 %, and Nafion NR50, a super-acidic perfluorinated resin-sulfonic acid, only 33 %. Other solid acids tested that gave even lower yields and are therefore wholly ineffective were tungstated zirconia (WZ), supported phosphoric acid (SPA), β-zeolite (an aluminosilicate molecular sieve), and ETS-10 (a titanosilicate molecular sieve). The low activity of β-zeolite was surprising to the authors as its acidic sites are fairly strong, however it is thought that the size of the pores (25 $Å^2$) was responsible. Triacetin is a very simple triacylglycerol however its conformational freedom is extremely restricted when in solution, which could limit diffusion of the molecule through porous solid materials.[63] Even if the triacetin is able to diffuse through the pores, there may not be enough room for necessary reaction intermediates to form, so most of the activity will be taking place on the surface of the catalyst. For most of the catalysts, rate of reaction decreased after multiple runs. The number of active sulfur sites remained the same, so it was hypothesised that this was due to blockage of the active sites by reaction products or intermediates. Nafion NR50 actually showed a increase in activity for its second run, due to the fact that resin catalysts tend to swell in highly polar solvents.[62]

Furuta *et al* tested their catalysts for both transesterification of soybean oil at high temperature (200-300 °C) and esterification of a FFA model with methanol at slightly lower temperatures.[64] Tungstated ZrO_2/Al_2O_3, sulfated ZrO_2/Al_2O_3, and sulfated SnO_2 were compared, and while all provided very good conversions for FFA (in this case *n*-octanoic acid) conversion, only the tungstated compound gave a good yield of FAME (90 %). Though it was the worst esterification catalyst tested, it still provided in excess of 90 % conversion, and thus is a promising catalyst for the processing of waste oils and fats, particularly as it remains stable under fairly high temperatures.[64]

A number of zinc compounds have also been proven to be good acid catalysts. Though often used as a support for base catalysts, ZnO has been recently shown to be itself capable of oil transesterification. In a 1:1 by weight mixture of rapeseed oil and methanol, 0.5 wt% ZnO gave a 92.7 % yield of FAME after 6 hours at 230 °C. Upon reuse of the catalyst under the same conditions, the yield actually increased to 94.3 %.[65] ZnO has also been grafted on to an alumina support, either by impregnation of an aqueous solution of $Zn(NO_3)$ and calcination at 500 °C (**A**), or simple mechanical mixing of Al_2O_3 and ZnO, followed by calcination at 600 °C (**B**). Both catalysts contain similar amounts of zinc and show similar activities for transesterification, with **A** yielding 91.4 % FAME after 1 hour, and **B** giving 94.3 % after the same time. The main active species in this zinc aluminate catalyst is thought to be a $ZnAl_2O_4$ phase which is formed during calcination, and leaching of Zn in to the biodiesel is negligible. One drawback of this system is the complete intolerance to water, as good yields will only occur if water content of the oil is less than 1500 ppm.[66]

Titanium alkoxides have been shown to be good homogeneous transesterification catalysts, and attempts have been made to make heterogeneous systems supporting $CH_3Ti(O^iPr)_3$ on silica.[66] However, as with the previous catalyst, it is permanently deactivated by water, so more stable catalysts have been proposed. $Ti(O^iPr)_4$ was grafted on to a silica support under an inert atmosphere, and this was followed by

steam hydrolysis and calcination. Catalysts with a TiO_2 content of between 3 and 11 wt % all gave FAME yields of approximately 65 % at 180 °C after 1 hour.[67] Higher levels of TiO_2, beyond a monolayer, led to a decrease in activity due to the unavailability of the active Lewis acid sites. With increased loading, many different types of titanium species were observed by Fourier transform infrared spectroscopy (FTIR), including titanium in both octahedral and tetrahedral environments, as well as single TiO_2 crystals. However, these stronger Lewis sites are not at all beneficial for catalytic activity, as they hinder release of the product.[67]

Titanium oxide has also been grafted on to alumina, as detailed in a 2005 patent application by Lacome *et al*.[68] Mixing of a titanium butoxide in heptane (other alkoxides or inorganic salts such as chlorides can also be used) with Al_2O_3 yielded a catalyst with a TiO_2 content of 12.5 wt% after drying and calcination at 500 °C. Catalyst testing was performed in an autoclave at 200 °C, and samples were removed from the reactor after 2, 5 and 7 hours. Any excess methanol was evaporated off and the glycerol removed, and the percentage of methyl esters in the product was 68 %, 89 % and 95 % respectively. Leaching of the Ti was minimal, confirming it as a completely heterogeneous catalyst, and the catalyst was reused three more times, and retained the same level of activity.[68] A ZrO_2/Al_2O_3 catalyst was also prepared, and under the same reaction conditions afforded slightly inferior results. The most active catalyst detailed in the patent contains antimony. Various production methods were reported however the most effective is the addition of a heptane solution of $Sb(OCH_2CH_2CH_2CH_3)_3$ to pre-prepared Al_2O_3, followed by drying at ambient temperature, and calcination at 350 °C. Antimony loading was determined to be 13.9 wt%, and testing under the conditions mentioned previously gave a FAME yield of 86 %, 96 % and 96 % after 2, 5, and 7 hours respectively. The antimony catalyst seems to have a much greater turnover rate than the Ti system, and a higher overall yield. The antimony concentration in the FAME produced was only 2 ppm, so no further refinement of the fuel would be necessary, and reuse of the catalyst again showed zero degradation in activity. The only drawback of

this system is the cost of the catalyst, as the antimony source is significantly more expensive than that used in the synthesis of TiO_2/Al_2O_3.[68]

Sreeprasanth *et al* recently reported an effective catalyst based on a double-metal cyanide (DMC) complex.[69] Double-metal cyanides have a zeolite-like structure which gives a high catalyst surface area, and they are also insoluble in almost all organic solvents.[70] A Zn-Fe DMC was shown to be a promising catalyst for the transesterification of numerous refined and unrefined oils. The material was prepared by the addition of an aqueous solution of $K_4Fe(CN)_6.3H_2O$ to $ZnCl_2$ dissolved in a 1:1 water/*tert*-butanol solvent, and stirring at 50 °C for 1 hour. To this mixture, a triblock copolymer with an average molecular weight of 5800 g mol^{-1} dissolved in a 1:20 water/*tert*-butanol solution was added and stirred for a further hour. Characterisation of the material showed Lewis acidic sites, but no Brønsted acidity. Conversion in the transesterification reaction was shown to increase with catalyst loads up to 2 wt%, and Fe-Zn DMC gave a conversion of 98.3 %, using ethanol and sunflower oil in a 15:1 molar ratio, at 170 °C. The reaction proceeded stepwise, as the triacylglycerols were converted first to diacylglycerols, and then monoacylglycerols, and finally glycerol, yielding 3 molar equivalents of ethyl esters in the process. In the first 2 hours of reaction glycerol yields were low, and NMR spectra of the reaction mixture taken at this time showed the majority of triacylglycerols had been converted, but mainly to di- and monoacylglycerols. After 8 hours however, these were not detectable by NMR and only glycerol and ethyl esters were found. Results for transesterification with methanol and other short chain alcohols were very similar to that quoted above. This catalyst is very promising as it is able to efficiently catalyse the esterification of FFA and the transesterification in one operation, even when oils with high FFA content such as rubber-seed oil are used. Water content also had no effect on methanol conversion data of the methanolysis of sunflower oil, most likely due to the highly hydrophobic nature of DMC complexes at the temperatures employed , however as the amount of water in the feedstock increased, so did the acidity of the product FAME. This is due to the hydrolysis of the FAME to FFA. Reusability of the catalyst

however was impressive, with no loss of activity even after 52 hours of continuous use.[69]

1.14 Summary of Research Aims

Both of the processes mentioned are an effort to move towards sustainable, 'green' chemistry, and reduce our dependence on oil. The main aim of this research was to synthesise, characterize, and test novel heterogeneous catalysts for the reaction of ethanol to 1,3-Butadiene. The aim was for a catalyst that provided high selectivity for the desired product, and operates at reasonable temperature and pressure. Also of importance was that selectivity towards ethylene and other butenes be suppressed to the fullest extent as to make the process economically viable on an industrial scale. The nature of catalyst-support interactions was also probed by the use of silsesquioxanes to model the binding of metals to a silica support. Also investigated were potential catalysts for the production of biodiesel using a vegetable oil and methanol feed. Results of this work are presented herein.

References

1. E. Marris, *Nature*, 2006, **444**, 670-672.
2. W. C. White, *Chemico-biological interactions*, 2007, **166**, 10-14.
3. J. Ostomisslensky, *Journal of the Russian Physical Chemistry Society*, 1915, **47**, 1472-1506.
4. D.J. Butterbaugh, R.L.E. Spence, *US patent*, **1948**, US2447181.
5. W. M. Quattlebaum, W. J. Toussant and J. T. Dunn, *Journal of the American Chemical Society*, 1947, **69**, 593-599.
6. J. Gorin and A. Yu, *Russian Journal of General Chemistry*, 1946, **16**, 1089.
7. I. Takahara, M. Saito, M. Inaba and K. Murata, *Catalysis Letters*, 2005, **105**, 249-252.
8. H. E. Jones, E. E. Stahly and B. B. Corson, *J. Am. Chem. Soc.*, 1949, **71**, 1822-1828.

9. W. Ponndorf, *Angewandte Chemie*, 1926, **39**.
10. T. Ooi, T. Miura and K. Maruoka, *Angewandte Chemie-International Edition*, 1998, **37**, 2347-2349.
11. Y. Ishii, T. Nakano, A. Inada, Y. Kishigami, K. Sakurai and M. Ogawa, *Journal of Organic Chemistry*, 1986, **51**, 240-242.
12. P. J. Kunkeler, B. J. Zuurdeeg, J. C. van der Waal, J. A. van Bokhoven, D. C. Koningsberger and H. van Bekkum, *J. Catal.*, 1998, **180**, 234-244.
13. J. Sanz, V. Fornes and A. Corma, *Journal of the Chemical Society-Faraday Transactions I*, 1988, **84**, 3113-3119.
14. E. Bourgeatlami, P. Massiani, F. Direnzo, P. Espiau, F. Fajula and T. D. Courieres, *Applied Catalysis*, 1991, **72**, 139-152.
15. A. Corma, M. E. Domine and S. Valencia, *J. Catal.*, 2003, **215**, 294-304.
16. K. Tanabe, *New solid acids and bases : their catalytic properties*, Elsevier, New York, N.Y., U.S.A., 1989.
17. V. A. Ivanov, J. Bachelier, F. Audry and J. C. Lavalley, *Journal of Molecular Catalysis*, 1994, **91**, 45-59.
18. H. Niyama, S. Morii and E. Echigoya, *Bulletin of the Chemical Society of Japan*, 1972, **45**, 655-659.
19. T. M. T. Ooi, Y. Itagaki, H. Ichikawa and K. Maruoka, *Synthesis*, 2002, 279-291.
20. A. Ramanathan, D. Klomp, J. A. Peters and U. Hanefeld, *Journal of Molecular Catalysis a-Chemical*, 2006, **260**, 62-69.
21. S. Kvisle, A. Aguero and R. P. A. Sneeden, *Applied Catalysis*, 1988, **43**, 117-131.
22. R. Cyril and J.T. Earl, *US patent*, **1957**, US2800517
23. R. Ohnishi, T. Akimoto and K. Tanabe, *Journal of the Chemical Society-Chemical Communications*, 1985, 1613-1614.
24. W.J. Toussaint and J.T. Dunn, *US patent*, **1947**, US2421361.
25. R.L.E.U Spence, D.J. Butterbaugh, D.G. Kundiger, *US patent*, 1948, US2438464.
26. S. K. Bhattacharyya and B. N. Avasthi, *Industrial & Engineering Chemisty Process Design and Development*, 1963, **2**, 45-51.
27. J. B. D. Delacaillerie, V. Gruver and J. J. Fripiat, *Journal of Catalysis*, 1995, **151**, 420-430.
28. V. Gruver, A. Sun and J. J. Fripiat, *Catalysis Letters*, 1995, **34**, 359-364.
29. Y. Kitayama and A. Michishita, *Journal of the Chemical Society-Chemical Communications*, 1981, 401-402.
30. *Japan Pat.*, 50172822
31. *Japan Pat.*, 58059928
32. T. Tsuchida, K. Atsumi, S. Sakuma and T. Inui, *US patent*, **2001**, US6323383.
33. T. Tsuchida, J. Kubo, T. Yoshioka, S. Sakuma, T. Takeguchi and W. Ueda, *Journal of Catalysis*, 2008, **259**, 183-189.
34. G. Knothe, J. Van Gerpen and J. Krahl, *The biodiesel handbook*, AOCS Press, Urbana, Ill., 2005.
35. B. P. p.l.c, *BP Statistical Review of World Energy 2009*, http://www.bp.com/liveassets/bp_internet/globalbp/globalbp_uk_english/reports_and_publications/statistical_energy_review_2008/STAGING/local_assets/2009_downloads/statistical_review_of_world_energy_full_report_2009.pdf, Accessed 8th April 2010.

36. A. K. Townsend, *Exploring sustainable biodiesel*, Schiffer, Atglen, Pa., 2008.
37. G. Knothe, C. A. Sharp and T. W. Ryan, *Energy & Fuels*, 2005, **20**, 403-408.
38. B. Freedman, Pryde, E.H., *Journal of the American Oil Chemistry Society*, 1984, **61**, 1638 - 1643

39. F. R. Ma and M. A. Hanna, *Bioresour. Technol.*, 1999, **70**, 1-15.
40. G. W. Huber, S. Iborra and A. Corma, *Chem Rev*, 2006, **106**, 4044-4098.
41. Y. Zhang, M. A. Dube, D. D. McLean and M. Kates, *Bioresour. Technol.*, 2003, **90**, 229-240.
42. M. Di Serio, R. Tesser, L. Pengmei and E. Santacesaria, *Energy & Fuels*, 2008, **22**, 207-217.
43. B. Bonelli, M. Cozzolino, R. Tesser, M. Di Serio, M. Piumetti, E. Garrone and E. Santacesaria, *J. Catal.*, 2007, **246**, 293-300.
44. M. Di Serio, B. Apicella, G. Grieco, P. Iengo, L. Fiocca, R. Po and E. Santacesaria, *Journal of Molecular Catalysis a-Chemical*, 1998, **130**, 233-240.
45. S. Gryglewicz, *Bioresour. Technol.*, 1999, **70**, 249-253.
46. M. Kouzu, T. Kasuno, M. Tajika, Y. Sugimoto, S. Yamanaka and J. Hidaka, *Fuel*, 2008, **87**, 2798-2806.
47. A. Demirbas, *Energy Conversion and Management*, 2007, **48**, 937-941.
48. C. Reddy, V. Reddy, R. Oshel and J. G. Verkade, *Energy & Fuels*, 2006, **20**, 1310-1314.
49. T. Tateno and T. Sasaki, *US patent*, **2004**, US6818026.
50. M. Verziu, B. Cojocaru, J. C. Hu, R. Richards, C. Ciuculescu, P. Filip and V. I. Parvulescu, *Green Chemistry*, 2008, **10**, 373-381.
51. K. Zhu, J. Hu, C. Kuebel and R. Richards, *Angewandte Chemie International Edition*, 2006, **45**, 7277-7281.
52. M. Di Serio, M. Ledda, M. Cozzolino, G. Minutillo, R. Tesser and E. Santacesaria, *Industrial & Engineering Chemistry Research*, 2006, **45**, 3009-3014.
53. E. Li and V. Rudolph, *Energy & Fuels*, 2008, **22**, 145-149.
54. W. L. Xie, H. Peng and L. G. Chen, *Journal of Molecular Catalysis a-Chemical*, 2006, **246**, 24-32.
55. D. G. Cantrell, L. J. Gillie, A. F. Lee and K. Wilson, *Applied Catalysis a-General*, 2005, **287**, 183-190.
56. G. S. Macala, A. W. Robertson, C. L. Johnson, Z. B. Day, R. S. Lewis, M. G. White, A. V. Iretskii and P. C. Ford, *Catalysis Letters*, 2008, **122**, 205-209.
57. Z. Q. Yang and W. L. Xie, *Fuel Process. Technol.*, 2007, **88**, 631-638.
58. W. L. Xie, Z. Q. Yang and H. Chun, *Industrial & Engineering Chemistry Research*, 2007, **46**, 7942-7949.
59. W. L. Xie and X. M. Huang, *Catalysis Letters*, 2006, **107**, 53-59.
60. X. Bo, G. M. Xiao, L. F. Cui, R. P. Wei and L. J. Gao, *Energy & Fuels*, 2007, **21**, 3109-3112.
61. L. M. Weinstock, J. M. Stevenson, S. A. Tomellini, S. H. Pan, T. Utne, R. B. Jobson and D. F. Reinhold, *Tetrahedron Letters*, 1986, **27**, 3845-3848.
62. D. E. Lopez, J. G. Goodwin, D. A. Bruce and E. Lotero, *Applied Catalysis a-General*, 2005, **295**, 97-105.

63. D. G. Papageorgiou, I. N. Demetropoulos, I. E. Lagaris and P. T. Papadimitriou, *Tetrahedron*, 1996, **52**, 677-686.
64. S. Furuta, H. Matsuhashi and K. Arata, *Catalysis Communications*, 2004, **5**, 721-723.
65. R. Stern, G. Hillion, J-J. Rouxel, and S. Leporq, *US patent*, **1999**, US5908946.
66. L. Bournay, G. Hillion, P. Boucot, J. Chodorge, C. Bronner and A. Forestiere, *US patent*, **2005**, US6878837.
67. M. Cozzolino, M. Di Serio, R. Tesser and E. Santacesaria, *Applied Catalysis a-General*, 2007, **325**, 256-262.
68. T. Lacome, G. Hillion, B. Delfort, R. Revel, S. Leporq and G. Acakpo, *US patent*, **2005**, US20050266139.
69. P. S. Sreeprasanth, R. Srivastava, D. Srinivas and P. Ratnasamy, *Applied Catalysis a-General*, 2006, **314**, 148-159.
70. P. Gravereau and E. Garnier, *Acta Crystallogr. Sect. C-Cryst. Struct. Commun.*, 1984, **40**, 1306-1309.

Chapter 2: Results and Discussion of Catalysts for the Conversion of Ethanol to 1,3-Butadiene

2.1 Catalytic Test Rig and Procedure

Catalysts for the conversion of ethanol to 1,3-BD were tested using a purpose-built catalytic rig. Over the course of the research many refinements were made to the structure of the rig as well as the operating procedure, in order to improve the integrity of the results. Catalytic testing was carried out by passing ethanol vapour in a stream of argon carrier gas over a fixed bed of catalyst, and the products analysed by both gas chromatography and ^{1}H NMR spectroscopy.

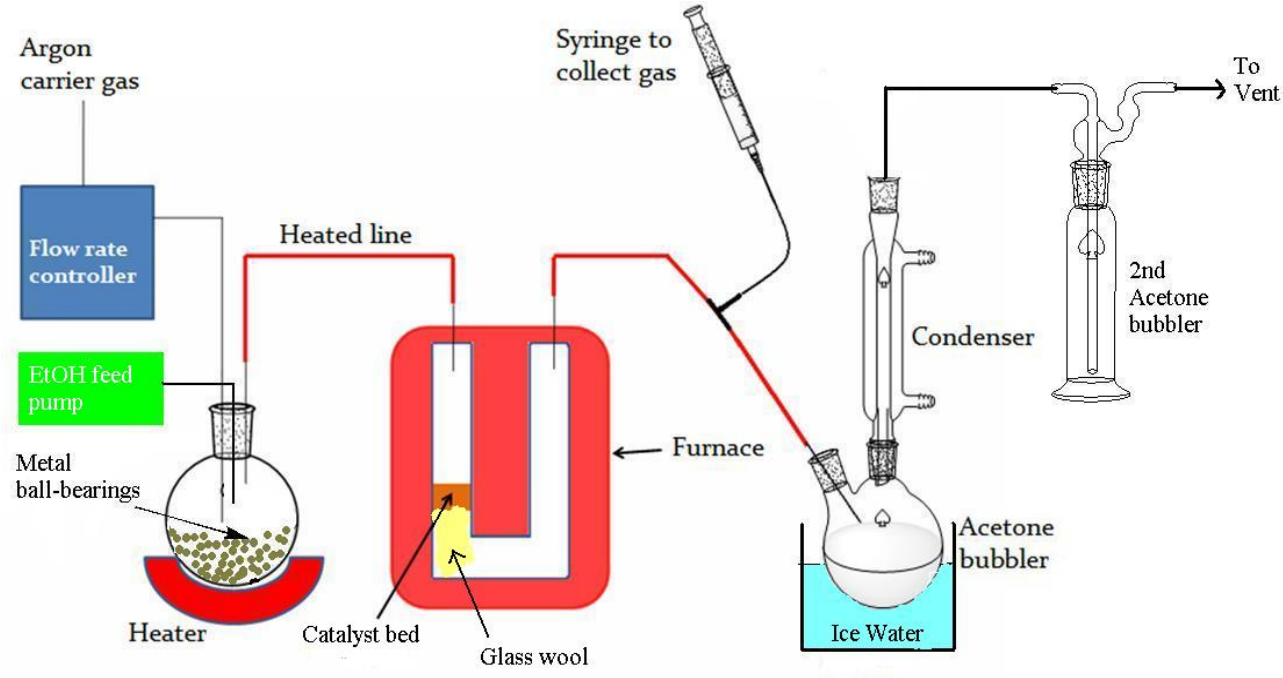

Figure 2.1.1: Schematic of the catalyst test rig

Argon gas was fed through the apparatus at all times, the flow rate controlled electronically using a mass flow controller. Ethanol is fed in to a flask via an HPLC pump, again at a known rate (either 0.1 or 0.05 ml min^{-1}). Both the Ar flow rate controller and HPLC pump were calibrated at regular intervals to ensure they remained consistent. The receiving flask was filled with metal ball-bearings and surrounded by a heating jacket set at 80 °C, to promote

ethanol vaporisation. Ethanol vapour in Ar carrier gas is then transported via a heated line to the reactor. This consisted of a U-shaped quartz tube, into which was place the catalyst on a bed of glass wool. The entire tube was enclosed in a furnace, operating at a set temperature, and under isothermal conditions. The furnace temperature ranged from 300 to 400 °C dependent upon the catalyst being tested. Exhaust gases then exit the furnace via more heated line, and bubbled through a flask of acetone, which is chilled to 0 °C. A condenser sat upon flask to prevent evaporation of products from the acetone. A second acetone bubbler was utilised to try and remove any residual products, and the remaining gas directed to a vent. Prior to the bubblers was a valve, enabling extraction of a sample of the exhaust stream for analysis by gas chromatography.

The apparatus shown underwent refinement throughout the whole project. Initially, an HPLC pump was not used to deliver the ethanol. Instead, the flask was filled with enough ethanol to submerge the incoming argon tubing, and the flask heated in the same manner. This required measurement of the mass of ethanol in the flask before and after a catalyst run to determine how much had been removed. This was obviously not ideal as a second weighing step introduces further possibility of errors. In addition problems were encountered getting the ethanol to vaporise, due to the high temperatures required to heat the significant amount of ethanol in the flask (approximately 200 ml). The introduction of ball bearings to provide an additional hot surface on which ethanol can vaporise was accompanied by the switch to the HPLC pump. Slow addition of ethanol at a constant and known rate to the hot flask provided much quicker vaporisation, but more importantly meant ethanol was passed over the catalyst at a constant rate. With the previous method, it was much more sporadic, which could by chance affect the gas chromatography analysis if a sample was taken during a period of low or high ethanol flow, and could lead to an inaccurate picture of catalyst activity and poor carbon balances. The ethanol feed flask was weighed at the end of the run to determine if any residual ethanol remained.

Problems were also encountered with ethanol condensing in the tubing that exits the feed flask and leads to the reactor, despite the majority of this tube being electronically heated.

This was solved by surrounding the area immediately above the ethanol flask with thick copper piping, through which water at 90 °C was passed.

To preserve reproducibility and integrity of results, a standard procedure was followed for each catalyst test.

1) Weigh 1 g of catalyst, and measure the volume to calculate the LHSV. Carefully add the quartz U-tube to the furnace, taking care to position the thermocouples in the correct place. The argon is set to the desired flow rate (25 or 12 ml min^{-1}) and directed through the reactor to purge the piping and U-tube of air.
2) Turn on water heater (90 °C), which pumps hot water through copper pipe, to heat the piping immediately above the ethanol flask, and the trace heater (120 °C) to heat the rest of the stainless steel pipe work.
3) Turn on the catalyst reactor furnace, and raise it to the required temperature.
4) Turn on the ethanol flask heater, and wait 10 minutes for it to achieve the desired temperature (80 °C).
5) The cooling system is then turned on, and Bubbler 1 immersed in ice.
6) The HPLC pump is switched on, and Ethanol added to the feed flask at the desired rate (0.1 or 0.05ml min^{-1}). This is time t=0
7) The apparatus is monitored for the entire run in case of abnormalities.
8) 2 minutes before the end of the run, a sample of the exhaust gas is taken for analysis by gas chromatography
9) At the desired end point, all heating elements are turned off and the argon and cooling system remain on. It is left in this state for 5 minutes.
10) The valves are then adjusted to bypass the reactor, and this is left for 10 minutes, to purge any remaining Ethanol.
11) All apparatus is switched off, and the trace heating unplugged.
12) The mass of acetone in Bubbler 1 and 2 is determined, and a sample taken for NMR analysis.
13) The final mass of the Ethanol feed flask is determined.

The Liquid Hourly Space Velocity {LHSV (h^{-1})} is defined as the volume of feed flowing per unit volume of catalyst per hour. A value of 1.5 h^{-1} was targeted, in line with the literature.

Exhaust gas samples were collected at the end of a given test, as well as at certain specific intervals during the test, dependant on length. For 1 hour catalyst tests, only a single sample is taken at the end. The majority of catalysts were tested over 3 hours, and samples analysed by gas chromatography at the 0.5, 1, 2, and 3 hour marks.

Gas chromatography (GC) is a common analytical method for determining the components of a mixture and their concentration. A gaseous sample is passed through a thin capillary tube called a column, which contains the stationary phase. This is a thin coating which interacts with the molecules in the sample, and it is the difference in the interaction of analytes with the stationary phase which leads to one being retained on the column for a longer time. This allows separation based on their retention times. Changing the chemistry of the stationary phase will give rise to different analyte-phase physical interactions, so one column may be able to separate components that another cannot. Using a column that is specific for the type of chemicals you wish to detect is therefore vital.

Generally columns are split in to two types – polar and non-polar. Non-polar columns are sufficient for detecting non-polar compounds, namely singly-bonded alkanes. The addition of other atoms other than carbon or hydrogen, such as oxygen, leads to polarity in the molecules and a polar column will separate these more efficiently. Retention times in a non-polar column are governed by molecule size as the interaction with the stationary phase is simply governed by Van der Waals forces, and is called a dispersive interaction. With a polar column, dipole interactions, acid/base chemistry and *pi-pi* interactions exist, and separation is determined by these as well as dispersive interaction. To detect polarisable compounds, name olefins, a highly polar column is required. In this research we were mainly detecting light C2-C4 olefins, and some light oxygenates (diethyl ether, acetaldehyde), thus a polar column was required. We utilised a Varian LowOx capillary column that is capable of accurately detecting C1-C10 oxygenates in a hydrocarbon stream.

The sample is passed through the column via a carrier gas, which can be argon, nitrogen, hydrogen, or a number of others. In this case we used helium, simply as a safety precaution. The flow rate of the carrier gas can have a profound effect on the results obtained. A high flow rate will in effect 'push' the sample through the column at a faster rate, which leads to quicker experiment times, but less separation between peaks. As such a compromise must be reached between experiment time and the required level of peak separation. The most important parameter in a GC analysis however is the temperature program employed. The columns are suspended in an oven, and the temperature imposed upon the column has a great effect on the adsorption of molecules on the stationary phase. The higher the temperature, the higher the rate at which the sample passes through the column. Again, a compromise must be reached between analysis time and peak separation. Though analysis is sometimes carried out under isothermal conditions, much more common is to ramp the temperature up at constant rate, or in steps. This can allow the analysis to be sped up in areas where good dissolution between peaks is unimportant. The LowOx column used is particularly insensitive to carrier gas flow rate, and elution time depends almost entirely on the temperature required in order to 'unstick' components from the stationary phase. The temperature profile used was 50 °C for 5 minutes, followed by ramping at 10 °C min^{-1} up to 180°C, where it is held for a further 7 minutes, giving a total analysis time of 25 minutes. This allows us good resolution of the early peaks which we are most interested in (ethylene, butenes, 1,3-BD), as well as the oxygenates which will come off at much higher temperature and therefore much later in the analysis, as they interact more strongly with the column.

Introduction of the sample in to the column can be via automated methods, however in this case the sample was collected using a gas-tight syringe and manually injected. A split injection method was utilised, where only a portion of the sample is passed into the column, and the remainder exhausted through a split vent. The split ratio was approximately 10:1. Dilution of the sample in this manner is required to keep peaks on the scale when the concentration of analytes in the sample is fairly high.

Once the sample has been separated by the column it must of course be detected in some way. There are a number of different detection methods that can distinguish components

however the most common, and what was utilised for this research, is a flame ionisation detector (FID). An FID is able to detect a wide range of components, and is primarily most sensitive to hydrocarbons, and other flammable species. It works by way of a compressed hydrogen-air flame, which burns the gaseous eluent at such a temperature that a complex ionisation process occurs which produces positively charged ions and electrons, creating a current between two electrodes on the detector. The advantages of FID are its high sensitivity for most hydrocarbons, and the fact that detection of the ions is mass- rather than concentration-sensitive. This means that a change in the flow rate of the carrier gas has no effect on results other than changing the retention time. The disadvantages of FID are that the sample is completely destroyed, and it is insensitive to water and carbon dioxide, which are possible products of the reaction performed. The flame jet is usually heated above the maximum operating temperature of the analysis to ensure there is no condensation of components. In this case the temperature was set at 250 °C.

The results of a GC are most commonly presented as a graph showing retention time (x-axis) against detector response (y-axis). Quantitative results can be obtained by measurement of the area beneath a peak. However, firstly a calibration must be performed, using a gas blend of a known concentration, in order to determine the response factor (*rf*) for each particular component. A calibration blend was purchased from BOC containing the components we wished to detect. The composition of the gas by volume was 1,3-BD 1.00 %, ethylene 1.00 %, 1-butene 0.50 %, diethyl ether 0.25 %, acetaldehyde 0.25 %, with N_2 making up the remainder. This was ran 3 times and an average peak area was used to calculate the *rf* using the formula,

$$rf = \frac{Average\ peak\ area}{Certified\ concenctration\ in\ calibration\ blend}$$

When analysing an unknown sample, we can then determine the contribution of each component (by volume) by dividing the peak area by the *rf*. The *rf* values and approximate retention times are given below (**Table 2.1.1**), as is an example of a calibration chromatograph with the relevant peaks assigned as appropriate (**Figure 2.1.1**).Of note is the characteristic broad peak for 1,3-BD. Retention times have been seen to vary from time to time, most likely due to water adsorbing on to the stationary phase, however the spacing

and shape of the peaks still allowed easy resolution of the chromatographs. The retention times of diethyl ether and acetaldehyde were confirmed by injection of authenticated samples.

Component	Approximate Retention Time (min)	Average Peak Area	Composition of Calibrant Blend (vol%)	Response Factor, *rf*
Ethylene	2.2	110	1.00	110
1-Butene	3.8	112	0.50	224
1,3-Butadiene	7.3	230	1.00	230
Diethyl Ether	18.8	48	0.25	195
Acetaldehyde	19.5	15	0.25	63

Table 2.1.1: Retention times and response factors (*rf*) for the detected products

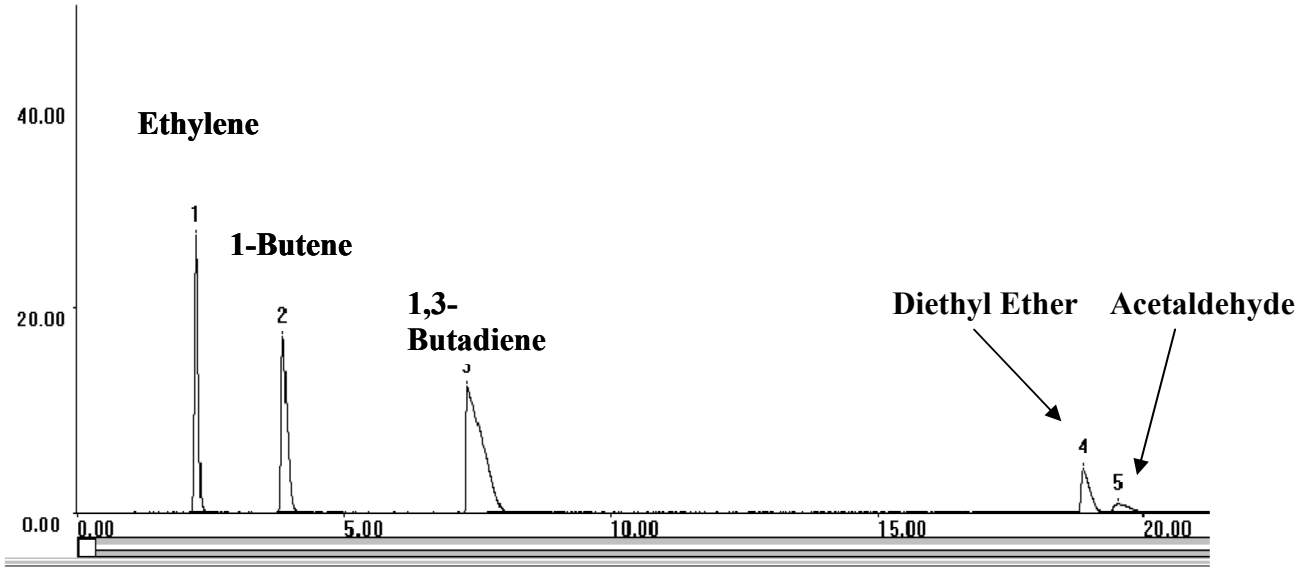

Figure 2.1.1: Peak positions as they appear for the calibration blend

As evidenced by the chromatograph shown, the peaks for the two oxygenates are much broader, less intense, and spaced quite closely together. This problem arises due to the FID detection technique which is not as sensitive for oxygenates.

This was overcome by the use of ^{1}H NMR to give a much more reliable indication of the amounts of these products we are making. During catalytic experiments, the exhaust gas

was bubbled through two vessels arranged in a series which were filled with chilled acetone, before being directed to vent. Acetaldehyde, ether, and 1,3-BD are readily soluble in acetone. At the end of each run, the mass of liquid in each of the bubblers was measured, and a ^{1}H NMR performed in $CDCl_3$. As well as providing information on the masses of products produced over the entire run, the bubblers will also contain any ethanol which has passed through the rig and not reacted. This information was used to determine a carbon balance for each run. A typical NMR is shown below (**Figure 2.1.2**).

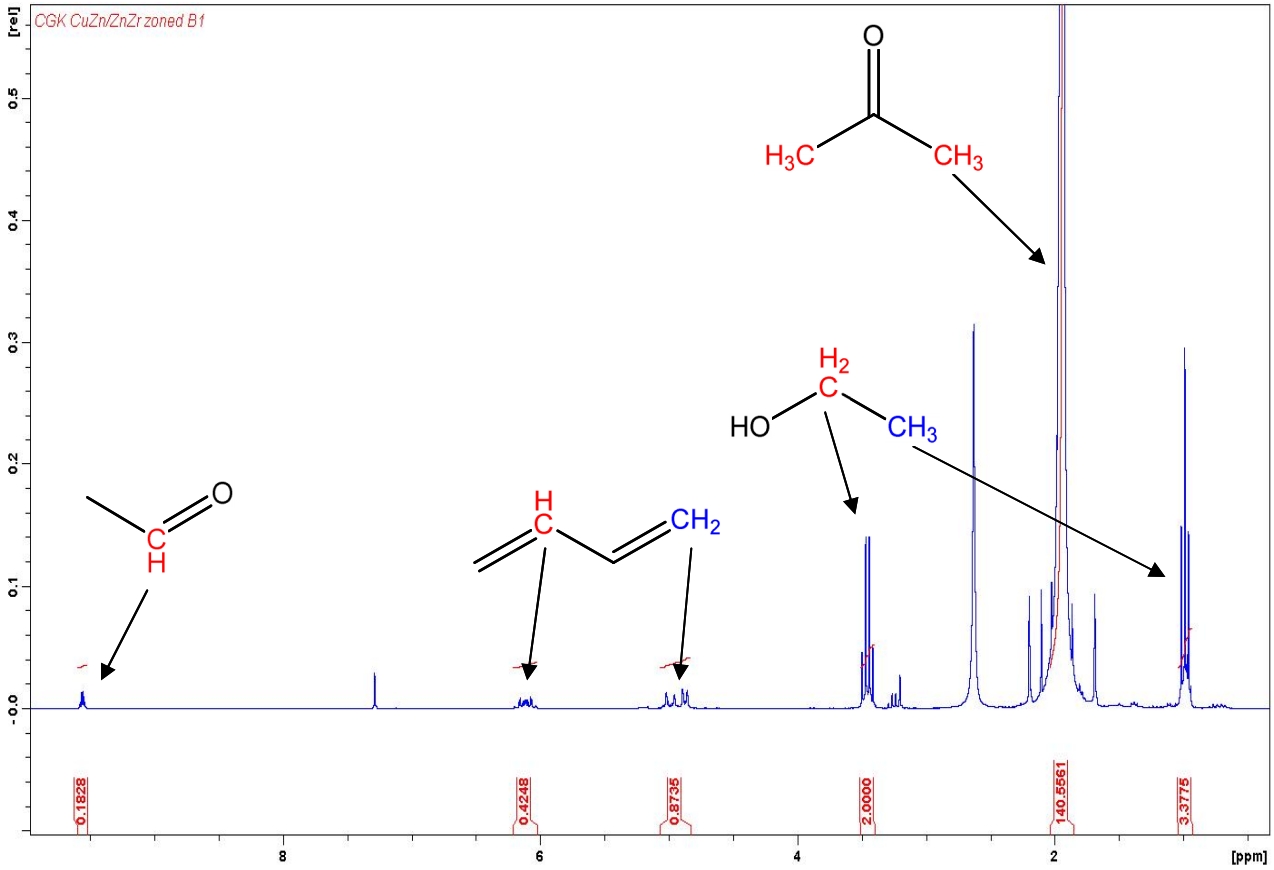

Figure 2.1.2: A typical NMR of the bubbler contents, with the relevant peaks indicated

To determine the content of the flask, we integrate the peaks relative to the Ethanol methylene which is found at 3.5 ppm, and calibrated to 2 as this is the number of protons it represents. Integration of the other peaks reveal the number of hydrogen atoms present in each specific environment, and from this the molar composition of the liquid contained in the bubbler can be established. The mass of liquid contained within the flasks is recorded, enabling calculation of the composition by mass. Ethanol also exhibits a peak at ≈ 1.0 ppm for the methyl group. Diethyl ether is a likely product of the dehydration of ethanol, and the

signal for the 2 equivalent methyl groups also occurs around 1 ppm, and will be obscured by the Ethanol methyl. If the integral is larger than 3, the excess is attributed to diethyl ether in the mixture. The largest peak present is for the 2 methyl groups of the acetone, which makes up the majority of the solution. 1,3-BD exhibits 3 peaks in the ^{1}H NMR spectrum. The *trans* and *cis* terminal methylene groups occur at 4.8 and 5.0 ppm respectively, whilst the CH exhibits a multiplet at 6.2 ppm. Acetaldehyde shows a peak around 2.2 ppm for the methyl group, however it is sometimes in danger of being obscured by the strong acetone signal. The CH signal at 9.7 ppm is therefore utilised as there are no other surrounding peaks.

The data abstracted from the GC and NMR spectra produced by each catalyst test was processed in order to determine selectivity and conversion values. For a 1 hour catalyst test, a single GC at the end of the run is taken, and the assumption must be made that activity remains constant throughout the entire run. Use of the HPLC pump to feed ethanol into the flask at a set rate means we know exactly how much has been used over a given time. If we subtract the mass of residual ethanol found in the flask from then we have a value for the mass of ethanol that has passed over the catalyst. This value was converted to moles, and then the volume of gaseous ethanol approximated using the ideal gas equation. Argon flow is also electronically regulated, so again the volume of Ar into the system over a given time is easily calculable. Addition of these two values yields the total volume of gas that has been passed over the catalyst. If we assume constant catalytic activity over the hour then the volume of product produced is simply the percentage composition as determined by the GC times the total volume of gas. From this the number of moles and mass of product can be calculated. Selectivity measurements are based solely on the 5 species we are detecting (ethylene, 1,3-BD, 1-butene, acetaldehyde, diethyl ether) using the following,

$$Selectivity\ of\ X\ (\%) = \frac{Moles\ of\ X}{Total\ moles\ of\ all\ products} \times 100$$

Conversion values are calculated based on the following,

$$Conversion\ (\%) = \frac{Mass\ of\ Carbon\ in\ GC}{Mass\ of\ carbon\ in\ to\ system} \times 100$$

The mass of carbon put in to the system using a pure ethanol feed is simply the carbon in the ethanol that has passed over the catalyst. At times, acetaldehyde was used as a co-feed, and in such cases the ethanol:acetaldehyde feed ratio was used to determine an average carbon content of the feed. The mass of carbon from the GC is the mass of carbon in the 5 products we are detecting. As there are a vast number of peaks in the GC which are unassigned due to their low intensity and poor resolution, conversion values given will be artificially lower than actual.

A carbon balance for each test is determined by also taking into account the mass of ethanol found in the 2 bubblers, as determined by ^{1}H NMR spectroscopy. Carbon balances were in excess of 80 % with a few notable exceptions.

$$C\ balance\ (\%) = \frac{Mass\ of\ carbon\ in\ GC + Mass\ of\ carbon\ in\ recovered\ EtOH}{Mass\ of\ carbon\ in\ to\ system} \times 100$$

For runs lasting in excess of an hour, an average of the exhaust gas composition was determined utilising the data from all of the available chromatographs. The individual chromatographs were used to follow activity of the catalyst over time. An example spreadsheet detailing how the data was worked up is included in the appendix.

Initial focus was on microporous aluminophosphate materials (ALPOs). Much work has been focused on the incorporation of other metals in to the aluminophosphate framework to enhance their reactivity.[1, 2] Metals with a similar ionic radius and coordination requirements can be isomorphously substituted in to the structure at both aluminium and phosphorous sites. Metal-substituted ALPO materials have been investigated as catalysts for a large number of reactions. Incorporation of metals such as iron, cobalt and manganese has yielded materials that are impressively active in alkylation reactions,[3] the oxidation of *p*-cresol to *p*-hydroxylbenzaldehyde,[4] and the dehydrogenation of ethane to ethene,[5] amongst others. **Ti-ALPO-5**, **Fe-ALPO-5**, **Mn-ALPO-5**, and **Ti-ALPO-11** were synthesised and characterised by pXRD. Catalytic performance for the conversion of ethanol to 1,3-BD was extremely poor due to the inherent Brönsted acidity of the materials, resulting in ethylene

being the only product observed by GC. Focus was then shifted to metal-exchanged sepiolite materials, which have been used successfully in the literature.[6, 7]

2.2 Metal-Exchanged Sepiolites for 1,3-Butadiene Production: Synthesis, Characterisation and Catalytic Activity

Sepiolite and metal-exchanged sepiolite materials have previously been investigated by others as potential heterogeneous catalysts for the conversion of ethanol to 1,3-BD.[6, 8] Most of the literature available concerns sepiolite in which Mn(II) ions have been impregnated. Synthesis of such a material has been carried out, as well as the production of Zn(II) and Cu(II) exchanged sepiolites. The materials were prepared by stirring sepiolite purchased from Aldrich at room temperature with an aqueous solution of $Mn(CH_3CO_2)_2$, $Zn(CH_3CO_2)_2.2H_2O$, and $Cu(CH_3CO_2)_2.H_2O$ to produce **Mn-Sep**, **Zn-Sep**, and **Cu-Sep** respectively. The reactions were carried out in an approximately 1:4 molar ratio of metal salt to sepiolite. As the exact degree of hydration of the mineral is not known, the molar mass of sepiolite was approximated to be 300 g mol^{-1} by taking in to account the mass lost upon heating, which can be attributed to water. In each case, after stirring for approximately 24 hours, material was filtered, washed with copious volumes of water, and dried at 80 °C. The single-exchanged material was then ground up to a fine powder, and placed in a fresh solution of the required metal salt. This process was then repeated a further two times. Performing three exchanges ensures that as many ions are exchanged as possible, for maximum metal loading. After the third exchange, the materials were then calcined at 450 °C for 3 hours, as stated in the literature, to give **Mn-SepC**, **Zn-SepC**, and **Cu-SepC**.[6]

The materials were characterised by powder X-ray diffraction (pXRD), energy dispersive X-ray (EDS) and ^{29}Si solid-state NMR spectroscopic methods, and scanning electron microscopy (SEM) was also utilised to gain further insight in to the structures. As-purchased sepiolite was also characterised for comparison. The pXRD patterns of sepiolite, **Mn-Sep**, **Zn-Sep**, and **Cu-Sep** are shown in **Figure 2.2.1**. All of the diffraction patterns are identical,

showing that there has been no alteration to the microporous sepiolite structure upon addition of the various metals.

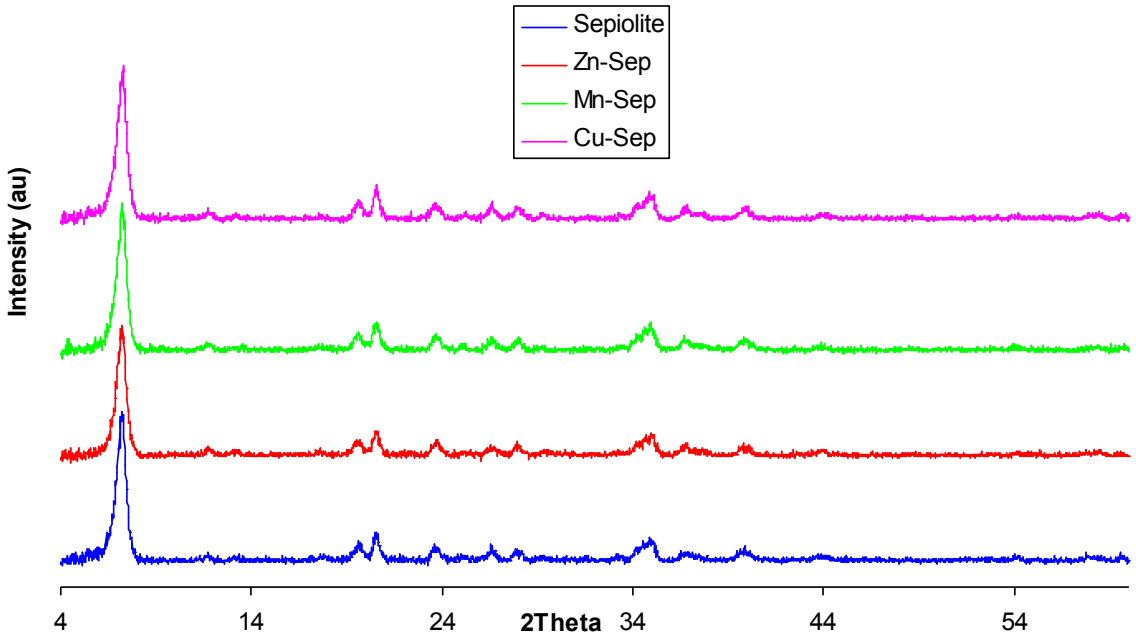

Figure 2.2.1 : Powder diffraction patterns of uncalcined sepiolite based catalysts

The powder diffraction patterns of the calcined materials **Zn-SepC**, **Cu-SepC** and **Mn-SepC** were all very similar in that they did not retain the structure of the uncalcined material. Using the diffraction pattern of **Mn-SepC** as an example (**Figure 2.2.2**), after calcination there exists a great degree of disorder in the sample, and it can be assumed that the structure breaks-down under the calcination conditions utilised.

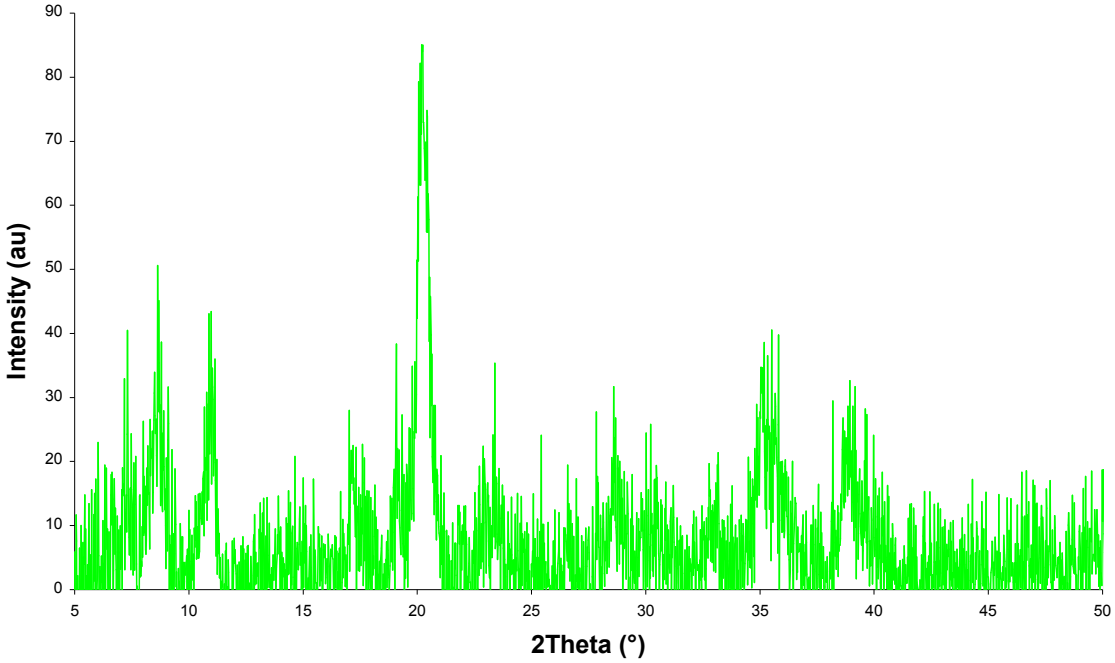

Figure 2.2.2 : pXRD of **Mn-SepC**

Calcination conditions were identical to those given in the literature,[6] however no pXRD was presented in this case.

All of the uncalcined materials, as well as **Zn-SepC** and **Mn-SepC**, were analysed using the JEOL JSM6310 Scanning Electron Microscope at University's Centre for Electron Optical Studies. Energy dispersive X-ray spectrometry (EDS) was also performed on the samples. This attachment is capable of elemental analysis of the sample, as it relies on the measurement of X-rays emitted by the material in response to stimulation by electromagnetic radiation. Each element has a unique electronic atomic structure, so can be identified by the characteristic X-rays that are emitted. The energy of the incident electron beam in this study was 20 keV. **Figure 2.2.3** shows some of the images captured by the electron microscope of the uncalcined **Cu-Sep** at various magnifications. The micrographs reveal a very fibrous material as expected, however further analysis of the catalyst surface was not possible due to the inability to produce clear pictures at higher magnification.

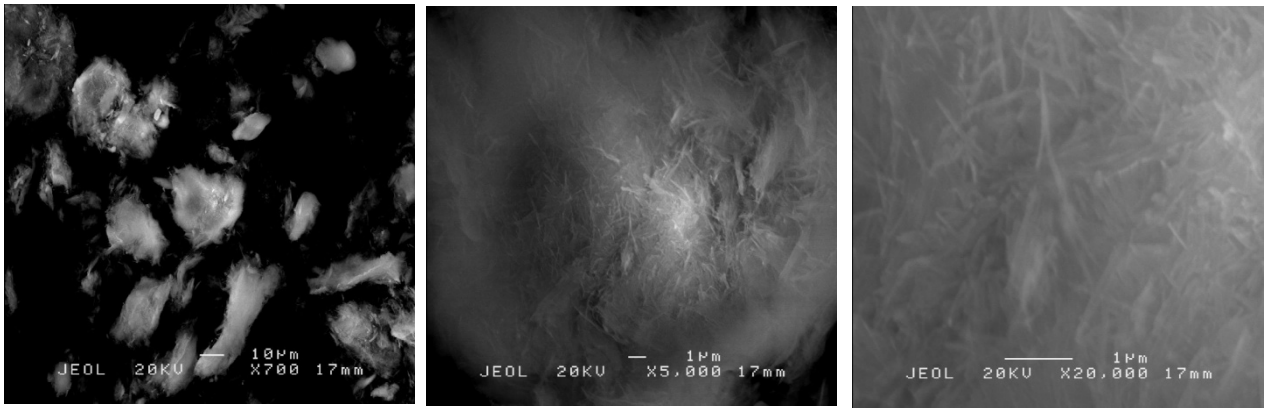

Figure 2.2.3 – SEM micrographs of **Cu-Sep** at various magnifications.

The EDS spectrum of **Mn-Sep** is shown in **Figure 2.2.4**. The chemical analysis shows that we have the three elements we would expect; manganese, magnesium, and silicon. The silicon peak dominates the spectrum and is not shown in its entirety. This single spectrum cannot be used for quantitative analysis due to the fact that peak sizes will change with the voltage (a high energy incident beam will increase the size of high-energy emissions). Absorbance of low energy X-rays by material other than the detector means that the early elements cannot be detected, hence there is no peak for oxygen in the spectrum. There are however peaks for some elements we were not expecting, such as aluminium, potassium, calcium and sulphur. EDS can usually detect elements in concentrations of 0.1 wt%, so these impurities in the sepiolite are most probably very minor.

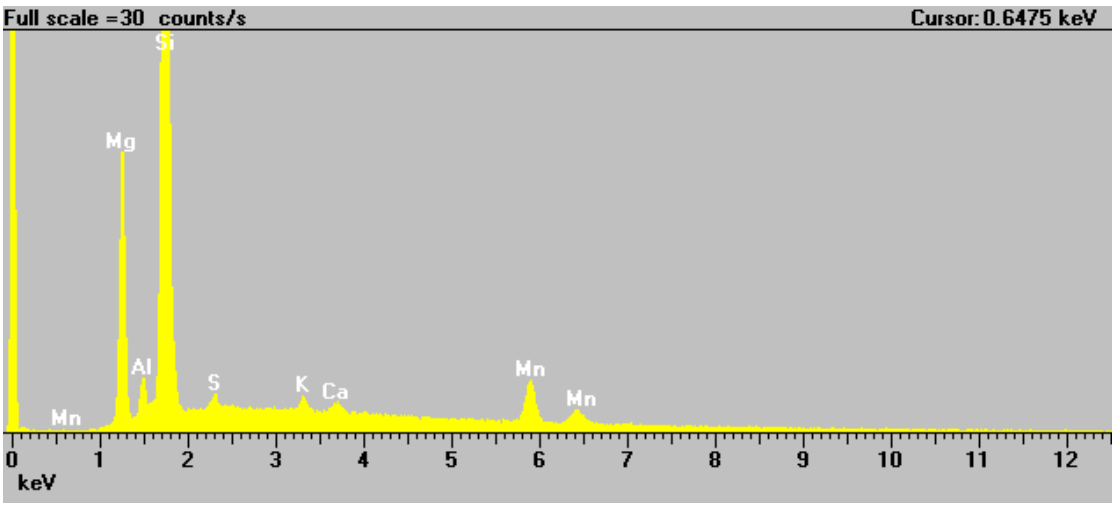

Figure 2.2.4: EDS spectrum of **Mn-Sep**

The EDS spectrum of **Mn-SepC** (**Figure 2.2.5**) shows it consists of the same elements, however some of the peaks for Mn, particularly that at approximately 5.9 keV, are larger in relation to the Mg and Si peaks than in the uncalcined material. However as the peaks are not strictly quantitative this cannot be rationalised.

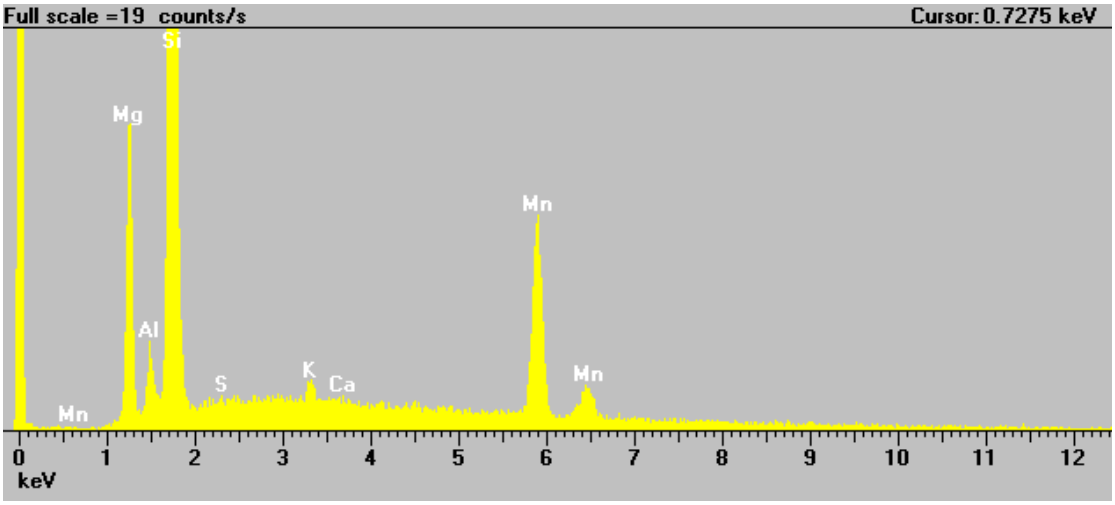

Figure 2.2.5: EDS spectrum of **Mn-SepC**

The EDS spectrum for **Zn-Sep** contains multiple peaks for zinc (**Figure 2.2.6**). Impurities are again seen with multiple peaks for iron, and also aluminium and potassium.

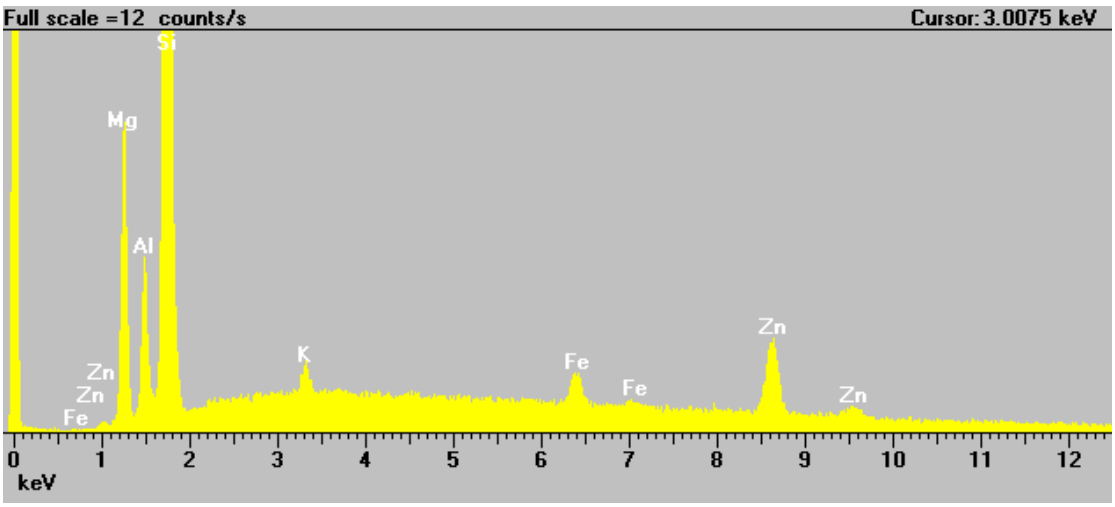

Figure 2.2.6: EDS spectrum of **Zn-Sep**

As with the **Mn-SepC**, one of the high-energy peaks for the added metal in the spectrum of **Zn-SepC** (**Figure 2.2.7**) is much larger than in the uncalcined sepiolite. The same impurities as in the uncalcined variant were detected, indicating the material has the same composition.

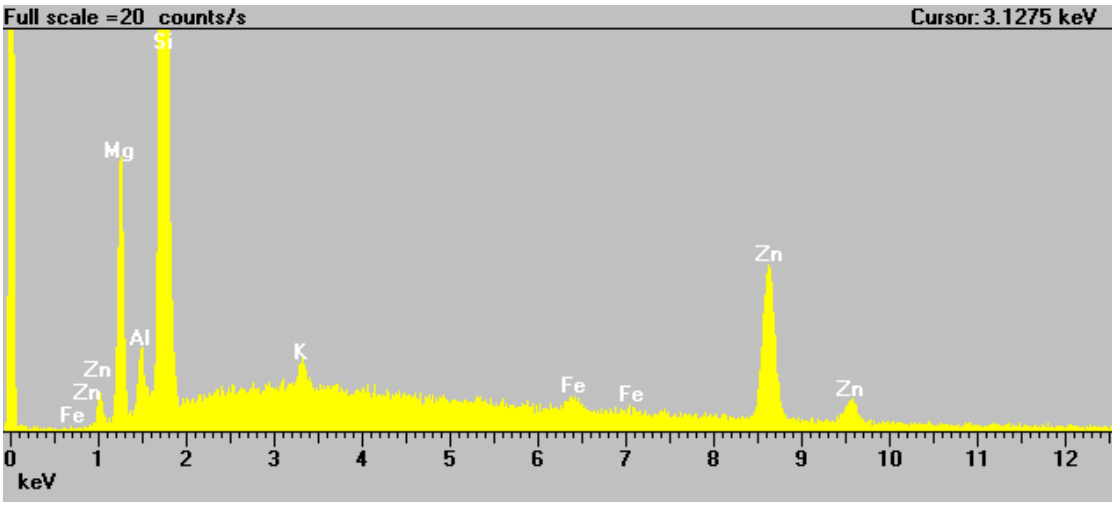

Figure 2.2.7: EDS spectrum of **Zn-SepC**

Finally, the spectrum of **Cu-Sep** (**Figure 2.2.8**) shows various peaks corresponding to copper being present, though they are all fairly weak. The fact that all the peaks, both high and low energy, are small, may mean that integration of the metal is not as efficient for Mn and Zn analogues.

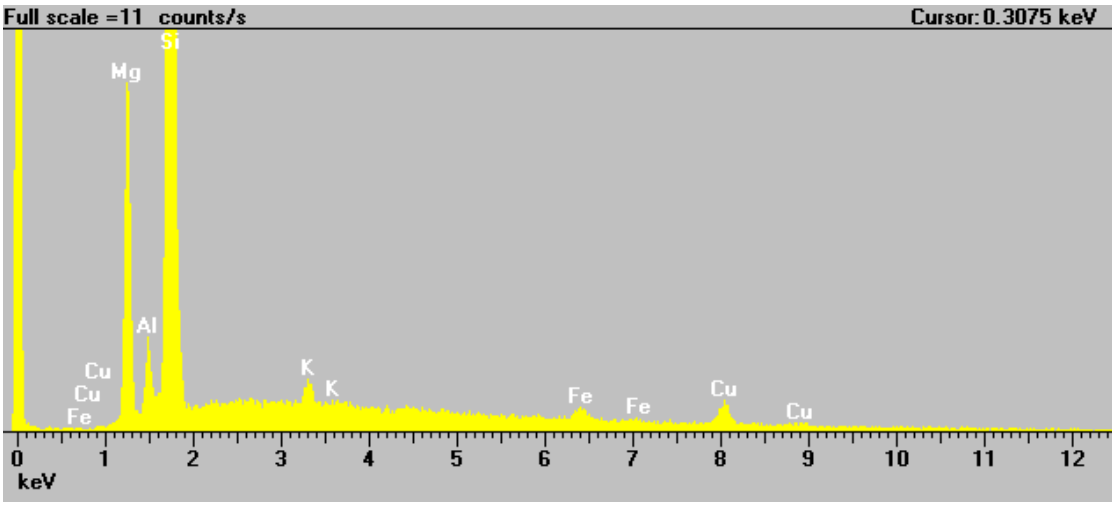

Figure 2.2.8: EDS spectrum for **Cu-Sep**

A number of the sepiolite based materials were also analysed by solid-state ^{29}Si NMR spectroscopy. Direct-polarisation (DP) as well as cross-polarisation (CP) methods were utilised. Direct-polarisation spectra are quantitative; however for nuclei with low gyromagnetic ratios such as silicon the spectra take a long time to acquire, as a considerable amount of time must be left between each scan to allow the nuclei to relax. CP-NMR works by transfer of polarisation from ^{1}H atoms which have a high gyromagnetic ratio.

Figure 2.2.9 shows the ^{29}Si CP-NMR spectra of sepiolite, **Mn-Sep** and **Mn-SepC**. The sepiolite NMR contains three sharp main resonances at -92, -95 and -98 ppm respectively for three chemically distinct silicate environments which is in accordance with that quoted in the literature.[9] The **Mn-Sep** spectra are qualitatively the same as the pure sepiolite spectra. Upon calcination the lines are significantly broadened, which in solid-state NMR implies a degree of disorder, in agreement with the pXRD of the calcined materials.

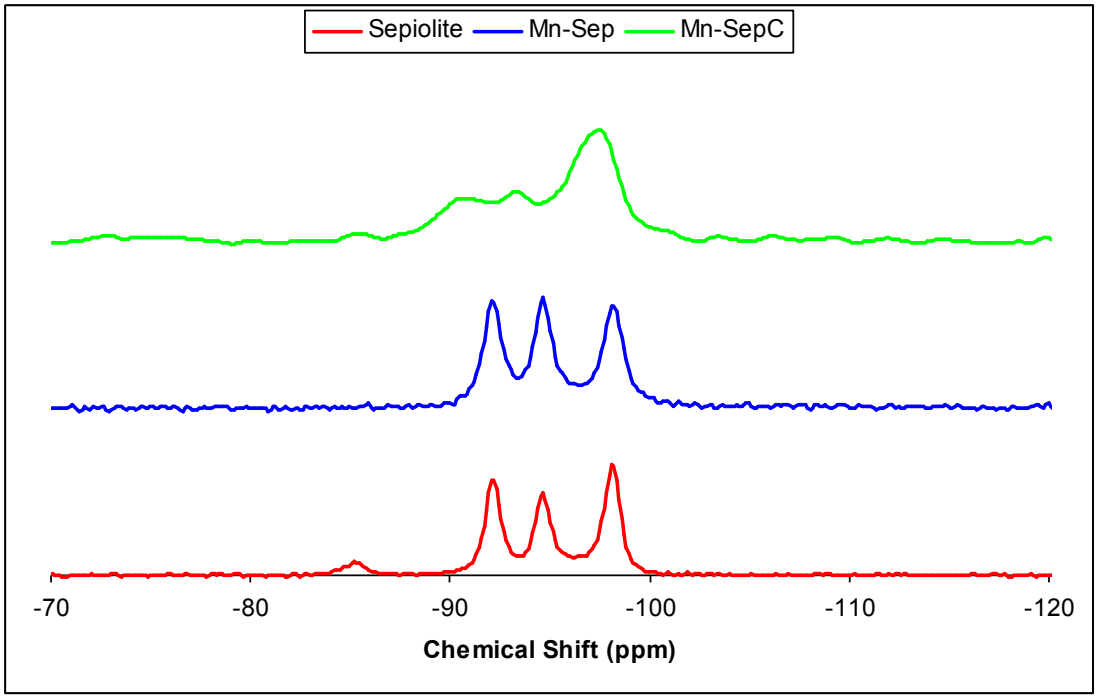

Figure 2.2.9: Comparison of the ^{29}Si NMR spectra for sepiolite, **Mn-Sep**, and **Mn-SepC**

Cu-SepC, **Mn-SepC**, and **Zn-SepC** were tested at 375 °C, with an ethanol feed rate of 0.1 ml min^{-1}, and an Ar flow rate of 25 ml min^{-1}.

Catalyst	LHSV (h^{-1})	Reactor Temp. (°C)	Time (min)	Conv. (%)	Selectivity (%)				
					1,3-BD	Ethylene	Acetaldehyde	Ether	1-Butene
Mn-SepC	1.61	375	60	28.71	5.78	55.31	11.68	26.29	0.92
Zn-SepC	2.79	375	180	22.47	7.64	44.79	26.04	24.80	0.69
Cu-SepC	1.61	375	60	28.88	9.98	12.09	53.05	20.83	0.41

Table 2.2.1: Catalyst test results for metal exchanged sepiolites

1,3-BD yields for all were poor, and ethylene was the major product for **Mn-SepC** and **Zn-SepC**. **Cu-SepC** gave considerably more acetaldehyde from the ethanol as would be expected, as copper is a well known alcohol dehydrogenation catalyst.[10, 11] Conversion values were fairly consistent for all catalysts.

The structural degradation of sepiolite upon heating is the major factor that limits its use as a support. Naturally occurring sepiolite contains water in 4 different environments. Water molecules may be adsorbed on the surface, as zeolitic water found in the channels, structurally present as hydroxl groups, and finally water molecules may be bound to magnesium ions on the edge of the channel walls.[12] The MgO moieties that make up the walls of the zeolitic channels are bound to 2 water molecules as well as 4 oxygen atoms. Most of the zeolitic water is removed by 120 °C, and removal of the first bound water occurs at temperatures in excess of 300 °C.[13] This causes Mg to adopt a distorted octahedral environment, by instead coordinating to an exposed oxygen atom within the channel. When the remaining water molecule is removed at 450 °C, further structural change is observed, causing the sepiolite channels to irreversibly fold over themselves.[7] The thermal stability of sepiolite has been shown to be improved by replacing Si and Mg sites with Al.[8] "Alumination" of sepiolite was not performed in this case to avoid the introduction of unwanted acidity to the catalysts which will promote ethylene production from ethanol. The ion exchange of Mg^{2+} ions in the structure with other divalent cations, including those of Mn, Zn, and Cu, has also been shown to increase the thermal stability of sepiolite.[14] Samples were heated to 700 °C, and powder diffraction patterns showed no discernible bending of the channels. For comparision, untreated sepiolite samples showed signs of structure bend after 2 hours at 400 °C. The difference in preparation method between that described in the

patent and that used to prepare the sepiolite catalysts tested herein is the pretreatment of sepiolite with a dilute solution of nitric or hydrochloric acid.[14] It is therefore assumed this process facilitates ion exchange by elution of the Mg ions into acid solution, creating a vacancy which can be filled by the incoming metal cation. As a result, poor integration of the metal into the structure is likely the cause of the poor thermal stability and catalytic activity of the sepiolite catalysts compared to those in the literature. Though EDS confirms the presence of the desired metals in the materials, it does not reveal information on the distribution or metal loading, nor can we discount the possibility the metals are simply adhered to the sepiolite surface. Based on these results it was decided to investigate alternative support materials.

2.3 Bimetallic Catalysts on a Silica Support

A catalyst containing cadmium and zirconium supported on silica has been shown to be active for the desired reaction by Quattlebaum *et al*.[15] A similar catalyst was synthesised where Cd was replaced with Zn, a fellow Group 12 metal, in order to eliminate potential toxicity. **ZnZrSi-60A** was prepared by stirring of Davisil grade 635 (60 Å pore diameter) silica gel into an aqueous solution of $Zn(NO_3)_2.6H_2O$ and $ZrO(NO_3)_2.xH_2O$. Metal loadings were 0.5 wt% and 1.5 wt% respectively. The material was left to stir at room temperature until the majority of water had evaporated, and then thoroughly dried and calcined 500 °C for a period of 5 hours. A sample was also analysed by inductively coupled plasma - optical emission spectrometry (ICP-EOS), which is used determine the concentration of metals in a sample, down to extremely low levels (~0.2-100 ppb).[16] It relies upon the use of a plasma to excite the constitutent ions or atoms so that they emit electromagnetic radiation at a wavelength characteristic to each particular element. The intensity of the emission corresponds to the concentration of that particular element in the sample. Metal loadings in **ZnZrSi-60A** found to be 0.30 wt% Zn and 1.82 wt% Zr. This is sufficiently close to the desired loading, as we cannot ensure completely even distribution. The pore diameter of the SiO_2 was also confirmed by N_2 adsorption experiments. A number of other bimetallic catalysts were prepared on 60 Å pore diameter SiO_2 using a similar synthetic procedure. The metals

were chosen due to their presence in other catalysts reported in the literature. The metal salts utilised were $Cu(CH_3CO_2)_2.H_2O$, $Co(NO_3)_3.6H_2O$, $Mn(CH_3CO_2)_2.4H_2O$, $Zn(NO_3)_2.6H_2O$, $Ce(NO_3)_3.6H_2O$ $ZrO(NO_3)6H_2O$, and HfO_2. Metal loadings were targeted at 1.0 wt%, and the catalysts were all calcined at 500 °C. The bimetallic catalysts were tested for 1 hour at a reactor temperature of 375 °C. Ethanol and argon flow rates were set to 0.1 and 25 ml min^{-1} respectively.

Catalyst	Conv. (%)	Selectivity (%)				
		1,3-BD	Ethylene	Acetaldehyde	Ether	1-Butene
ZnZrSi-60A	45.97	38.94	41.09	10.34	6.67	2.95
TiZnSi-60	5.51	0.82	61.00	21.88	16.06	0.24
CoZnSi-60	16.54	6.49	29.76	47.40	16.13	0.22
CuZnSi-60	28.76	20.91	42.07	30.09	4.64	2.29
MnZrSi-60	10.58	29.16	46.10	9.07	15.54	0.13
CuMnSi-60	17.79	10.30	10.48	62.16	15.10	1.95
MnZnSi-60	16.98	18.74	28.19	35.65	16.58	0.83
CuCoSi-60	17.00	10.83	39.28	37.55	10.98	1.36
CoMnSi-60	12.93	22.90	46.88	19.26	9.63	1.33
CeZnSi-60	29.64	26.68	39.91	27.84	3.48	2.09

Table 2.3.1: Results for bimetallic catalysts on 60 Å silica support

Conversions vary considerably, with few reaching above 20%. As SiO_2 is a fairly acidic support, ethylene and diethyl ether selectivity was high for all runs. The catalysts containing copper and zinc produced considerable amounts of acetaldehyde. Copper supported on rice husk ash has been shown to highly active for ethanol dehydrogenation to acetaldehyde.[10] The cobalt containing catalysts all gave considerably poorer carbon balances, in the region of 30 %. Cobalt catalysts are well documented in the literature to be capable catalysts for the steam reformation of ethanol (**Figure 2.3.1**). [17, 18]

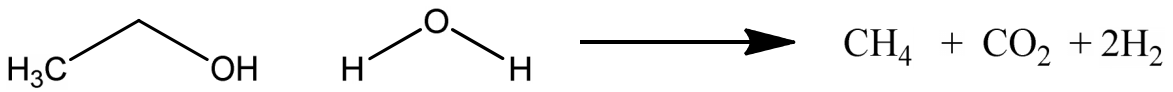

Figure 2.3.1: The steam reformation of ethanol

Steam reformation of ethanol requires water, which will be present in reasonable quantities within the catalyst tube. Residual moisture may be present in the pores of the SiO_2 support,

and the reaction mechanism itself contains several dehydration steps which will produce water. Carbon dioxide cannot be detected by the GC using an FID detector.

The standout catalyst in terms of both conversion and ethylene:1,3-BD product ratio is clearly **ZrZnSi-60A**. It is assumed that Zn is active for the dehydrogenation of ethanol, the silica support and/or a combination of the Lewis acidic metal centres could catalyse the subsequent aldol condensation of ethanol with acetaldehyde, and Zr catalyses the Meerwein-Ponndorf-Verley reaction.[19, 20] Dehydration of the alcohol to yield 1,3-BD is assumed to readily occur under the process conditions.

2.4 Optimisation of Zinc/Zirconium Catalysts

A batch of **ZnZrSi-60A** was calcined at a lower temperature (300 °C) to see if this affected activity. The lower calcination temperature showed some improvement in 1,3-BD selectivity. The 300 °C calcined **ZnZrSi-60A** was tested for 1 hour at varying reactor temperatures (**Table 2.4.1**).

Catalyst	Reactor Temp. (°C)	Conv. (%)	Selectivity (%)				
			1,3-BD	Ethylene	Acetaldehyde	Ether	1-Butene
ZnZrSi-60A	300	4.27	8.10	17.37	64.84	6.95	2.70
ZnZrSi-60A	350	27.53	43.97	29.03	19.56	7.28	1.56
ZnZrSi-60A	375	44.26	42.86	32.62	15.42	6.10	3.00
ZnZrSi-60A	400	49.64	45.84	30.71	13.81	5.98	3.65
ZnZrSi-60B	375	34.92	37.04	35.70	9.70	14.21	3.34
ZnZrSi-60C	375	30.35	43.78	39.02	6.78	6.45	3.96

Table 2.4.1: Catalytic activity of **ZnZrSi-60A**, **ZnZrSi-60B** and **ZnZrSi60-C**. All catalysts were calcined at 300 °C. All tests lasted 1 hour. EtOH and Ar flow was 0.1 and 25 ml min^{-1} respectively.

ZnZrSi-60A performed poorly at 300 °C. The conversion is extremely low, as is 1,3-BD selectivity (7.99 %), with the major product being acetaldehyde. As expected conversion

significantly increased with reactor temperature up to 375 °C after which the difference is minimal. Ethylene and 1,3-BD selectivities for the tests at 350 °C and above remained fairly consistent. The increased 1,3-BD selectivity appears to coincide with falling acetaldehyde selectivity. The results imply that temperatures in excess of 300 °C are needed to drive the condensation of acetaldehyde and the ensuing reaction steps to form 1,3-BD. 375 °C was chosen as the optimum temperature for subsequent runs. The difference in conversion and 1,3-BD selectivity at 375 and 400 °C is small, and as the potential applications of this work are 1,3-BD production on a large scale, a 25 °C reduction in operating temperature could considerably reduce production costs.

ZnZrSi-60B and **ZnZrSi-60C** were synthesised to investigate any possible effect the metal loading may have on the catalytic activity. The composition of **ZnZrSi-60B** was Zn 1.00 wt%, Zr 1.50 wt%, and **ZnZrSi-60C** Zn 1.00 wt%, Zr 3.00 wt%. Both were calcined at 300 °C and tested under the same conditions as before (**Table 2.4.1**). Results indicate that metal loading has no significant effect upon selectivity, but is seen to have a detrimental effect upon conversion values.

Focus then shifted to reducing selectivity towards ethylene. As the dehydration of ethanol to ethylene is a competing process, a resultant increase in 1,3-BD selectivity would be expected. Attempts were initially made to reduce the acidity of the SiO_2 by a number of methods. Ohnishi *et al* noted that washing of their MgO/SiO_2 catalysts with a dilute solution of NaOH increased 1,3-BD yield.[21] **ZnZrSi-60Na** was synthesised as per previous catalysts, using 0.1 M NaOH in place of water when making up the SiO_2 slurry. Evaporation and subsequent steps were identical as for the synthesis of **ZnZrSi-60A**. A catalyst was also prepared where 100 mg of $Ba(OH)_2$ was thoroughly stirred in to 10.0 g of **ZnZrSi-60A** before calcination, to give **ZnZrSi-60Ba**.

Further attempts to reduce acidity focused on varying the support material. SiO_2 with pore diameters of 40 and 60 Å respectively were purchased. **ZnZrSi-40** and **ZnZrSi-150** were synthesised by the same procedure as for the 60 Å equivalent, and calcined at 500 °C. ^{29}Si solid state NMR spectra of the 3 catalysts was performed, and the spectra deconvoluted to

determine the relative proportions of the spectroscopically different Si environments on the catalyst surface, or which there are 3 (**Figure 2.4.1**).

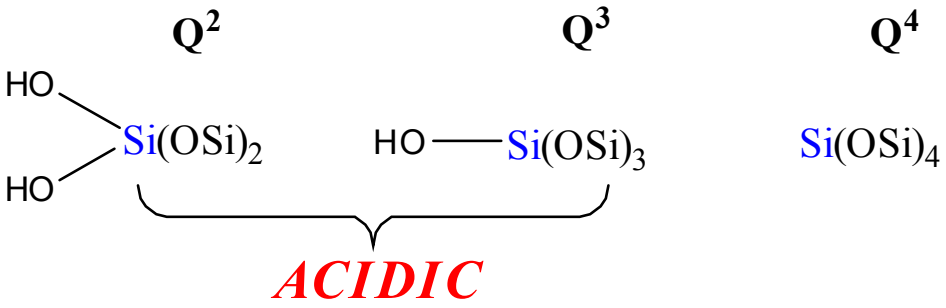

Figure 2.4.1: Representation of the 3 different silica surface environments.

The Q^2 and Q^3 environments both have Brönsted acidic OH groups, whereas the Q^4 has no such acidity. The ^{29}Si NMR spectroscopic data (**Table 2.4.2**) shows that the 150 Å catalyst exhibits a significantly lower proportion of the 2 acidic environments, and consequently a higher proportion of the Q^4 environment (75.7 % for 150 Å vs 69.9 % for 60 Å), resulting in a less acidic catalyst.

Silica Pore Size / Å	Composition of Catalyst / %		
	Q^2	Q3	Q^4
40	2.5	27.8	69.8
60	3.4	26.7	69.9
150	2.6	21.7	75.7

Table 2.4.2: Silica surface composition of Zn/Zr catalysts of varying silica pore diameter (Å)

Investigations into an alternative to SiO_2 were also made. **ZnZr-ZrO_2** was made, containing 0.5 wt% Zn and 1.5 wt% Zr respectively grafted on to ZrO_2.

The results as given in **Table 2.4.3** indicate that the pore diameter of the SiO_2 support has a considerable effect on catalytic activity. Conversions for the 40, 60, and 150 Å pore diameter catalysts remain similar, however a marked decrease in ethylene selectivity is observed, as well as a corresponding increase in selectivity for 1,3-BD, up to 47.9 % for **ZnZrSi-150**. This is assumed to arise from the decrease in Brönsted acidity as we increase the pore diameter. Other attempts to reduce the acidity of the catalyst, by basic pre-treatment or addition of a basic alkaline earth metal, resulted in a thoroughly poor performing catalyst, with extremely low selectivity for 1,3-BD, particularly in the case of **ZnZrSi-60Na**, where over 70 % of the reaction product was diethyl ether. This implies some degree of acidity is required to produce 1,3-BD. Use of ZrO_2 as a support also resulted in diminished activity, implying the SiO_2 is playing a vital role in the reaction.

Catalyst	Calc. Temp (°C)	Conv. (%)	Selectivity (%)				
			1,3-BD	Ethylene	Acetaldehyde	Ether	1-Butene
ZnZrSi-40	500	55.06	27.74	48.93	8.08	15.00	0.25
ZnZrSi-60A	500	45.97	38.94	41.09	10.34	6.67	2.95
ZnZrSi-150	500	48.37	47.91	25.78	9.34	13.96	3.01
ZnZrSi-60Ba	500	20.72	25.21	51.23	18.99	2.46	2.11
ZnZrSi-60Na	300	18.48	0.10	1.91	21.29	76.64	0.04
ZnZr-ZrO_2	500	16.91	13.77	29.16	51.51	5.35	0.21

Table 2.4.3: Results of attempts to reduce support acidity. All tests were for 1 hour, with a reactor temperature of 375 °C. EtOH and Ar flow was 0.1 and 25 ml min^{-1} respectively. LHSV for all silica catalysts was ~1.5 h^{-1}. For **ZnZr-ZrO_2** it was 8.4 h^{-1} due to the difference in density of the support.

2.5 Longevity Studies of Bimetallic Catalysts

The longevity of the most promising catalysts was tested by conducting runs for 3 hours. By taking a sample of exhaust gas at the ½, 1, 2, and 3 hour marks, a profile of catalyst activity over time can be determined. All catalyst showed a reduction in conversion compared to the 1 hour runs, and the significant results are tabulated below (**Table 2.5.1**).

Catalyst	Conv. (%)	Selectivity (%)				
		1,3-BD	Ethylene	Acetaldehyde	Ether	1-Butene
ZnZrSi-60A	34.82	28.81	47.24	7.98	13.06	2.09
ZnZrSi-150(1st)	20.69	39.11	27.06	14.88	16.24	2.71
ZnZrSi-150(2nd)	22.95	33.48	24.98	13.31	26.00	2.23
CuZrSi-60	20.72	25.21	51.23	18.99	2.46	2.11

Table 2.5.1: Longevity study of various bimetallic catalysts. All tests were for 3 hours, with a reactor temperature of 375 °C. EtOH and Ar flow was 0.1 and 25 ml min^{-1} respectively

ZnZrSi-60A exhibits lower overall 1,3-BD selectivity over 3 hours, and the cause of this can be seen from the gas composition over time profile (**Figure 2.5.1**). Selectivity for both 1,3-BD and ethylene peaks at 1 hour, however ethylene production remains fairly steady whilst selectivity for 1,3-BD is reduced significantly between 1 and 2 hours.

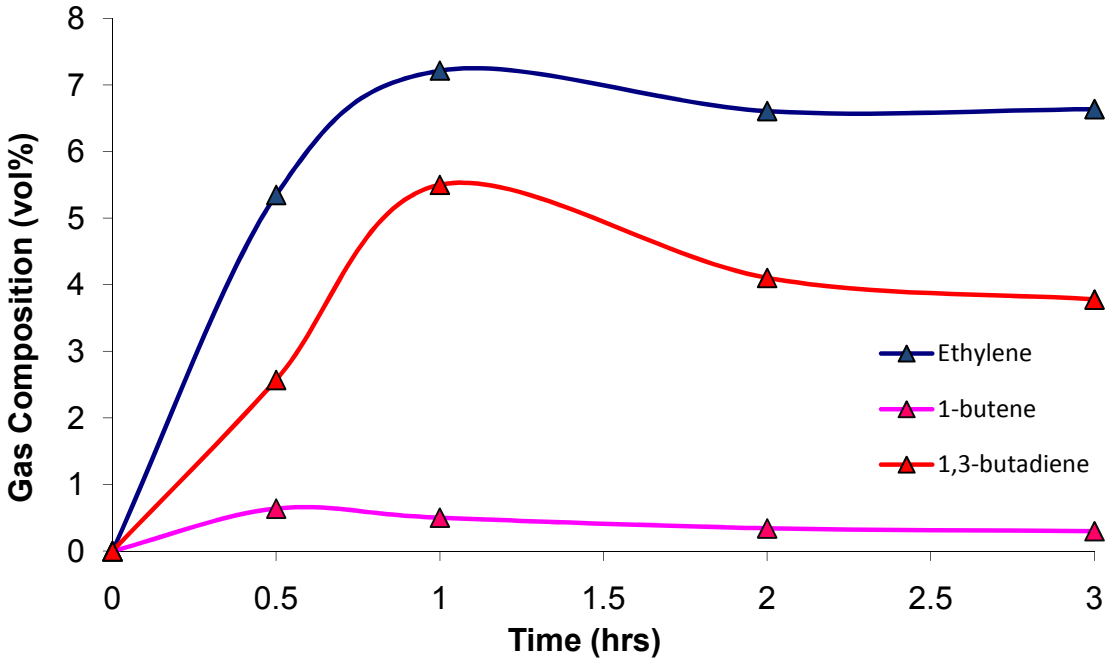

Figure 2.5.1: Gas composition over time for the 3 hour test of **ZnZrSi-60A**

As with the shorter runs, **ZnZrSi-150** exhibited increased selectivity for 1,3-BD compared to the 60 Å catalyst. The catalyst was initially ran for a period of 3 hrs {**ZnZrSi-150(1st)**} after which the rig was shut down as usual and the catalyst allowed to cool. This catalyst was then

reused later in the day to gauge the recyclability {**ZnZrSi-150(2nd)**}. Conversion remained consistent, and there is a small drop in the average 1,3-BD selectivity for the recycled catalyst. **Figure 2.5.2** shows the real-time GC data for both the fresh and recycled materials.

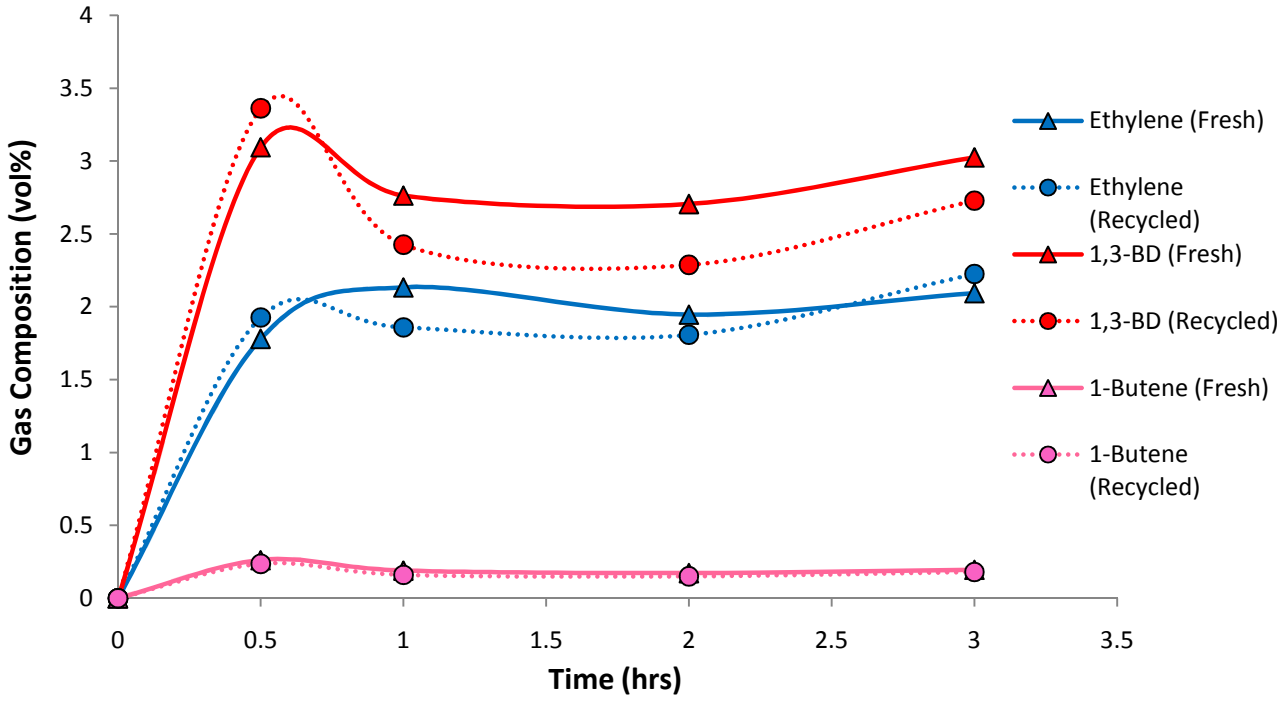

Figure 2.5.2: Real-time GC measurement of 1,3-BD, ethylene, and 1-butene for **ZnZrSi-150**, both fresh and recycled.

Little to no coking of the catalyst was observed, which remained an off-white colour once removed from the reactor. Thermogravimetric (TGA) analysis on approximately 10 mg of spent catalyst, taken in both air and nitrogen, showed an average a loss of ~4 wt%. The majority of weight loss occurs early in the analysis and fairly low temperature, and is believed to be due to the loss of adsorbed ethanol, acetaldehyde, or water.

CuZrSi-60 was prepared and consisted of 1.00 wt% of Cu and Zr supported on 60 Å SiO_2. Initial tests were promising and the catalyst exhibited high selectivity for 1,3-BD when tested for 1 hour, however the average selectivity over 3 hours is poor. The GC data shows that selectivity for 1,3-BD falls rapidly after 1 hour, whilst ethylene production remains stable (**Figure 2.5.3**).

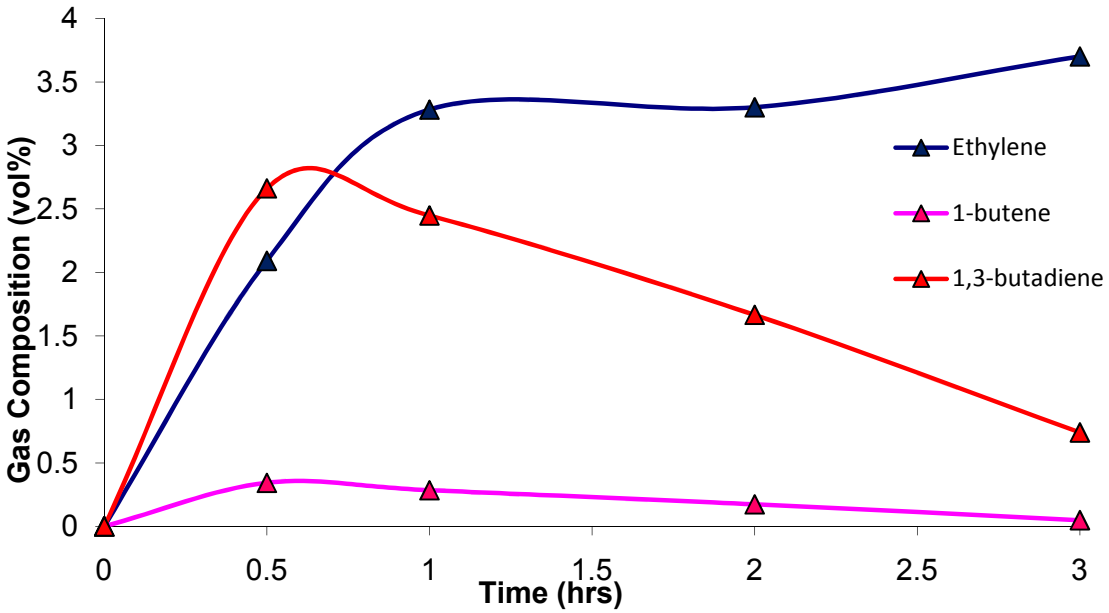

Figure 2.5.3: Gas composition over time for 3 hour test of **CuZrSi-60**.

X-ray photoelectron spectroscopy (XPS) was performed on samples of fresh, calcined (500 °C), and spent **ZnZrSi-60A**, and a fresh and spent sample of **CuZrSi-60**. XPS is a technique that can measure the composition of a material, as well as the electronic state of its components. It is primarily a surface technique; however etching of a surface allows measurement of compositional uniformity as a function of depth. It works on the basis that irradiating a sample with an intense X-ray beam causes ejection of electrons, which are then collected. The kinetic energy of these electrons is measure and used to determine the binding energy of the emitted electron. Each element will produce a characteristic XPS spectrum of peaks at binding energies that specifically relate to the electronic configuration of the element. The number of electrons detected is directly related to the concentration of that element within the irradiated area. The data gathered from the XPS analysis is shown in **Table 2.5.2**.

Catalyst	State	Binding Energy (kj mol^{-1})			Composition (mol %)		
		Zr	*Zn*	*Cu*	*Zr*	*Zn*	*Cu*
ZrZnSi-60A	**Uncalcined**	334.11	1045.11	-	0.44	0.22	-
ZrZnSi-60A	**Calc. 500 °C**	333.39	1044.39	-	0.37	0.09	-
ZrZnSi-60A	**Spent**	334.12	1042.12	-	0.33	0.05	-
ZrCuSi-60	**Uncalcined**	334.22	-	933.22	0.37	-	0.54
ZrCuSi-60	**Calc. 500 °C**	333.29	-	933.29	0.35	-	0.51
ZrCuSi-60	**Spent**	333.92	-	932.92	0.31	-	0.25

Table 2.5.2: XPS data for **ZnZrSi-60** and **CuZrSi-60**.

Interestingly, there is a significant reduction of the surface concentration of some metals after both calcination and a catalytic run, presumably due to migration in to the bulk material. In particular, zinc concentration in spent **ZnZrSi-60A** is less than a quarter of the value pre-calcination, however these catalysts are reusable with only a minor loss of activity. Zirconium ions are not affected to such a degree. Binding energies are consistent with the literature for Zr(IV), Zn(II), and Cu(II) species.[22-25]

2.6 Trimetallic Catalysts on a Silica Support

Though the bimetallic Zn/Zr systems produce good yields of 1,3-BD, ethylene selectivity remains high. To further promote ethanol dehydrogenation over dehydration, copper was added to make a trimetallic catalyst. **CuZnZrSi-60** was synthesised using the silica slurry method described previously from **$Cu(CH_3CO_2)_2.H_2O$**, **$Zn(NO_3)_2.6H_2O$**, **$ZrO(NO_3)_2.xH_2O$**, and 60 Å pore diameter SiO_2. Loading was 1 wt% of each metal, and the catalyst was calcined at 500 °C. A variation of the synthetic procedure was attempted, in which fast evaporation of the water from the slurry was facilitated by a rotary evaporator. However the catalyst appeared “speckled” (**Figure 2.6.1**) in comparison to that produced by the slow evaporation, which remained the preferable method.

Figure 2.6.1: **CuZnZrSi-60** as produced by slow and fast evaporation methods.

Initial 1 hour tests (**Table 2.6.1** and **Figure 2.6.2**) were performed to determine the optimum operating temperature of the catalyst. At 300 °C, the 1,3-BD : ethylene product ratio is extremely high, however conversion is poor and acetaldehyde is the major product. As seen with previous catalysts, the dehydrogenation of ethanol occurs fairly readily at lower temperatures, however higher temperatures are required to promote the later reaction steps to give a reasonable yield of 1,3-BD, whilst also increasing the conversion. Unfortunately this also promotes ethylene production. The test at 375 °C exhibits the highest 1,3-BD selectivity for catalysts on a 60 Å SiO_2**.**

Catalyst	Reactor Temp (°C)	Conv. (%)	Selectivity (%)				
			1,3-BD	Ethylene	Acetaldehyde	Ether	1-Butene
CuZnZrSi-60	300	20.74	29.61	4.06	45.84	10.14	10.34
CuZnZrSi-60	350	35.25	25.30	23.02	33.46	14.72	3.48
CuZnZrSi-60	375	38.53	50.08	24.87	15.60	4.64	4.81

Table 2.6.1: Catalytic data for **CuZnZrSi-60** at varying reactor temperature. All tests were for 1 hour. EtOH and Ar flow was 0.1 and 25 ml min^{-1} respectively.

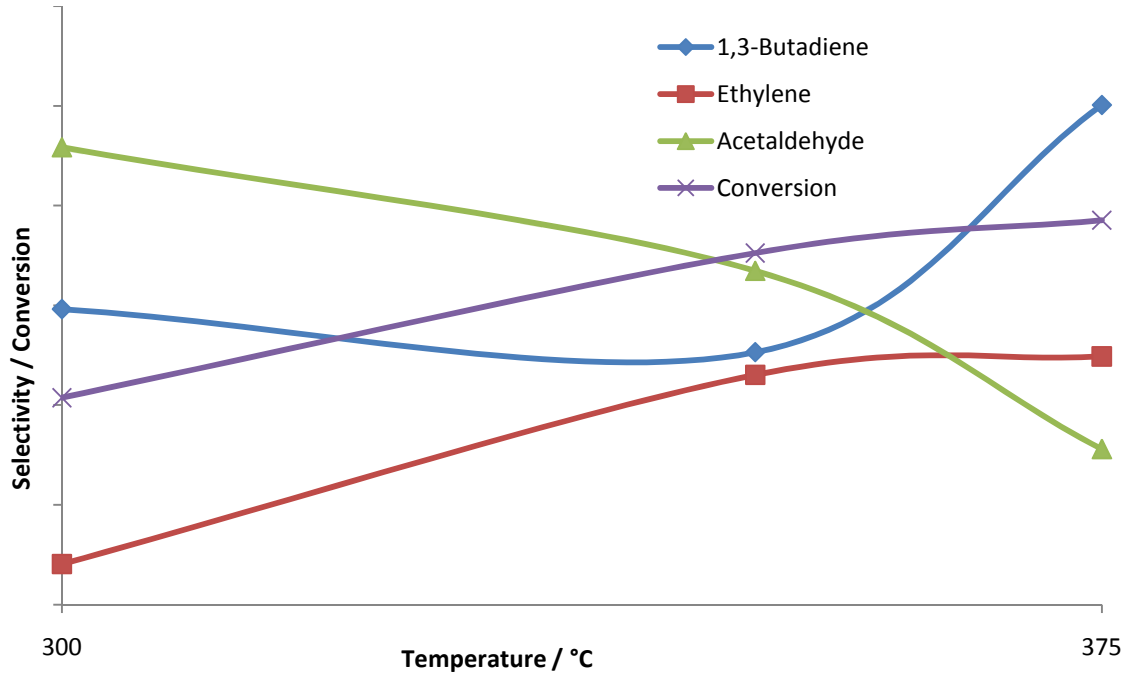

Figure 2.6.2: Changes in product selectivity and conversion with reactor temperature for **CuZnZr-60**

As with the promising bimetallic catalysts, attempts were made to reduce ethylene selectivity by the use of a SiO_2 support with a larger pore size. **CuZnZrSi-150** and **CuZnZrSi-500** were synthesised as previously described using 150 and 500 Å pore diameter SiO_2 respectively. Both were calcined at 500 °C. Catalytic data of the trimetallic catalysts, including the 60 Å catalyst for comparison, tested at 375 °C for a run time of 3 hours, is shown in **Table 2.6.2**.

Catalyst	Conv. (%)	Selectivity (%)				
		1,3-BD	Ethylene	Acetaldehyde	Ether	1-Butene
CuZnZrSi-60	27.00	32.98	26.62	32.79	5.23	2.38
CuZnZrSi-150	44.60	67.44	20.84	5.26	2.81	3.65
CuZnZrSi-500	35.23	32.60	6.04	44.11	14.71	2.53

Table 2.6.2: Catalytic data for trimetallic catalysts. All were calcined at 500 °C. All tests were for 3 hours. EtOH and Ar flow was 0.1 and 25 ml min^{-1} respectively.

The 3 hour result for **CuZnZrSi-60** exhibits a drop in conversion compared to the 1 hr test, consistent with previous findings. Overall selectivity for 1,3-BD is also reduced. **Figure 2.6.3** shows that both 1,3-BD and ethylene production peaks at 30 minutes, with comparative

selectivity far in favour of 1,3-BD. Activity then drops, and remains constant over the remainder of the run, however the 1,3-BD:ethylene ratio is considerably reduced, though 1,3-BD remains the major product.

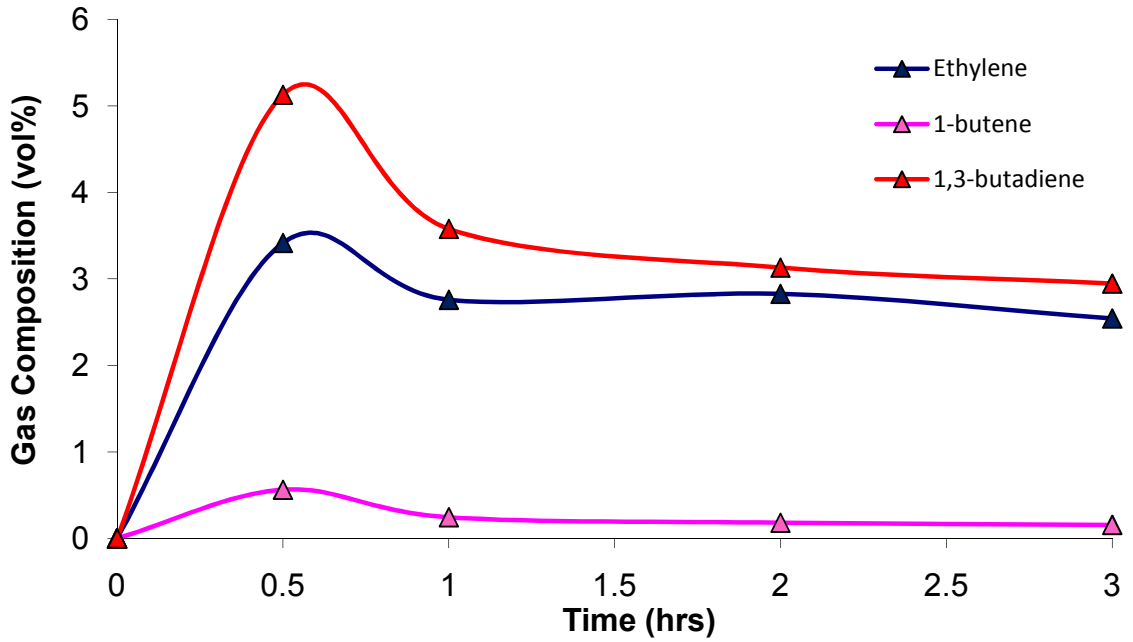

Figure 2.6.3: Gas composition over time for 3 hour test of **CuZnZrSi-60**

CuZnZrSi-150 does not exhibit an initial surge in activity as found with previous catalysts (**Figure 2.6.4**). Instead Ethanol conversion is in excess of 17 % higher than the 60 Å catalyst, but most impressive is 1,3-BD selectivity, which constitutes 67.44 % of the detected products, and at times exceeds 12 vol% of the exhaust emissions which is more than double that of the previous catalyst. Catalytic activity at 30 minutes is poor, but increases dramatically at 1 hour and results show no sign of catalyst deactivation over the tested period.

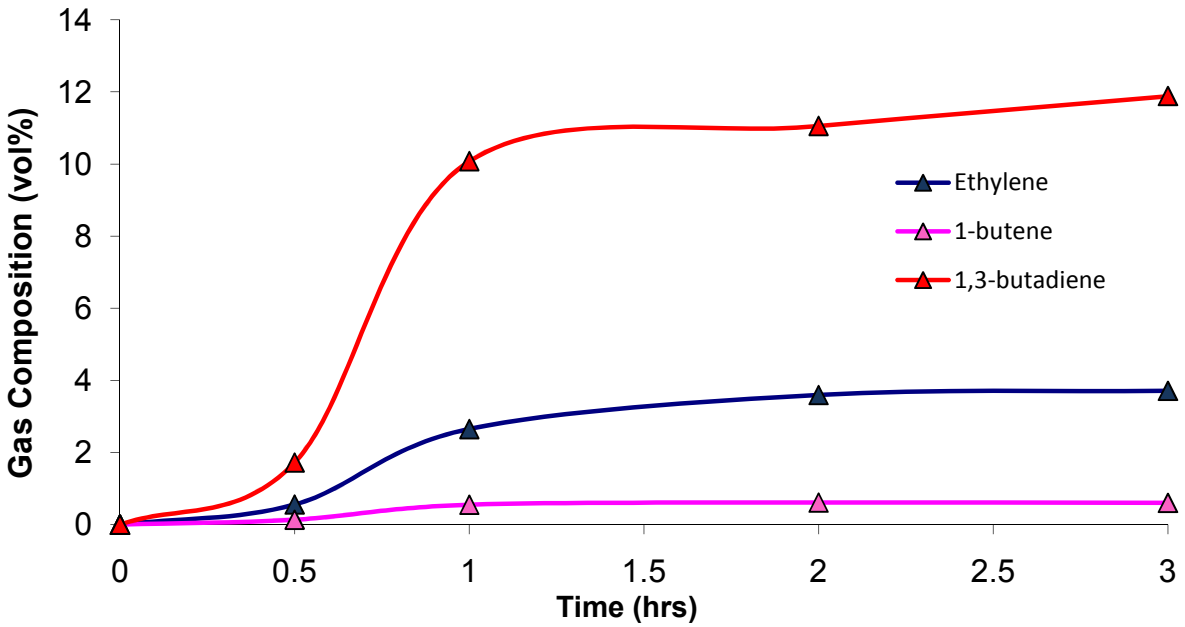

Figure 2.6.4: Gas composition over time for 3 hour test of **CuZnZrSi-150**

CuZnZrSi-500 exhibits interesting behaviour (**Figure 2.6.5**). Conversion is in-between the two other trimetallic catalysts, and as with **CuZrZnSi-150** a steady initial increase in activity is observed. Comparison of gas composition as determined by GC reveals the catalyst is no more active for 1,3-BD production than **CuZnZrSi-60**, however of great importance is the suppression of ethylene production, which results in an average 1,3-BD:ethylene ratio of 5.4:1, far in excess of previously tested catalysts. Of note is the large quantity of acetaldehyde detected, implying some degree of acidity in the support is required to promote further reaction to the desired products. On an industrial scale, this is not necessarily a problem, as acetaldehyde could be easily separated from the exhaust gas stream and fed back in to the reactor.

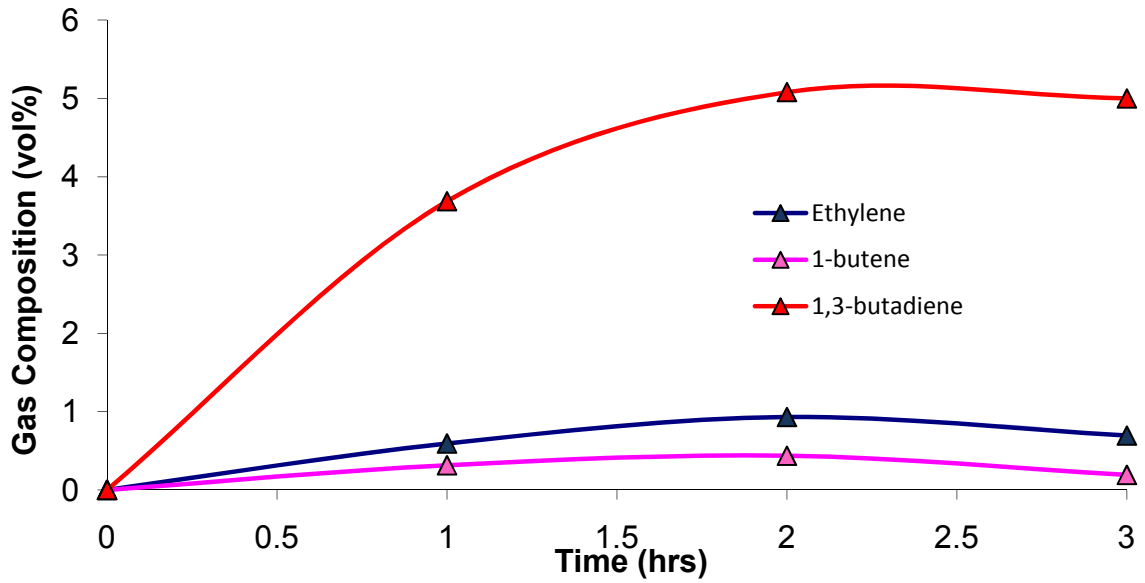

Figure 2.6.5: Gas composition over time for 3 hour test of **CuZnZrSi-500**

2.7 Acetaldehyde and Ethanol Co-Feed Experiments

Tests then moved on from a pure ethanol feed to include acetaldehyde. A number of catalysts were tested with an EtOH:acetaldehyde feed ratio of 9:1 or 8:2 respectively. The feed solution for these tests was prepared fresh the morning of the run to ensure minimal decomposition of the acetaldehyde. All other aspects of the run were carried out according to the standard procedure. Efforts were made to modify our method of mass- balancing to include the mixed feedstock, however quoted conversion values for these runs will be higher than actual, as will acetaldehyde selectivity. The mass of acetaldehyde detected in the ^{1}H NMR of the bubbler content is assumed to have arisen from the dehydrogenation of ethanol, though in reality much of this will be from the feed. It was not possible to distinguish the acetaldehyde from the two different sources. For these runs the flow rate of both Ar and the liquid feed was reduced to 12 and 0.05 ml min^{-1} respectively, in order to reduce any pressure build-up that may accompany the use of a more volatile feedstock.

A number of zinc/zirconium bimetallic catalysts were tested using a feed containing acetaldehyde and the results are given in **Table 2.7.1**. For comparison, catalysts were also tested using a pure ethanol feed under the revised flow conditions.

Catalyst	EtoH : Acetal. Ratio	Conv. (%)	Selectivity (%)				
			1,3-BD	Ethylene	Acetaldehyde	Ether	1-Butene
ZnZrSi-60A	10 : 0	41.91	35.72	42.90	9.75	6.82	4.81
ZnZrSi-60A	9 : 1	53.30	44.73	33.28	11.51	4.49	5.99
ZnZrSi-150	10 : 0	38.96	42.10	31.09	13.86	8.61	4.34
ZnZrSi-150	9 : 1	40.79	58.73	17.90	14.79	3.33	5.25
ZnZrSi-150	8 : 2	45.19	65.98	9.82	14.66	4.77	4.76

Table 2.7.1: Results upon variation of EtOH : Acetaldehyde feed ratio. The LHSV for all runs was ≈ 0.75 at a feed flow of 0.05 ml min^{-1} and in all cases an Ar flow of 12 ml min^{-1} was used. The time for these runs was 3 hours at a temperature of 375 °C. All catalysts were calcined at 500 °C

Conversions for all tests are on the whole higher than previously observed, due to the increased residence time of ethanol on the catalyst, a consequence of the lower Ar and feed flow rates. Comparison of a pure ethanol feed against one containing 10 % acetaldehyde for **ZnZrSi-60A** (**Figure 2.7.1**) reveals a dramatic increase in selectivity towards 1,3-BD over ethylene. Comparison of ethylene content of the exhaust gas for both runs reveals a slight reduction in ethylene production upon introduction of acetaldehyde in to the feed. This implies a small amount of ethanol is being preferentially utilised in the aldol condensation step with acetaldehyde, rather than being dehydrated. The marked increase in 1,3-BD content of the exhaust gas reveals the shortcoming of the catalyst is its inability to effectively dehydrogenate ethanol, one which is addressed with the addition of copper to make the trimetallic catalyst.

ZnZrSi-150 exhibits the same behaviour when acetaldehyde is introduced to the feed (**Figure 2.7.2**). Conversion values are also seen to rise with increasing acetaldehyde content. Ethylene suppression is more pronounced than the previous catalyst, and again suggests preferential reaction of ethanol in the aldol condensation step. A greater acetaldehyde content in the feed means more available with which the ethanol can react to form acetaldol, and as such we would expect that increasing acetaldehyde content further would lead to less ethylene. 1,3-BD production increases dramatically with added acetaldehyde, and at an ethanol : acetaldehyde ratio of 8:2 the selectivity for the desired product is nearly 66 %.

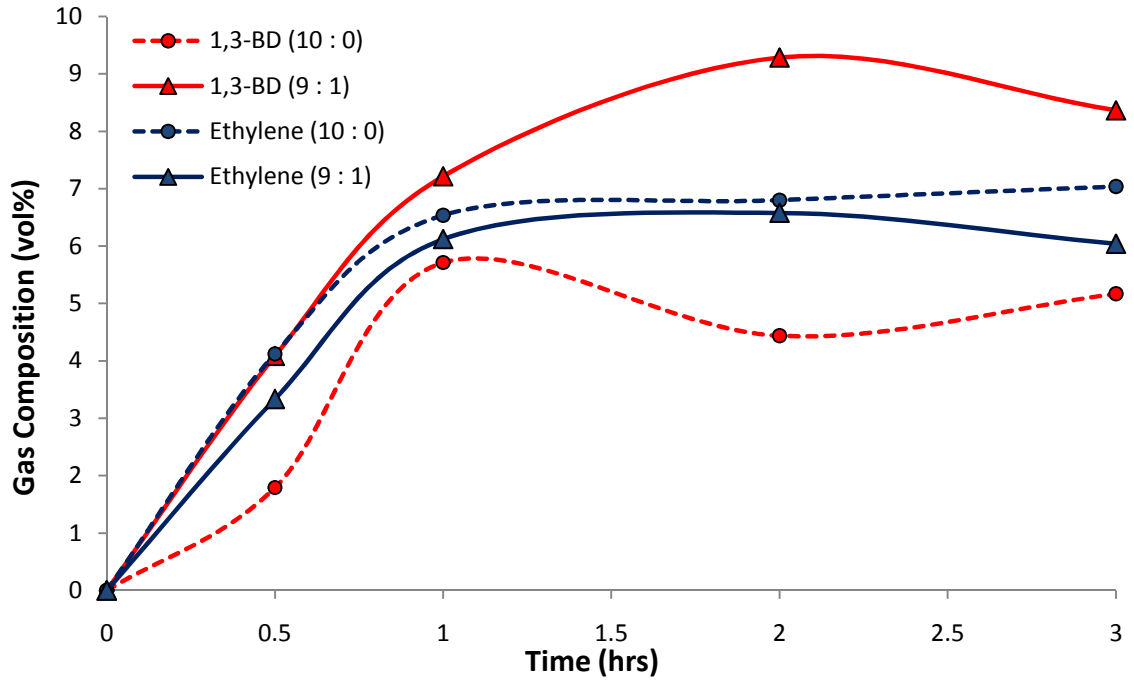

Figure 2.7.1: Gas composition over time for **ZnZrSi-60A** with varying EtOH : acetaldehyde feed ratio

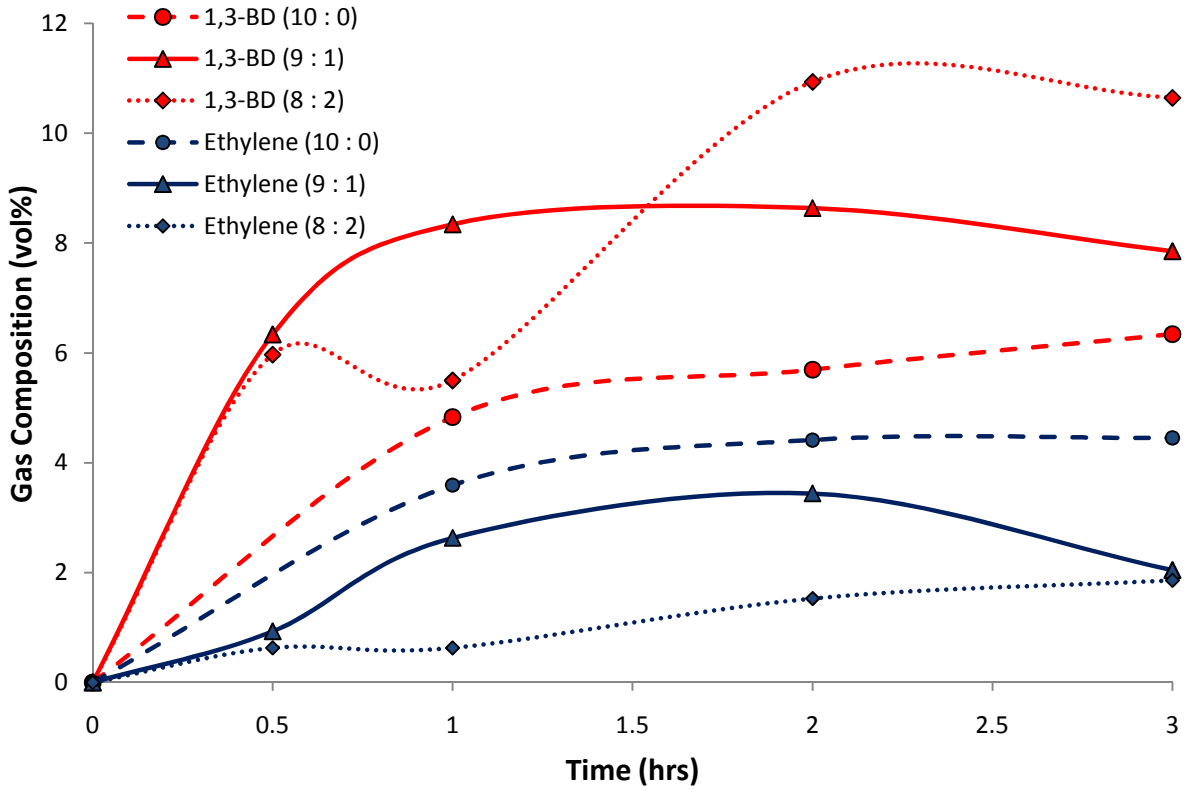

Figure 2.7.2: Gas composition over time for **ZnZrSi-150** with varying EtOH : acetaldehyde feed ratio

A number of trimetallic catalysts were also tested with acetaldehyde in the feed to see if 1,3-BD selectivity was enhanced. **Table 2.7.2** details the results for **CuZnZrSi-500**. Conversion and 1,3-BD selectivity values do not vary considerably between runs, indicating that the dehydrogenation of ethanol to acetaldehyde is not rate limiting for this particular catalyst. Catalysts that performed poorly with a pure ethanol feed, such as **HfZnSi-60** and **CuZnSi-60**, also underwent tests with a mixed feed, however neither showed improvement.

Catalyst	EtoH : Acetal. Ratio	Conv. (%)	Selectivity (%)				
			1,3-BD	Ethylene	Acetaldehyde	Ether	1-Butene
CuZnZrSi-500	10 : 0	35.23	34.60	6.05	44.12	12.71	2.53
CuZnZrSi-500	9 : 1	35.55	39.85	5.80	40.59	11.35	2.40
CuZnZrSi-500	8 : 2	32.70	39.07	4.41	44.97	9.70	1.85

Table 2.7.2: Results upon variation of EtOH : Acetaldehyde ratio for **CuZnZrSi-500**. The LHSV for all runs was ≈ 0.75 at a feedrate of 0.05 ml min^{-1} and in all cases an Ar flow of 12 ml min^{-1} was used. The time for these runs was 3 hours at a temperature of 375 °C. All catalysts were calcined at 300 °C

2.8 Conclusions

A number of materials have been prepared, characterised via a number of methods, and tested as possible catalysts for the production of 1,3-butadiene (1,3-BD) from ethanol. Catalysts were tested on a fixed-bed continuous flow reactor, and the selectivity towards established products and conversions calculated via analysis by GC and ^{1}H NMR spectroscopy. Microporous aluminophosphate materials were tested due to their extensive use as catalysts for other processes.[3-5] However, the only observed product was ethylene, due to the inherent Brönsted acidity of the materials. Focus then moved to metal-exchanged sepiolite materials, which have previously been shown to catalyse 1,3-BD production with much success.[6-8] Attempts were made to exchange atoms within the porous structure with divalent manganese, zinc, and copper atoms. The presence of these metals in the materials was confirmed by EDS. These materials were found to produce small quantities of 1,3-BD, however the major product was ethylene and the conversion was

similarly poor. After a catalytic run the sepiolite catalysts appeared heavily coked. The inactivity of the catalysts was thought to have arisen from their poor thermal stability, characteristic of sepiolite.[13] X-ray diffraftion patterns of the materials post-calcination revealed no order, indicating structure collapse at the calcination temperatures employed. It is hypothesised that pre-treatment of the sepiolite with a dilute acid solution prior to exchange of the atoms with the metal ions would facilitate the exchange process, and produce materials with considerably higher thermal stability, as has been reported in the literature.[14]

Much more promising catalysts were produced by anchorage of metals to a silica support. A catalyst containing zinc and zirconium metals was shown to be the most active bimetallic combination. Metal loadings were confirmed by ICP-EOS and XPS. It is assumed that ZnO is active for the dehydrogenenation of ethanol, the silica support and/or a combination of the Lewis acidic metal centres could catalyse the subsequent aldol condensation of ethanol and acetaldehyde and ZrO_2 the Meerwein-Ponndorf-Verley reduction of the aldehyde produced to the alcohol. Investigations in to the nature of the support reveal that catalytic activity is related to the pore diameter of the silica. Between a range of 40 and 150 Å, conversion and 1,3-BD activity is seen to increase with pore diameter. This is due to reduced acdity of the materials, as confirmed by ^{29}Si solid-state NMR spectroscopy, and the observed reduction of the acidic Q^2 and Q^3 silicon environments that occur within silica. Use of acetaldehyde within the feed resulted in significantly increased activity for **ZnZrSi-60A**, indicating the catalyst struggles with the dehydrogenation of ethanol to acetaldehyde.. Comparison of results with that of a pure ethanol feed reveal a slight decrease in ethylene production, implying ethanol is preferentially reacting in the aldol condensation step rather than being dehydrated. Metal loadings in excess of 0.5 wt% Zn and 1.5 wt% Zr were found to have a negative impact upon conversion values. Longevity studies upon catalysts resulted in a universal decrease in conversion. ZnZr on 150 Å silica was tested over a combined period of 6 hours, with little deterioration in activity. Catalysts did not appear to be heavily coked, and TGA analysis of spent materials showed only minor weight loss early in the run, consistent with the loss of absorbed water, ethanol, or acetaldehyde.

The shortcomings of the bimetallic catalyst were addressed by the inclusion of copper to produce a trimetallic CuZnZr catalyst. Variation of the silica support material resulted in a catalyst that exhibited a 67 % selectivity towards 1,3-BD (**CuZnZrSi-150**). Increasing the silica pore diameter to 500 Å did not further enhance catalytic activity. Large amounts of acetaldehyde were detected, implying some degree of acidity is required in the support to catalyse the aldol condensation.

A number of other bimetallic catalysts were tested with limited success. Of particular interest was the poor carbon balance found with cobalt containing catalysts. It is thought this is likely to be due to the cobalt catalysing the steam reformation of ethanol, giving rise products that are unable to be detected by the GC.[17, 18]

The mechanism of the reaction of ethanol to produce butadiene contains a considerable amount of chemistry, therefore producing a catalyst that is capable of promoting every step is a difficult task. Catalysts may be dismissed as inactive if butadiene yields are poor, yet they may be extremely active for most of the reaction scheme, but struggle with one particular transformation. There are many examples, both in the literature and this work, where acetaldehyde as been co-fed in to the reactor, and butadiene yields have increased by a large degree.[26] This suggests the catalyst is not an effective dehydrogenation catalyst, therefore cannot by itself produce the all-important intermediate acetaldehyde from ethanol. To bypass these potential problems, a novel approach to this reaction would be to have sequential catalyst zones within a single reactor bed. A series of catalysts can be arranged to catalyse each reaction step individually. The three main steps of the reaction are thought to be the dehydrogenation of ethanol to acetaldehyde, the aldol condensation to form acetaldol, and finally the MPVO reaction to form the dehydratable C4 compound. Testing of materials for each of these steps, and then combining the most promising, could be a good approach, and opens up the scope of potential catalyst. Once a successful combination has been established, further study can determine the optimum depth of each zone, ethanol residence time, temperature etc.

2.9 Experimental

General Experimental Procedures

The products of the catalyst testing were analysed by a Hewlett Packard 5890 GC using He as the carrier gas, a Varian CP-LowOx column (10 m x 0.53 mm) and FID as the detection method. The GC was calibrated using a 5-gas blend of the major expected products (ethylene, 1,3-BD, 1-butene, acetaldehyde, diethyl ether). ^{1}H NMR (250 MHz, $CDCl_3$) of the bubbler content was performed on a Bruker 250 MHz spectrometer. SEM microscopy and EDS spectra were performed on a JEOL JSM6310 scanning electron microscope at the University of Bath's Centre for Electron Optical Studies. ICP-OES measurements were carried out by MEDAC Ltd on a Varian Vista MPX system. BET measurements were carried out on a BELSORP Mini-II gas adsorption instrument. ^{29}Si {^{1}H} Solid-State NMR spectra were recorded at the EPSRC National Solid-state NMR service centre, Durham, using a Varian VNMRS 400 MHz spectrometer and referenced to TMS. A pulse delay of 60 seconds was utilised. The spectra for certain materials were deconvoluted to determine the relative proportion of each silicon environment.

Mn-SepC, Zn-SepC, Cu-SepC

All sepiolite catalysts were synthesised via the same procedure. Sepiolite was purchased from Aldrich and used without further purification. The metal ion sources employed were $Mn(CH_3CO_2)_2$, $Zn(CH_3CO_2)_2.2H_2O$, and $Cu(CH_3CO_2)_2.H_2O$. As an example, for **ZnSep-C:** $Zn(CH_3CO_2)_2.2H_2O$ (2.50 g, 11.39 mmol) was dissolved in 100 ml of water. Sepiolite (14 g) was added with stirring, giving an approximately 1:4 molar ratio (exact degree of hydration of the mineral is not specified). The mixture was stirred for 24 hours, and a further 30 ml of water was added as it became increasingly viscous. The mixture was then filtered and washed with cold water, before being partially dried, ground to a fine powder, and placed in to a fresh aqueous solution of $Zn(CH_3CO_2)_2.2H_2O$ of the same concentration as before. The exchange was repeated a further time, and the product was dried at 80 °C to give **Zn-Sep**. Calcination in air at 450 °C for 1 hour yielded **Zn-SepC**.

Bi- and Tri-metallic Catalysts on a Solid Support

The 4 grades of silica support used and their respective pore diameter were Davisil 635 (60 Å), Davisil 645 (150 Å), Davisil XWP500A (500 Å) and Merck 10181 (40 Å). Metal loadings were targeted at 1 wt% of the metal in the final catalyst, with the exception of **ZrZnSi-60A** (0.5 wt% Zn, 1.5 wt% Zr), **ZrZnSi-60B** (1.0 wt% Zn, 1.5 wt% Zr), and **ZrZnSi-60C** (1.0 wt% Zn, 3.0 wt% Zr). The general procedure was to dissolve the appropriate metal salt in water, and add the silica to form a slurry which is vigorously stirred until the solvent has evaporated. The catalyst is then dried in an oven at 80 °C and calcined. The materials were calcined by heating at 5 °C per minute until the desired temperature (300 or 500 °C), at which point the sample was held at this temperature for a further 5 hours before being allowed to cool to room temperature. The metal salts used were $Cu(CH_3CO_2)_2.H_2O$, $Co(NO_3)_3.6H_2O$, $Mn(CH_3CO_2)_2.4H_2O$, $Zn(NO_3)_2.6H_2O$, $Ce(NO_3)_3.6H_2O$ $ZrO(NO_3)6H_2O$, and HfO_2.

As an example, for **CuZnSi-60**: $Cu(CH_3CO_2)_2.H_2O$ (0.31 g, 1.55 mmol) and $Zn(NO_3)_2.6H_2O$ (0.41 g, 1.38 mmol) were dissolved in water (200 ml) and Davisil 635 silica added (9.80 g). The powder was calcined at 500 °C.

For **CuZnZrSi-150**: $ZrO(NO_3)_2.6H_2O$ (0.375 g, 1.62 mmol), $Cu(CH_3CO_2)_2.H_2O$ (0.31 g, 1.55 mmol) and $Zn(NO_3)_2.6H_2O$ (0.41 g, 1.38 mmol) were dissolved in water (200 ml) and Davisil 645 silica added (9.70 g). The powder was calcined at 500 °C.

Slight modifications to the procedure were required in the following examples;

For **ZnZrSi-60Na**: $ZrO(NO_3)_2.6H_2O$ (0.38 g, 1.64 mmol) and $Zn(NO_3)_2.6H_2O$ (0.23 g, 0.76 mmol) were dissolved in 0.1 M NaOH (200 ml) and Davisil 635 silica added (9.80 g). The powder was calcined at 300 °C.

For **ZnZrSi-60Ba**: $ZrO(NO_3)_2.6H_2O$ (0.38 g, 1.64 mmol) and $Zn(NO_3)_2.6H_2O$ (0.23 g, 0.76 mmol) were dissolved in water (200 ml) and Davisil 635 silica added (9.80 g). After drying, 100 mg of $Ba(OH)_2$ was thoroughly mixed in, and the powder was calcined at 500 °C.

For **ZnZr-ZrO_2**: $ZrO(NO_3)_2.6H_2O$ (0.375 g, 1.62 mmol) and $Zn(NO_3)_2.6H_2O$ (0.41 g, 1.38 mmol) were dissolved in water (200 ml) and ZrO_2 added (9.80 g). The powder was calcined at 500 °C.

References

1. M. Hartmann and L. Kevan, *Research on Chemical Intermediates*, 2002, **28**, 625-695.
2. B. M. Weckhuysen, R. R. Rao, J. A. Martens and R. A. Schoonheydt, *European Journal of Inorganic Chemistry*, 1999, 565-577.
3. K. J. A. Raj and V. R. Vijayaraghavan, *Catalysis Letters*, 2004, **96**, 67-70.
4. M. P. J. Peeters, M. Busio and P. Leijten, *Appl. Catal. A-Gen.*, 1994, **118**, 51-62.
5. P. Concepcion, A. Corma, J. M. L. Nieto and J. PerezPariente, *Appl. Catal. A-Gen.*, 1996, **143**, 17-28.
6. Y. Kitayama and A. Michishita, *Journal of the Chemical Society-Chemical Communications*, 1981, 401-402.
7. Y. Kitayama and A. Abe, *Nippon Kagaku Kaishi*, 1989, 1824-1829.
8. V. Gruver, A. Sun and J. J. Fripiat, *Catalysis Letters*, 1995, **34**, 359-364.
9. P. F. Barron, *American Mineralogist*, 1985, **70**, 758-766.
10. F. W. Chang, H. C. Yang, L. S. Roselin and W. Y. Kuo, *Appl. Catal. A-Gen.*, 2006, **304**, 30-39.
11. J. Cunningham, G. H. Al-Sayyed, J. A. Cronin, J. L. G. Fierro, C. Healy, W. Hirschwald, M. Ilyas and J. P. Tobin, *Journal of Catalysis*, 1986, **102**, 160-171.
12. M. Vivaldi, J. L. Fenoll and P. Hach-Ali, in *Differential Thermal Analysis*, ed. R. C. Mackenzie, Academic Press, London, Editon edn., 1969, pp. 553-573.
13. J. E. Post, D. L. Bish and P. J. Heaney, *Am. Miner.*, 2007, **92**, 91-97.
14. M. Horio, K. Suzuki, S. Tomura and K. Inukai, *Euorpean patent*, **1999**, EP0731057
15. W. M. Quattlebaum, W. J. Toussant and J. T. Dunn, *Journal of the American Chemical Society*, 1947, **69**, 593-599.
16. J. M. Mermet, *Journal of Analytical Atomic Spectrometry*, 2005, **20**, 11-16.
17. M. S. Batista, R. K. S. Santos, E. M. Assaf, J. M. Assaf and E. A. Ticianelli, *J. Power Sources*, 2004, **134**, 27-32.
18. F. Haga, T. Nakajima, H. Miya and S. Mishima, *Catalysis Letters*, 1997, **48**, 223-227.
19. Y. Ishii, T. Nakano, A. Inada, Y. Kishigami, K. Sakurai and M. Ogawa, *Journal of Organic Chemistry*, 1986, **51**, 240-242.
20. A. Ramanathan, D. Klomp, J. A. Peters and U. Hanefeld, *Journal of Molecular Catalysis a-Chemical*, 2006, **260**, 62-69.
21. R. Ohnishi, T. Akimoto and K. Tanabe, *Journal of the Chemical Society-Chemical Communications*, 1985, 1613-1614.
22. J. Agrell, H. Birgersson, M. Boutonnet, I. Melian-Cabrera, R. M. Navarro and J. L. G. Fierro, *Journal of Catalysis*, 2003, **219**, 389-403.
23. P. H. Matter and U. S. Ozkan, *Journal of Catalysis*, 2005, **234**, 463-475.
24. S. Velu, K. Suzuki, C. S. Gopinath, H. Yoshida and T. Hattori, *Physical Chemistry Chemical Physics*, 2002, **4**, 1990-1999.
25. Z. Xu, Z. H. Qian, L. Mao, K. Tanabe and H. Hattori, *Bulletin of the Chemical Society of Japan*, 1991, **64**, 1658-1663.
26. S. Kvisle, *Applied catalysis. A, General*, 1988, **43**, 117-131.

Chapter 3: Results and Discussion of Biodiesel Catalysts

3.1 Introduction to Schiff-base Ligands

Schiff-bases, or imines, contain a carbon-nitrogen double bond where the nitrogen atom is also bound to an aryl or alkyl group, and are the product of the reaction of a primary amine with a carbonyl compound. Schiff-bases have been used extensively as ligands for a number of years, and for a multitude of reasons. Of great importance is their ease of synthesis, which allows large quantities of a ligand to be produced, and at relatively little cost. Schiff-base formation is via an S_N2 mechanism (**Figure 3.1.1**), with the lone-pair of the nitrogen attacking the electrophilic, leading to a carbolamine intermediate.[1] This is then followed by the loss of water, which is usually acid catalysed. In the ligand preparation described herein the solvent, methanol, is acting as the proton source.

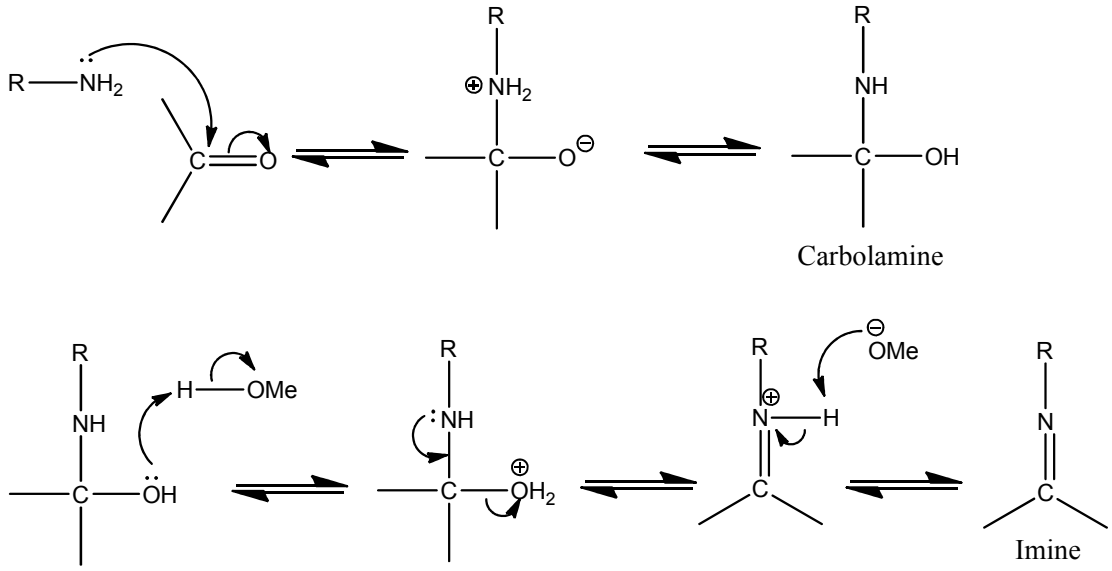

Figure 3.1.1: Mechanism of imine/Schiff-base formation

Schiff-bases designed to coordinate to a metal centre often use an aryl aldehyde, such as 2-hydroxybenzaldehyde, commonly known as salicylaldehyde. Substitution of the aromatic ring means we are able to alter the steric and electronic properties of the ligand. Due to the ease of synthesis, a series of ligands with different

properties can be quickly and cheaply prepared, coordinated to a metal, and screened for catalytic activity. Ligands of this kind are well-utilised in catalysis as they are multi-dentate, binding through the nitrogen and the oxygen of the hydroxyl group on the aromatic ring, and leaving vacant sites on the metal where there is the potential for catalytic activity. Further control over the steric properties of the ligand can be achieved by using substituted anilines as the starting amine.

Schiff-base complexes have been utilised as catalysts for a vast number of processes. Examples in the literature include the use of titanium and zirconium complexes of chiral Schiff-base ligands as catalysts for the ring-opening polymerisation of *rac*-lactide to give polylactide (PLA), a biodegradable thermoplastic.[2] Others have utilised tetranuclear Cu(II) Schiff-base complexes as catalysts for the oxidation of cyclohexane and toluene,[3] or Ni(II) or Ru(II) Schiff-base complexes as catalysts for the reduction of benzene,[4] amongst many other applications.

The ligands prepared in this study were complexed with zinc, due to its low cost, affinity for the oxygen donor present on the ligands, and previous use for transesterification catalysis in the literature.

3.2 Ligand Synthesis

A variety of Schiff-base ligands were synthesised by the reaction of a number of substituted aldehydes with different aniliness. Eight ligands in total were prepared, with the general procedure consisting of the addition of the aniline to a methanolic solution of the aldehyde.[2] In most cases, a yellow solid precipitated from the reaction mixture after approximately 1 hour, though some of the ligands containing bulky substituents required refluxing methanol to drive the reaction to completeness. Yields for all ligands were generally very high, and the **Figure 3.2.1** shows the ligands prepared.

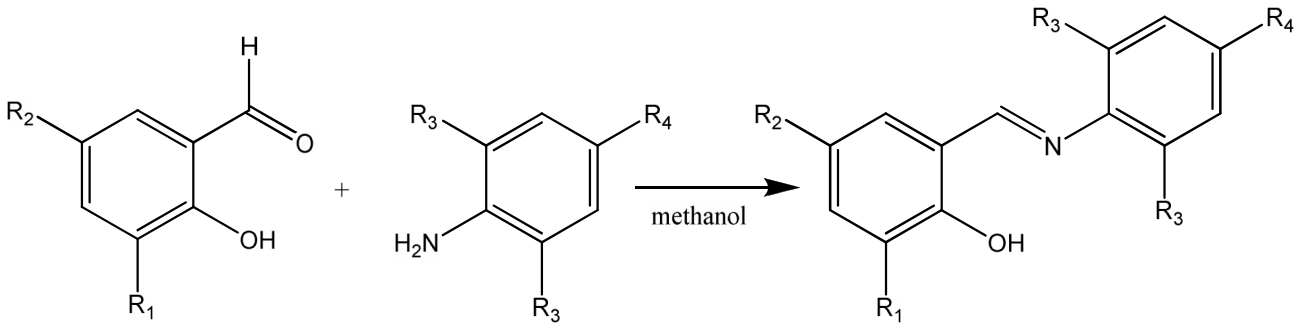

L_1: $R_1=R_2=R_3=R_4=H$
L_2: $R_1=R_2=R_4=H$, $R_3=i$Pr
L_3: $R_1=R_2=H$, $R_3=R_4=Me$
L_4: $R_1=R_2=Cl$, $R_3=R_4=H$
L_5: $R_1=R_2=Cl$, $R_3=R_4=Me$
L_6: $R_1=R_2=Cl$, $R_3=i$Pr, $R_4=H$
L_7: $R_1=Me$, $R_2=R_3=R_4=H$
L_8: $R_1=OMe$, $R_2=H$, $R_3=R_4=Me$
L_9: $R_1=OMe$, $R_2=R_4=H$, $R_3=i$Pr

Figure 3.2.1: The ligands prepared in this study.

Though most of the ligands synthesised used an aldehyde with the hydroxyl group in the ortho position on the aromatic ring, to further investigate the coordination geometry two ligands was prepared from 4-hydroxy-3-methoxybenzaldehyde (**Figure 3.2.2**).

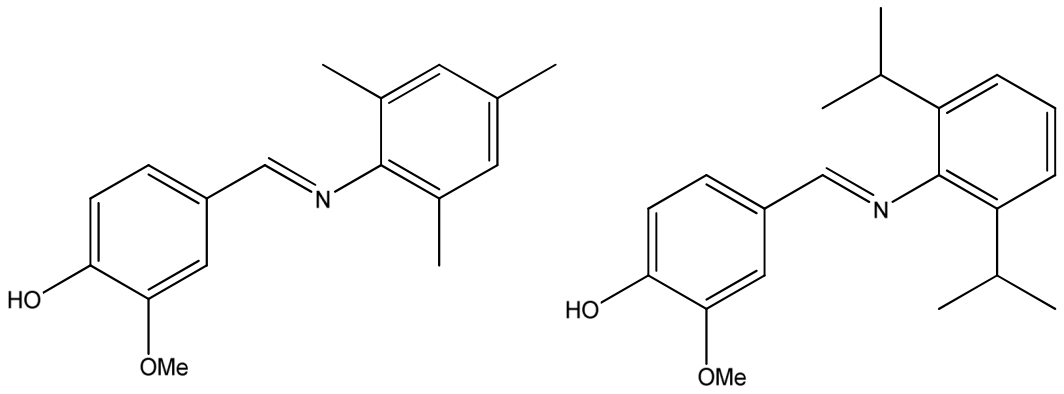

L10 **L11**

Figure 3.2.2: The structure of **L10** and **L11**

A ligand was also synthesised from a bis(aldehyde) and two equivalents of aniline, to form the Schiff base ligand **L12** with two imine bonds, and therefore three atoms capable of metal coordination. This synthesis was again carried out in methanol,

with a bright yellow powder isolated after several hours stirring (**Figure 3.2.3**). The ^{1}H NMR of **L12** showed broad multiplets which were difficult to assign, particularly in the aryl hydrogen region, which indicates a degree of fluxionality in the ligand on the NMR timescale, high resolution mass spectrometry confirmed the identity of **L12.**

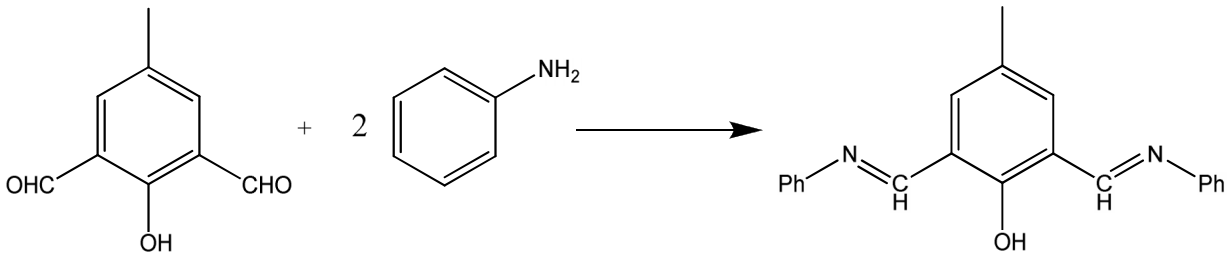

L12

Figure 3.2.3: Synthetic route to **L12**

All ligands were confirmed by ^{1}H and ^{13}C NMR spectroscopy.

3.3 Zinc Complex Synthesis and Characterisation

Complexation of the ligands was then attempted by a 1:1 stoichiometric reaction with $Zn(CH_3CO_2)_2.2H_2O$ in methanol. In most cases, the mixture was left to stir for a number of hours, before a crystalline solid was observed forming. Once again, for the more bulky ligands the solution needed to be heated to reflux (80 °C) to facilitate complexation. The Zn complexes were extracted by filtration of the solid, and recrystallised from hot methanol if possible, or a mixed-solvent route, with chloroform added to aid the solubility of the complex. **L1** to **L7** and **L12** gave crystals of the corresponding Zn complex that were sufficient for structural analysis by single crystal X-ray diffraction. All complexes were characterised by ^{1}H and ^{13}C NMR spectroscopy and elemental analysis. **L1-L2** and **L12** gave a trimetallic species, whilst **L3**-**L7** gave monometallic complexes. The structure of the trimetallic complexes for **L1-L2** consists of three Zn atoms, two Schiff-base ligands, and four acetate groups derived from the Zn salt starting material. The molecular structure for **$Zn_3(L2)_2(CH_3CO_2)_4$** is given (**Figure 3.3.1**).

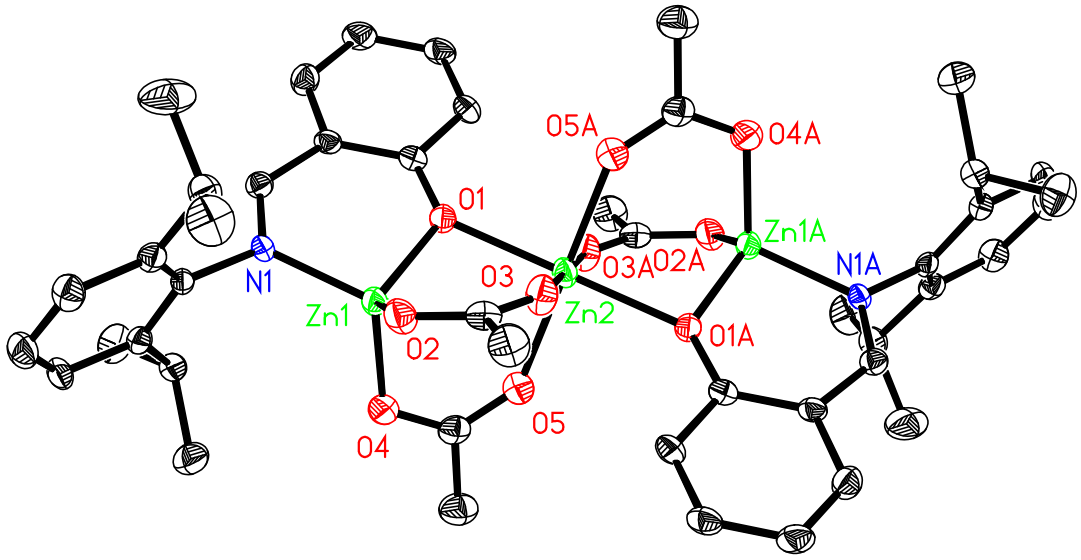

Figure 3.3.1: Molecular structure of $\mathbf{Zn_3(CH_3CO_2)_4(L2)_2}$. Ellipsoids are shown at the 50% probability level and the hydrogen atoms have been removed for clarity. Labels with suffix A relate to those in the asymmetric unit by the –x , –y, –z symmetry operation.

The three metal atoms, Zn(1), Zn(2), and Zn(1A) are bridged by the two ligands and the four acetate groups. The central Zn atom is in a pseudo-octahedral environment, and is bound to all four acetate groups as well as the oxygen atoms on the ligands. The structure is centrosymmetric with the inversion centre lying on Zn(2), meaning Zn(1) and Zn(1A) are crystallographically equivalent. Each is bound to two acetate groups, as well as an imine and phenoxide group of one of the Schiff-base ligands. They are in a pseudo-tetrahedral environment, as exemplified by the N(1)-Zn(1)-O(1) bond angle of 114.43(14) °, which is slightly large, most likely due to steric constraints caused by the isopropyl groups in the 2 and 6 positions on the aromatic ring. In comparison, the same bond in $\mathbf{Zn_3(L1)_2(CH_3CO_2)_4}$, which features hydrogen atoms in the positions on the ring, is much closer to the ideal value for a tetrahedron at 109.10(11) °. Bond lengths and angles are in agreement with zinc carboxylate structures in the literature.[5, 6]

^{1}H and ^{13}C solution NMR spectra of $\mathbf{Zn_3(L2)_2(CH_3CO_2)_4}$ confirms the symmetry of the structure, with a single resonance in the proton spectrum for the N=C<u>H</u> imine of

each ligand, at 8.25 ppm, and a peak for the acetate methyls at 1.79 ppm, in the ratio of 2:12, as would be expected from the solid-state structure. Selected bond lengths are shown below for both $\mathbf{Zn_3(L1)_2(CH_3CO_2)_4}$ and $\mathbf{Zn_3(L2)_2(CH_3CO_2)_4}$ (**Table 3.3.1**)

	$Zn_3(L1)_2(CH_3CO_2)_4$	$Zn_3(L2)_2(CH_3CO_2)_4$
Zn(1)-O(1)	1.939(3)	1.938(3)
Zn(1)-O(2)	1.964(3)	1.932(3)
Zn(1)-O(4)	1.938(2)	1.938(3)
Zn(2)-O(1)	2.150(2)	2.161(3)
Zn(2)-O(3)	2.104(3)	2.077(3)
Zn(2)-O(5)	2.060(2)	2.091(3)
Zn(1)-N(1)	1.984(3)	1.989(3)
O(1)-Zn(2)-O(3)	89.42(9)	90.06(12)
O(3)-Zn(2)-O(5)	92.34(10)	92.08(13)
O(1)-Zn(1)-N(1)	98.39(10)	96.92(13)
O(2)-Zn(1)-N(1)	109.10(11)	114.44(14)

Table 3.3.1: Selected bond lengths (Å) and angles (°) for the two trimetallic complexes

In comparing the structures of these two trimetallic complexes, the two aromatic rings which make up each ligand are almost coplanar in $\mathbf{Zn_3(L1)_2(CH_3CO_2)_4}$, however in $\mathbf{Zn_3(L2)_2(CH_3CO_2)_4}$ there is significant rotation of an N-C bond, to direct the isopropyl substituents above and below the plane of the newly formed 6-membered, Zn-containing ring.

L3 to **L7** produced monometallic complexes, all with a Zn(II):ligand ratio of 1:2. The complexes $\mathbf{Zn(L2)_2}$ –$\mathbf{Zn(L5)_2}$ and also $\mathbf{Zn(L7)_2}$ exhibited very similar structures, with the Zn atom in a pseudo-tetrahedral environment.[7, 8] **Figure 3.3.2** shows the molecular structure of $\mathbf{Zn(L4)_2}$.

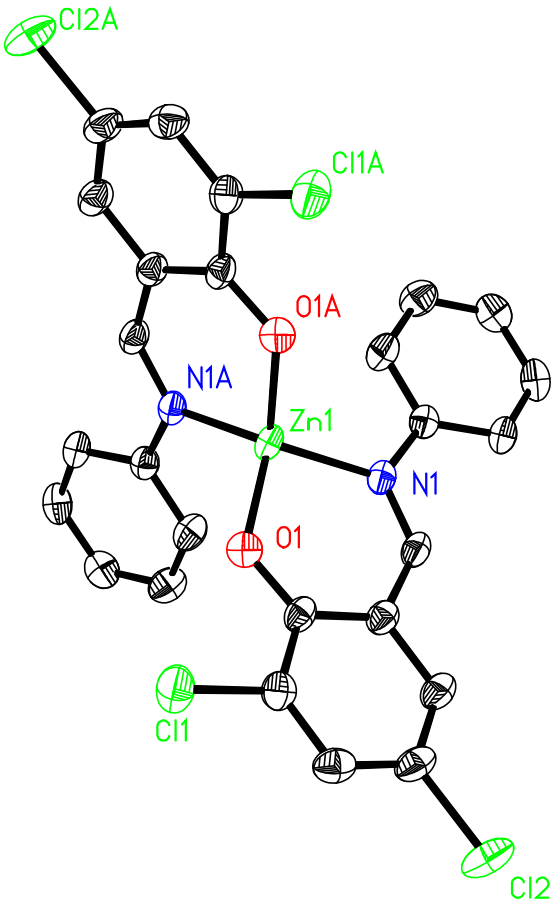

Figure 3.3.2: Molecular structure of **Zn(L4)$_2$**. Ellipsoids are shown at the 50% probability level and the hydrogen atoms have been removed for clarity.

The Zn-phenoxide bond Zn(1)-O(1) in these structures is considerably shorter than that in the trimetallic complexes due to it being terminal, whereas in the trimetallic structures the phenoxide is bridging and shares its electron density between two Zn centres, resulting in a weaker bond. A comparison of bond lengths and angles of the monometallic species is given in **Table 3.3.2.**

	Zn(L3)$_2$	**Zn(L4)$_2$**	**Zn(L5)$_2$**	**Zn(L6)$_2$(MeOH)$_2$**	**Zn(L7)$_2$**
Zn(1)-O(1)	1.9109(14)	1.9210(14)	1.923(3)	2.0218(11)	1.9088(14)
Zn(1)-O(2)	1.9256(14)	-[b]	-[b]	1.9864(11)	1.9174(14)
Zn(1)-O(3)	-[a]	-[a]	-[a]	2.0562(13)	-[a]
Zn(1)-N(1)	2.0167(17)	2.0135(15)	2.012(3)	2.0822(14)	2.0238(16)
Zn(1)-N(2)	2.0000(16)	-[b]	-[b]	2.0700(13)	2.0182(16)
O(1)-Zn(1)-N(1)	95.64(6)	97.08(6)	95.33(11)	88.00(5)	96.17(6)
O(2)-Zn(1)-N(2)	96.27(6)	-[b]	-[b]	90.27(5)	96.11(6)
O(1)-Zn(1)-O(3)	-[a]	-[a]	-[a]	85.87(5)	-[a]
[a]Not applicable. [b]Only one crystagraphically unique ligand					

Table 3.3.2: Selected bond lengths (Å) and angles (°) for all the monometallic Zn complexes prepared

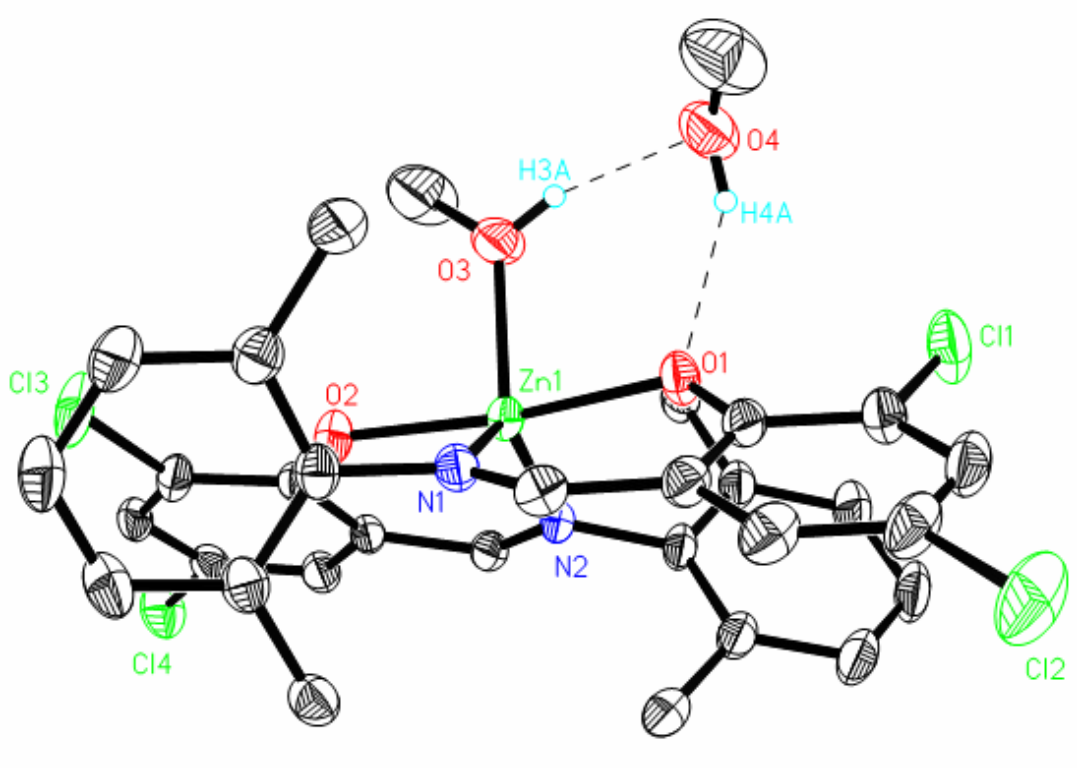

Figure 3.3.3: Molecular structure of **$Zn(L6)_2(MeOH)_2$**. Ellipsoids are shown at the 50% probability level and the hydrogen atoms not involved in hydrogen bonding have been removed for clarity

The Zn complex of **L6** is unique in that the isolated material contained two molecules of methanol within the crystal structure. The Zn centre is pseudo-square based pyramidal, and is bound to both the N and O of each ligand, as well as a methanol molecule in the axial position. Furthermore, this methanol is hydrogen bonded to another lattice MeOH, which in turn hydrogen bonds to the phenoxide oxygen of one of the ligands, forming a six-membered ring. As expected, Zn(1)-(O1) and Zn(1)-N(1) bond distances are longer in **$Zn(L6)_2(MeOH)_2$** than in the other monometallic complexes, due to the bulkiness of the ligand and the distorted geometry inflicted upon the ligands as a result of the methanol coordination.

The final complex was prepared using **L12**, a Schiff-base ligand containing two imine bonds, which proved to be an effective tridentate ligand. Equimolar reaction with zinc acetate yielded a trimetallic species **$Zn_3(L12)_2(CH_3CO_2)_4$**, containing two ligands and four acetate groups. There is no centre of inversion as with the other trimetallic species, and all three Zn atoms are inequivalent. The outermost metal atoms, Zn(1)

and Zn(3) are in a pseudo-tetrahedral environment. Each is bonded to one of the imines and the phenol oxygen of the ligand, as well as two acetates. The ligand forces one of the acetates to bond terminally through a single oxygen atom, O(2) and O(9) respectively, while another acetate bridges the outer Zn atoms to the central one, which is also pseudo-octahedral. The bond lengths for Zn(1)-O(2) and Zn(3)-O(9) are 1.951(2) Å and 1.9550(18) respectively. The bridging acetates exhibit slightly longer Zn-O bonds for the central zinc {Zn(1)-O(1)} than the outer ones {Zn(2)-O(5)}. The remaining imine of each ligand is bound to the central Zn, with Zn(2)-N(2) being 2.1814(19) Å, somewhat longer than the central Zn-imine bond {Zn(1)-N(1)} which measures 2.040(2) Å. The ^{1}H NMR spectrum of the complex in $CDCl_3$ showed very broad peaks, indicating some form of fluxionality exists within the structure on the NMR timescale at room temperature. Cooling to -40 °C slows this dynamic behaviour, and the peaks appear sharper and more easily identifiable. The solution structure of **$Zn_3(L12)_2(CH_3CO_2)_4$** is in agreement with the solid state structure shown below (**Figure 3.3.4**).

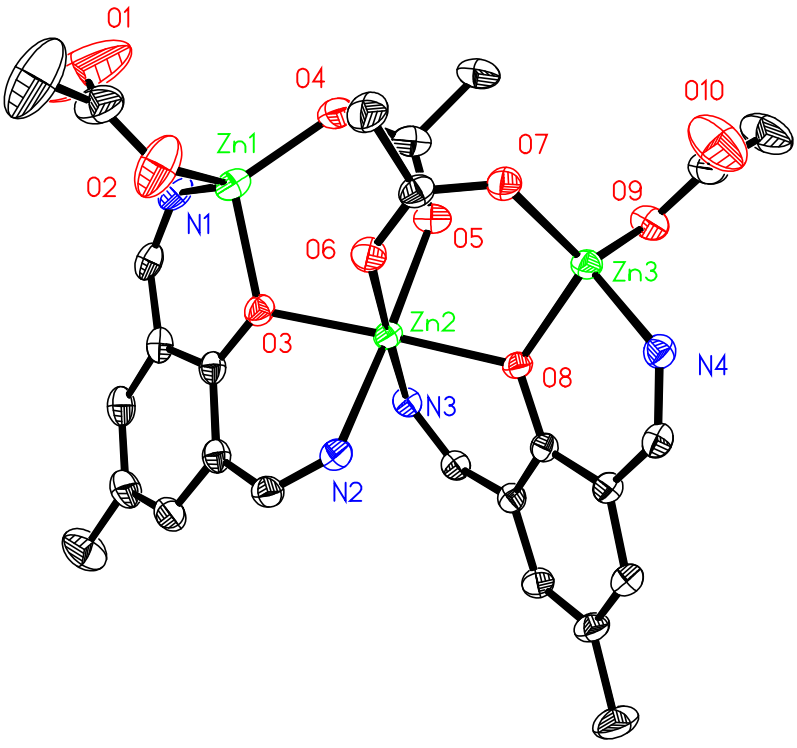

Figure 3.3.4: Structure of **$Zn_3(L12)_2(CH_3CO_2)_4$**. Ellipsoids are shown at the 50% probability level, and the hydrogen atoms have been removed for clarity, as have the carbons of the phenyl rings {attached to N(1), N(2), N(3) and N(4)} and the methyl carbon of the ligand

Some of the ligands did not yield isolatable products when reacted with zinc acetate. The reaction mixtures of $Zn(CH_3CO_2)_2.2H_2O$ with **L8-L11** were analysed by ^1H NMR spectroscopy, which revealed the presence of the starting materials. The lack of a reaction with **L8**, even under reflux conditions, is not easily explained as there are no steric or electronic factors that should inhibit reactivity. **L9** did likely not yield any product due the bulkiness of the isopropyl groups of the ligand hindering the approach of the Zn ion. The reaction with **L10** and **L11** did not proceed due to the hydroxyl group of the benzaldehyde residing in the 4 position on the aromatic ring. This does not facilitate the coordination of both the OH and the imino nitrogen to the metal, due to the two groups being orientated in completely different directions and the limited flexibility of the ligand. The Zn would be coordinatively unsaturated, and fitting more than two ligands around a single metal site is not possible due to their size.

3.4 Activity for the Transesterification of Vegetable Oil

All of the Zn complexes mentioned previously were tested as homogeneous catalysts for transesterification of vegetable oil with methanol to produce FAME. Zinc is a Lewis acidic metal and therefore should be active as a catalyst, by coordination and polarisation of the carbonyl group of the triacylglycerols. The same conditions were used for every test so their activities could be compared. The reactions were carried out in a sealed autoclave which was heated to 195° by use of a graphite-bath, with the reaction time being 2 hours. 20 g of store-bought vegetable oil was combined with 8.5 g (a 1:12 molar ratio) of methanol and 2 mol% catalyst. A blank run was also conducted to determine the baseline activity of the reactor when no catalyst was loaded.

Monitoring of the transesterification reaction and the conversion of triacylglycerols to FAME can be done using ^1H NMR spectroscopy.[9] The conversion of vegetable oil was determined by taking the FAME layer and measuring the integral of the signals

relative to the methoxy (A_1) and α carbon CH_2 (A_2) groups, and utilisation of the formula;

$$\text{Percent conversion} = 100 \times (2A_1 \,/\, 3A_2)$$

The methoxy signal (a strong singlet peak around 3.6 ppm) will be as a result of any FAME produced, whilst the methylene signal (a multiplet at approximately 2.3 ppm) arises from CH_2 groups in both the triacylglycerols and the methyl ester products (**Figure 3.4.1**). The factors 2 and 3 arise from the number of protons in each particular group. The ^{1}H NMR spectrum of the biodiesel test conducted using $\mathbf{Zn_3(L2)_2(CH_3CO_2)_4}$ is shown, and the relevant peaks noted (**Figure 3.4.2**).

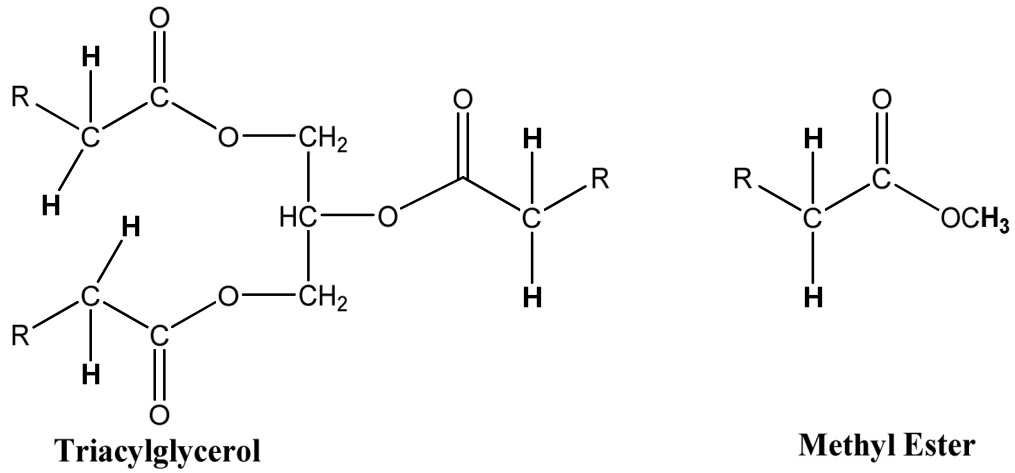

Figure 3.4.1: The structure of a triacylglycerol and a methyl ester. Integration of the peaks for the highlighted protons will lead to conversion values.

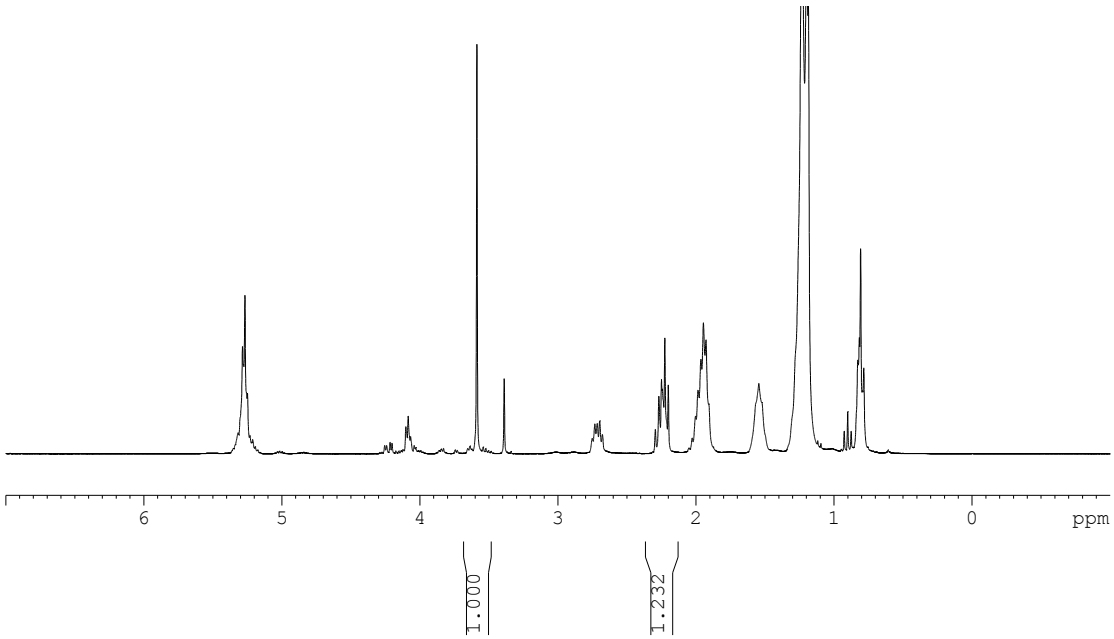

Figure 3.4.2: ^{1}H NMR ($CDCl_3$) spectrum of the FAME produced by $\mathbf{Zn_3(L2)_2(CH_3CO_2)_4}$. Percentage conversion = 100 × (2 × 1.00 / 3 × 1.232) = 54%.

The results for the seven homogeneous complexes, and in addition a heterogeneous Mn-exchanged sepiolite material, are tabulated below (**Table 3.4.1**). The affect of the reaction temperature on the activity of $\mathbf{Zn_3(L2)_2(CH_3CO_2)_4}$ is also investigated.

Catalyst	Reaction Conditions	Conversion (%)
none	195 °C for 2 hours	6
$Zn_3(L1)_2(CH_3CO_2)_4$	2 mol% of Zn, 195 °C for 2 hours	60
$Zn_3(L2)_2(CH_3CO_2)_4$	2 mol% of Zn, 195 °C for 2 hours	54
$Zn_3(L2)_2(CH_3CO_2)_4$	2 mol% of Zn, 165 °C for 2 hours	41
$Zn_3(L2)_2(CH_3CO_2)_4$	2 mol% of Zn, 125 °C for 2 hours	28
$Zn(L3)_2$	2 mol% of Zn, 195 °C for 2 hours	52
$Zn(L4)_2$	2 mol% of Zn, 195 °C for 2 hours	70
$Zn(L5)_2$	2 mol% of Zn, 195 °C for 2 hours	46
$Zn(L6)_2(MeOH)_2$	2 mol% of Zn, 195 °C for 2 hours	39
$Zn(L7)_2$	2 mol% of Zn, 195 °C for 2 hours	55
Mn-Sep	5 wt% of catalyst, 195 °C for 4 hours	14
Mn-SepC	5 wt% of catalyst, 195 °C for 4 hours	22

Table 3.4.1: Results for the homogeneous Zn catalysts and a heterogeneous Mn catalyst. In all cases, 20 g of vegetable oil and 8.5 g of methanol was used.

The most active catalyst was **$Zn(L4)_2$** which achieved a conversion of 70% after two hours. This complex has two chlorine atoms bound to the phenyl ring, which withdraw electron density from the aromatic system, as does the oxygen atom. With three species now competing for electron density, there is less electron density on the oxygen to donate to the Zn, which in turn increases the Lewis acidity of the metal. Increased Lewis acidity gives a higher conversion as the catalyst is able to more strongly polarise the carbonyl bond in the triacylglycerol, making it susceptible to nucleophilic attack. However, **$Zn(L5)_2$** and **$Zn(L6)_2(MeOH)_2$** also contain chlorine atoms and give substantially lower yields. The lower activity can only be rationalised by the steric affects of the methyl and isopropyl groups respectively on the aryl ring. The Lewis acidity of the metal should not differ greatly from **$Zn(L4)_2$** in either case.

$Zn(L1)_2(CH_3CO_2)_4$ gave a conversion of 60%, with the next most active being **$Zn(L7)_2$** with 55%. This complex contains no bulky substituents, but its lower activity can be rationalised by the electron-donating methyl group increasing the availability of electron density with which the hydroxyl group can bind to the Zn, which will in turn decrease its Lewis acidity, and therefore catalytic activity.

Variation of reaction temperature on with **$Zn(L2)_2(CH_3CO_2)_4$** clearly shows that conversion increases with temperature up until at least 195 °C. Though the catalyst was not tested at a higher temperature, it has shown by others that temperatures in excess of 200 °C can lead to polymeric products, due to degradation of the triacylglycerols and FFA that compose the oil.[10]

The results of the heterogeneous Mn-exchanged sepiolite catalysts **Mn-Sep** and **Mn-SepC** are surprisingly poor. Heterogeneous catalysts are known to proceed at slower rates than homogeneous catalysts, hence the reaction time was increased to four hours, but this did not lead to impressive results. Lewis acidic Mn^{2+} ions on the sepiolite surface should effectively catalyse the transesterification reaction, and basic sites are also present in sepiolite. However, while EDS experiments have confirmed the presence of manganese in the sepiolite, the amount loaded has not been determined, nor has the distribution. The zeolitic pores that sepiolite possesses

may also hinder the reaction, due to trapping of intermediate products and prevention of further reaction or not facilitating the transport of the triglyceride through the material. The calcined material gave a slightly higher conversion, which could be for various reasons. Removal of residual water and other contaminants that would have a detrimental effect on activity occurs during the calcination, but pXRD of the calcined sepiolite materials have indicated disorder, likely due to structure collapse. This may give rise to leaching of free manganese ions in to the liquid medium, so they essentially are acting as a homogeneous catalyst.

3.5 Conclusions

Schiff-base ligands **L1-L12** were synthesised, and complexation with zinc was attempted, with many forming novel mono- and trimetallic complexes, the structure of which have been elucidated by X-ray crystallography. All of these complexes have been shown to be active as homogeneous catalysts for biodiesel production from vegetable oil and methanol, with the most active being **$Zn(L4)_2$**. Those ligands that did not form isolatable complexes using zinc acetate as a reagent may do so if a more reactive zinc source such as $Zn(CH_3)_2$ is utilised. In keeping with the theme of this study, any future work would be to produce heterogeneous equivalents of those catalysts that performed well (**Figure 3.5.1**). This could involve anchorage of the ligands to a solid support such as silica. This can be achieved by reaction of silica with 3-aminopropyltrimethoxysilane (AMPS), to form the heterogenised amine SiO_2-AMPS. Reaction of this with the appropriate aldehydes as utilised for ligand synthesis, and then treatment with $Zn(CH_3CO_2)_2.2H_2O$, should yield the appropriate heterogeneous catalyst.[11]

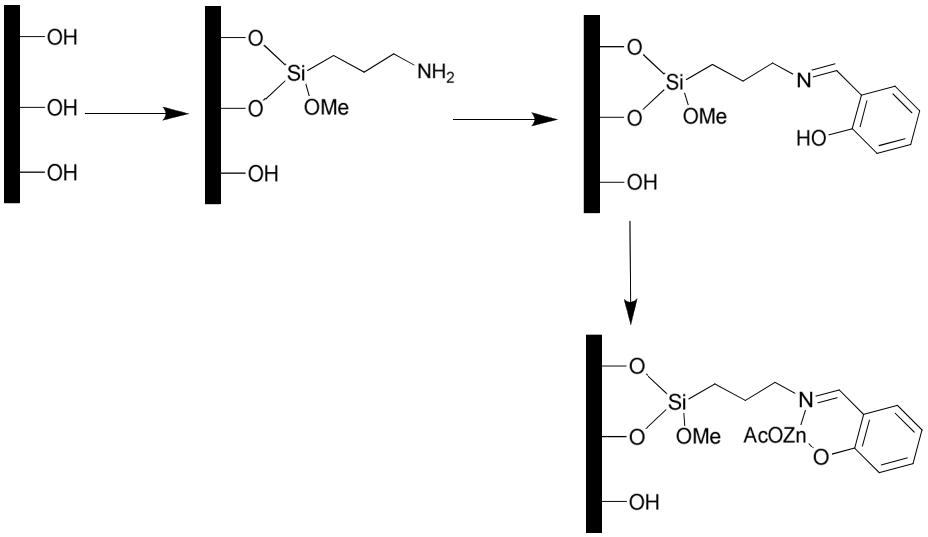

Figure 3.5.1: Example of the preparation of a heterogeneous catalyst for biodiesel production

3.6 Experimental

General Experimental Details

$Zn(CH_3CO_2)_2.2H_2O$ was purchased from Aldrich and used without further purification. ^1H and $^{13}C\{^1H\}$ NMR spectra were recorded on a Bruker 300 MHz or a Bruker 250 MHz spectrometer. Chemical shifts are reported in ppm and referenced to residual solvent peaks. Coupling constants are given in Hertz. High resolution mass spectrometry was performed on the micrOTOF (ESI-TOF) by the Mass Spectrometry Service at the University of Bath. Elemental analysis was performed by Mr A. K. Carver at the University of Bath. Crystallographic data was collected on a Nonius Kappa CCD area detector diffractometer using Mo-Kα radiation (λ = 0.71073 Å) at a temperature of 150 K. Structures were solved by direct methods and refined on all F^2 data using the SHELXL-97 program suite. Hydrogen atoms were included in idealised positions and refined using the riding model, except those involved in hydrogen bonding which were located in difference maps and refined freely.

Synthesis of Ligands

L1

2-Hydroxybenzaldehyde (5.0 ml, 46.8 mmol) was dissolved in 40 ml of methanol. Addition of aniline (5.0 ml, 54.9 mmol) and vigorous stirring for 30 minutes yielded a bright yellow precipitate. This was filtered, washed with methanol, and then left to dry at ambient temperature. ^{1}H NMR (250 MHz, $CDCl_3$) : δ 6.92 – 7.10 (m, 2H, ArH), 7.25 – 7.50 (m, 7H, ArH), 8.63 (s, 1H, N=CH). MS ESI (+ve), $C_{13}H_{12}NO$, Actual: 198.0899, Theoretical: 198.0919

L2

2-Hydroxybenzaldehyde (2.8 ml, 26.50 mmol) was added to 30 ml of methanol, and to this solution was added 2,6-diisopropylaniline (5.0 ml, 26.50 mmol). Vigorous stirring for approximately 4 hours and removal of solvent yielded a pale yellow solid, which was dried *in vacuo*. ^{1}H NMR (250 MHz, $CDCl_3$) : δ = 1.18 (d J = 6.79 Hz, 12H, $CH(CH_3)_2$, 2.99 (m, 2H, $CH(CH_3)_2$), 6.98 (m, 1H, ArH), 7.10 (d J = 6.79 Hz, 1H, ArH), 7.20 (s, 3H, ArH), 7.37 (m, 1H, ArH), 7.44 (m, 1H, ArH) , 8.30 (s, 1H, N=CH)

L3

2-Hydroxybenzaldehyde (3.80 ml, 35.60 mmol) was dissolved in 30 ml of methanol. 2,4,6-Trimethylaniline (5.00 ml, 35.60 mmol) was added, and an immediate colour change was observed from dark purple to yellow/green. The reaction was stirred vigorously overnight, and the majority of the methanol removed by rotary evaporation. Two layers were observed indicating the product was an oil, however subsequent addition of fresh methanol yielded a pale yellow solid. This was filtered and dried *in vacuo*. Yield 3.15g, 37 %. ^{1}H NMR (300 MHz, $CDCl_3$) : δ = 2.17 (s, 6H, CH3), 2.30 (s, 3H, CH3), 6.93 (s, 2H, ArH), 6.96 (m, 1H, ArH), 7.07 (d J = 8.29 Hz, 1H, ArH), 7.33 (m, 1H, ArH), 7.40 (m, 1H, ArH), 8.32 (s, 1H, N=CH).

L4

3,5-Dichloro-2-hydroxybenzaldehyde (3.00 g, 15.63 mmol) was dissolved in 40 ml of methanol, to which aniline (1.45 ml, 15.91 mmol) was added. A yellow precipitate

formed after several minutes stirring, which was filtered, washed with methanol, and dried *in vacuo*. ^{1}H NMR (300 MHz, $CDCl_3$) : δ = 7.28 – 7.42 (m, 4H, ArH), 7.44 – 7.54 (m, 3H, ArH), 8.61 (s, 1H, N=CH). MS ESI (+ve), $C_{13}H_{12}Cl_2NO$, Actual: 266.0140, Theoretical: 266.01394

L5

3,5-Dichloro-2-hydroxybenzaldehyde (6.83 g, 35.60 mmol) was dissolved in 30 ml of hot methanol, to which was added 2,4,6-trimethylaniline (5.00 ml, 35.60 mmol) while stirring. An orange colour was observed upon addition of the aniline, and within 2 minutes a fine, bright yellow precipitate had formed. The reaction was left to stir for 48 hours, after which the product was filtered off and dried *in vacuo.* ^{1}H NMR (300 MHz, $CDCl_3$) : δ = 2.18 (s, 6H, CH3), 2.31 (s, 3H, CH3), 6.95 (s, 2H, ArH), 7.25 (d= J 2.45 Hz, 1H, ArH), 7.50 (d J = 2.45 Hz, 1H, ArH), 8.28 (s, 1H, N=C

L6

3,5-Dichloro-2-hydroxybenzaldehyde (5.06 g, 2.65 mmol) was partially dissolved in 40 ml of methanol, and to this was added 2,6-diisopropylaniline (5.00 ml, 2.65 mmol). Within 1 minute of stirring a bright yellow precipitate was observed forming. This was filtered, washed with fresh methanol and dried *in vacuo*. ^{1}H NMR (250 MHz, $CDCl_3$) : δ = 1.17 (d J = 6.95 Hz, 12H, CH3), 2.93 (m, 2H, C*H*$(CH_3)_2$), 7.21 (s, 3H, ArH), 7.27 (d J = 2.37 Hz, 1H, ArH), 7.51 (d J = 2.37 Hz, 1H, ArH), 8.24 (s, 1H, N=CH).

L7

2-Hydroxy-3-methylbenzaldehyde (1.00 ml, 8.25 mmol) was dissolved in 40 ml of methanol, and to this solution was added aniline (0.75 ml, 8.23 mmol). The mixture was stirred for 1 hour, and the solution concentrated *in vacuo* to aid precipitation of the yellow solid. This was followed by filtration, washing with cold methanol, and drying in air. ^{1}H NMR (250 MHz, $CDCl_3$) : δ = 2.26 (s, 3H, Ar-CH_3), 6.67 – 6.80 (m, 1H, ArH), 7.12 – 7.40 (m, 7H, ArH), 8.53 (s, 1H, N=CH).

L8

2-Hydroxy-3-methoxybenzaldehyde (5.41 g, 35.60 mmol) was reacted with 2,4,6-trimethylaniline (5.00 ml, 35.60 mmol) in a similar procedure to the above. Evaporation of the methanol solvent left a viscous orange oil. ^{1}H NMR (250MHz, $CDCl_3$) : δ = 2.09 (s, 6H, *o*-CH_3 on aniline), 2.21 (s, 3H, *p*-CH_3 on aniline), 4.02 (s, 3H, O-CH_3), 6.94-6.75 (m, 5H, ArH), 8.24 (s, 1H, N=CH).

L9

3,5-Ditertbutyl-2-hydroxybenzaldehyde (6.20 g, 26.50 mmol) was dissolved in methanol to give a yellow solution, to which was added 2,4,6-trimethylaniline (5.00 ml, 26.5 mmol). A colour change from yellow to green was observed immediately. The reaction was stirred vigorously for approximately 16 hours, after which a bright yellow precipitate had formed. This was filtered through a sintered glass frit, washed with cold methanol, and dried under vacuum. Yield 7.86 g, 85 %. ^{1}H NMR (300 MHz, $CDCl_3$): δ = 1.33 (s, 9H, CH_3), 1.49 (s, 9H, CH_3), 2.19 (s, 6H, *o*-CH_3 on aniline), 2.30 (s, 3H, *p*-CH_3 on aniline), 6.91 (s, 2H, ArH), 7.14 (d J = 2.44 Hz, 1H, ArH), 7.47 (d J = 2.58 Hz, 1H, ArH), 8.32 (s, 1H, N=CH).

L10

4-Hydroxy-3-methoxybenzaldehyde (5.41g, 35.60 mmol) was dissolved in 45 ml of methanol, and to this solution 2,4,6-trimethylaniline (5.00 ml, 35.60 mmol) was added. A colour change from deep purple to green was observed over the opening minutes of the reaction, which was stirred for 20 minutes. Removal of all the solvent gave a pale yellow solid which was thoroughly dried *in vacuo.* ^{1}H NMR (250 MHz, $CDCl_3$) : δ = 2.09 (s, 6H, *o*-CH_3 on aniline), 2.21 (s, 3H, *p*-CH_3 on aniline), 3.86 (s, 3H, O-CH_3), 6.94-6.75 (m, 5H, ArH), 8.24 (s, 1H, N=CH).

L11

4-Hydroxy-3-methoxybenzaldehyde (4.04 g, 26.50 mmol) was dissolved in 30 ml of methanol, and 2,6-diisopropylaniline (5.00 ml, 26.50 mmol) was added while stirring. The reaction was left stirring for approx. 14 hours, after which there was no apparent colour change. Refluxing at 80 °C for 3 hours, followed by rotary

evaporation to remove the majority of the solvent yielded an off-white powder, which was dried *in vacuo*. Yield 6.83 g, 90 %. ^{1}H NMR (300 MHz, $CDCl_3$) : δ = 1.17 (d J = 6.78 Hz, 12H, $CH(CH_3)_2$), 2.99 (m, 2H, $CH(CH_3)_2$), 4.02 (s, 3H, O-CH_3), 7.01 (d J = 7.88 Hz, 1H, ArH), 7.14 (m, 3H, ArH), 7.23 (m, 2H, ArH), 8.24 (s, 1H, N=CH).

L12

2-Hydroxy-5-methylisophthalaldehyde (1.00 g, 6.09 mmol) was reacted with aniline (1.13 g, 12.19 mmol) in 30 ml of methanol. After 2 hours a yellow powder had precipitated from the solution, and this was filtered, washed with cold methanol, and dried *in vacuo*. ^{1}H NMR (300 MHz, $CDCl_3$) : δ = 2.31 (s, 3H, CH_3), 7.19-7.37 (m, 12H, ArH), 8.76 (s, 2H, N=CH). MS ESI (+ve), $C_{21}H_{18}N_2O$, Actual: 337.1307, Theoretical: 337.1316

Zn(II) Complex Synthesis

$Zn_3(L1)_2(CH_3CO_2)_4$

$Zn(CH_3CO_2)_2.2H_2O$ (1.10 g, 5.1 mmol) was dissolved in methanol (20 ml) to which L1 (1.0 g, 5.1 mmol) was added. The solution was stirred for 1 hour, during which time a yellow solid precipitated out of solution. The solution was filtered and washed with cold methanol. The product was recrystallised from hot methanol. ^{1}H NMR (300 MHz, MeOD): δ = 1.99 (s, 12H, O_2C-CH_3), 6.76 (m, 2H, ArH), 6.90 (m, 2H, ArH), 7.25 – 7.47 (m, 14H, ArH), 8.62 (s, 2H, N=CH). $^{13}C\{^{1}H\}$ (300 MHz, MeOD): 22.3 (CH_3 acetate), 120.6 (C), 122.8 (CH), 123.4 (CH), 128.3 (CH), 130.9 (CH), 137.3 (CH), 137.3 (CH), 138.6 (CH), 150.5 (C), 171.1 (CH=N), 181.8 (CO_2). Calc. for $C_{34}H_{32}N_2O_{10}Zn_3$ C, 49.5; H, 3.91; N, 3.40. Found C, 49.5; H, 3.91; N, 3.40.

$Zn_3(L2)_2(CH_3CO_2)_4$

$Zn(CH_3CO_2)_2.2H_2O$ (0.51 g, 2.32 mmol) was reacted with L2 (0.65 g, 2.32 mmol) in 30 ml of methanol. The reaction was stirred vigorously at room temperature for approximately 5 hours, and cessation of stirring lead to a precipitate within minutes. The product was heated back in to solution with the addition of 10 ml of chloroform to aid recrystallisation. ^{1}H NMR (300 MHz, $(CD_3)_2SO$) : δ = 1.11 (s, 24H, $CH(CH_3)_2$),

1.79 (s, 12H, O_2C-C*H*$_3$), 2.99 (m, 4H, C*H*$(CH_3)_2$), 6.52 (s, 2H, ArH), 6.71 (s, 2H, ArH), 7.12-7.40 (m, 10H, ArH), 8.25 (s, 2H, N=CH). $^{13}C\{^1H\}$ NMR (300 MHz, $(CD_3)_2SO$) : δ = 22.4 (CH_3), 25.3 (CH_3 acetate), 27.5 (CH), 114.1 (CH), 118.4 (C), 122.5 (CH), 123.3 (CH), 126.3 (CH), 135.3 (CH), 137.0 (CH), 141.0 (C), 146.3 (C), 169.9 (C), 173.4 (CH=N), 177.4 (CO_2). Calc. for $C_{46}H_{56}N_2O_{10}Zn_3$ C, 55.6; H, 5.68; N, 2.82; Found C, 55.9; H, 5.77; N, 2.90.

Zn(L3)$_2$

$Zn(CH_3CO_2)_2.2H_2O$ (1.00 g, 4.56 mmol) was reacted with L3 (1.09 g, 4.56 mmol) in 40 ml of methanol. The reaction was refluxed at 80 °C for 16 hours with stirring. Cooling allowed a yellow precipitate to form. This was recrystallised from a 2:1 methanol/dichloromethane solution (30 ml). Crystals were grown over a period of 5 days at 5 °C. ^1H NMR (300 MHz, $(CD_3)_2SO$) : δ = 1.79 (s, 12H, CH_3), 2.25 (s, 6H, CH_3), 6.60 (m, 2H, ArH), 6.74 (d J=8.48 Hz, 2H, ArH), 6.88 (s, 4H, ArH), 7.35 (m, 4H, ArH), 8.26 (s, 2H, N=CH). $^{13}C\{^1H\}$ (300 MHz, $(CD_3)_2SO$) : δ = 17.4 (CH_3), 20.4 (CH_3), 114.3 (CH), 118.0 (CH), 122.5 (CH), 129.1 (CH), 130.0 (C), 135.2 (C), 135.8 (CH), 137.1 (CH), 145.5 (C), 170.7 (C), 175.3 (N=CH). Calc. for $C_{32}H_{32}N_2O_2Zn_1$ C, 70.9; H, 5.95; N, 5.17. Found C, 70.5; H, 5.92; N, 5.19.

Zn(L4)$_2$

$Zn(CH_3CO_2)_2.2H_2O$ (0.82 g, 3.73 mmol) was reacted with L4 (1.00 g, 3.77 mmol) in 40 ml of hot methanol. The mixture was stirred for 60 minutes, after which a precipitate had formed. Recrystallisation was from methanol. ^1H (300 MHz, $(CD_3)_2SO$) : δ = 7.19 – 7.43 (m, 6H, ArH), 7.44 – 7.64 (m, 8H, ArH), 8.51 (s, 2H, HC=N). $^{13}C\{^1H\}$ (300 MHz, $(CD_3)_2SO$) : δ = 115.5 (C), 120.4 (C), 122.6 (CH), 126.3 (C), 126.5 (CH), 128.9 (CH), 132.7 (CH), 133.8 (CH), 150.5 (C), 163.4 (C), 167.9 (CH=N). Calc. for $C_{26}H_{16}Cl_4N_2O_2Zn_1$ C, 52.4; H, 2.71; N, 4.70. Found C, 52.4; H, 2.68; N, 4.68.

Zn(L5)$_2$

L5 (1.40 g, 4.57 mmol) was dissolved in 50 ml of a methanol/chloroform mixture (4:1). To this solution was added $Zn(CH_3CO_2)_2.2H_2O$ (1.00 g, 4.56 mmol). The reaction was heated to reflux at 80 °C and after a few minutes a yellow precipitate was

formed. The reaction was left refluxing with vigorous stirring for 5 hours. After being left to cool, it was filtered through sintered glass and washed with methanol, before being thoroughly dried *in vacuo*. The product was recrystallised from a mixture of methanol, dichloromethane, and chloroform. ^{1}H NMR (300 MHz, $(CD_3)_2SO$) : δ = 1.89 (s, 12H, CH_3), 2.21 (s, 6H, CH_3), 6.80 (s, 4H, ArH), 7.36 (m, 4H, ArH), 8.22 (s, 2H, N=CH). $^{13}C\{^{1}H\}$ NMR (300 MHz, $(CD_3)_2SO$) : δ = 17.9 (CH_3), 20.4 (CH_3), 114.9 (C), 119.0 (C), 126.6 (C), 128.6 (CH), 129.2 (C), 132.9 (CH), 133.4 (CH), 134.4 (C), 146.5 (C), 163.8 (C), 173.4 (CH=N). Calc. for $C_{32}H_{28}Cl_4N_2O_2Zn_1$ C, 56.5; H, 4.15; N, 4.12. Found C, 56.2; H, 4.08; N, 4.11.

$Zn(L6)_2(MeOH)_2$

L9 (1.60 g, 4.57 mmol) was dissolved in 30 ml of hot methanol, to which $Zn(CH_3CO_2)_2.2H_2O$ (1.01 g, 4.56 mmol) was added immediately. The reaction was stirred for 12 hours, and the solvent then removed by rotary evaporation. The product was recrystallised from a 2:1 methanol/chloroform mixture (15 ml), which yielded yellow crystals. ^{1}H NMR (300 MHz, $CDCl_3$) : δ = 0.79 (s, 9H, CH_3), 0.98 (d J=6.73 Hz, 12H, CH_3), 1.10 (d J=6.71 Hz, 3H, CH_3), 1.99 (s, 2H, H_3C-O*H*), 2.85 (m, 4H, *H*C(CH_3)$_2$), 3.36 (s, 6H, *H*$_3$C-OH), 6.86 (d J=2.82 Hz, 2H, ArH), 6.99 (m, 4H, ArH), 7.10 (m, 2H, ArH), 7.31 (d J=2.83 Hz, 2H, ArH), 7.86 (s, 2H, N=CH). $^{13}C\{^{1}H\}$ NMR (300 MHz, $CDCl_3$) : δ =22.6, 23.5 (H*C*(CH_3)$_2$), 25.0, 28.3 (HC(*C*H_3)$_2$), 50.7 (CH_3OH), 117.3 (C), 118.1 (C), 124.0 (CH), 127.2 (CH), 128.1 (C), 132.8 (CH), 134.6 (CH), 140.9 (C), 145.9 (C), 164.8 (C), 173.4 (CH=N). Calc. for $C_{40}H_{48}Cl_4N_2O_4Zn_1$ C, 58.02; H, 5.84; N, 3.38; Found C, 57.9; H, 5.83; N, 3.44.

$Zn(L7)_2$

$Zn(CH_3CO_2)_2.2H_2O$ (1.45 g, 6.61 mmol) was reacted with L7 (1.00 g, 4.74 mmol) in 30 ml of methanol. The yellow precipitate was filtered and washed with cold methanol. Recrystallisation was from hot methanol. ^{1}H NMR (300 MHz, $(CD_3)_2SO$) : δ = 2.12 (s, 6H, CH_3), 6.52 – 6.61 (m, 2H, ArH), 7.15 – 7.51 (m, 14H, ArH), 8.71 (s, 2H, N=CH). $^{13}C\{^{1}H\}$ (300 MHz, $(CD_3)_2SO$) : δ = 17.0 (CH_3), 114.2 (CH), 117.7 (C), 121.4 (CH), 126.7 (CH), 129.5 (CH), 130.2 (C), 135.3 (CH), 135.7 (CH), 148.9 (C), 169.3 (C), 170.5 (CH=N). Calc. for $C_{28}H_{24}N_2O_2Zn_1$ C, 69.2; H, 4.98; N, 5.77. Found C, 70.0; H, 5.04, N,5.83.

$Zn_3(L8)_2(CH_3CO_2)_4$

An analogous procedure was carried out, except recrystallisation was from cold methanol. ^{1}H NMR (500 MHz, $CDCl_3$ – 40 °C) : δ = 1.91 (s, 6H, O_2C-C*H*$_3$), 2.17 (s, 6H, Ar-C*H*$_3$), 2.25 (s, 6H, O_2C-C*H*$_3$), 6.78 (m, 6H, ArH). 6.92 (m, 6H, Ar-H), 7.10 (s, 2H, ArH), 7.45 (m, 10H, ArH), 7.79 (s, 2H, N=CH), 7.85 (s, 2H, N=CH). ^{13}C{^{1}H} NMR (500 MHz, $CDCl_3$ – 40 °C) : δ = 19.6, 22.1, 23.6 (CH_3), 121.3, 122.8, 125.1, 125.6, 127.4, 127.9, 129.6, 141.2, 142.4, 148.0, 151.6 (Ar), 163.3 (Ar-O), 166.6, 168.4 (CH=N), 179.0, 180.3 (CO_2). Calc. for $C_{50}H_{46}N_4O_{10}Zn_3$ C, 56.7; H, 4.34; N, 5.29. Found C, 56.5; H, 4.36; N, 5.16.

Biodiesel Testing Procedure

Vegetable oil (20 g), methanol (8.5 g), and the catalyst are placed in an autoclave reactor along with a magnetic stirrer bar. The autoclave is securely closed to ensure that no methanol vapour can escape. The graphite bath is preheated to 195 °C, after which the autoclave is placed within it, and the reaction is stirred vigorously for the allotted time (usually 2 hours). The autoclave is then removed and the vessel cooled in cold water before opening. The reaction mixture is then poured in to a flask of cold deionised water, which aids separation of the FAME from the glycerol. The mixture will separate in to three distinct layers, with the FAME being the top. A portion of this can be removed using a pipette, and analysed by ^{1}H NMR in $CDCl_3$ to determine the conversion using the method reported in the literature.[9]

References

1. M. Jones, *Organic Chemistry*, 2nd edn., W.W. Norton and Company Inc., London, 2000.
2. A. J. Chmura, D. M. Cousins, M. G. Davidson, M. D. Jones, M. D. Lunn and M. F. Mahon, *Dalton Trans.*, 2008, 1437-1443.
3. P. Roy and M. Manassero, *Dalton Trans*, 2009, **39**, 1539-1545.

4. V. Arun, N. Sridevi, P. P. Robinson, S. Manju and K. K. M. Yusuff, *J. Mol. Catal. A-Chem.*, 2009, **304**, 191-198.
5. M. Dey, C. P. Rao, P. Saarenketo, K. Rissanen and E. Kolehmainen, *Eur. J. Inorg. Chem.*, 2002, 2207-2215.
6. P. de Hoog, L. D. Pachon, P. Gamez, M. Lutz, A. L. Spek and J. Reedijk, *Dalton Trans.*, 2004, 2614-2615.
7. J. F. Xie, J. Qiao, L. D. Wang, J. Xie and Y. Qiu, *Inorg. Chim. Acta*, 2005, **358**, 4451-4458.
8. L. Tatar, D. Ulku and O. Atakol, *Acta Crystallogr. Sect. C-Cryst. Struct. Commun.*, 1999, **55**, 508-510.
9. G. Gelbard, O. Bres, R. M. Vargas, F. Vielfaure and U. F. Schuchardt, *Journal of the American Oil Chemists Society*, 1995, **72**, 1239-1241.
10. M. G. Kulkarni, R. Gopinath, L. C. Meher and A. K. Dalai, *Green Chemistry*, 2006, **8**, 1056-1062.
11. M. D. Jones, M. G. Davidson, C. G. Keir, L. M. Hughes, M. F. Mahon and D. C. Apperley, *European Journal of Inorganic Chemistry*, 2009, 635-642.

Chapter 4: Results and Discussion on the use of Silsesquioxanes as Homogeneous Model Compounds

4.1 Introduction to Silsesquioxanes

Silsesquioxanes are compounds of the general formula $(RSiO_{1.5})_a(H_2O)_{0.5\,b}$, where R is a hydrogen or organic group, and *a* and *b* are integers, with *a* representing the number of siloxane units and *b* the degree of condensation. The most useful are the incompletely condensed *a*7b*3* variants, as the lack of a silicon vertex allows them to bind through three silanol groups (**Figure 4.1.1**).

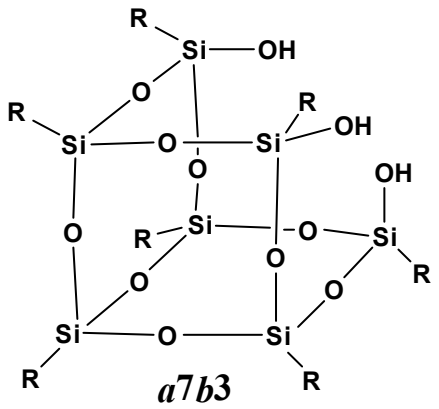

Figure 4.1.1: Molecular diagram of an *a*7*b*3 silsesquioxane, where R = isobutyl, isooctyl, cyclopentyl, cyclohexyl, phenyl etc.

Silsesquioxanes are extremely useful as soluble homogeneous models for silica surface sites. This leads to a greater understanding of how a metal may bind to a silica or zeolite support in heterogeneous catalysts. A great variety of metal-silsesquioxane complexes have been reported in the literature.[1] For example, Ducahteau *et al* have created half-sandwich Ti(IV) and Zr(IV) complexes stabilised by a condensed silsesquioxane, as models for silica grafted alkene polymerisation catalysts (**Figure 4.1.2**).[2]

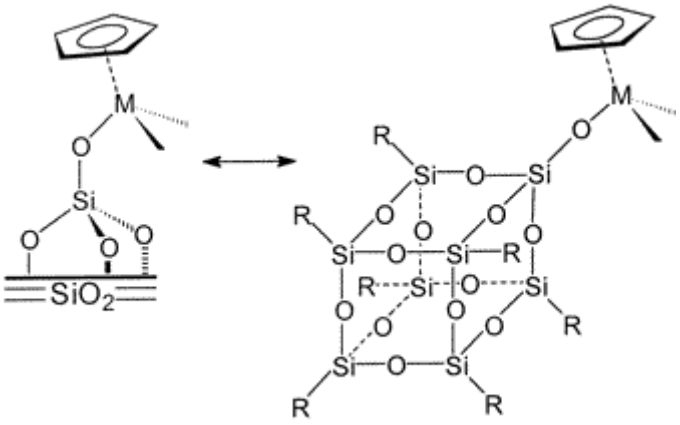

Figure 4.1.2: Example of how silsesquioxanes can be used to model silica surfaces

The same group has also prepared Zn-alkyl silsesquioxane complexes as models for the copolymerisation of cyclohexene oxide and CO_2,[3] as well as Al(III) and Ga(III) silsesquioxane complexes.[4,5] Pescarmona *et al* have prepared osmium silsesquioxanes as models for the dehydroxylation of alkenes.[6] In this work, novel silsesquioxane complexes were synthesised utilising titanium, zinc and aluminium metals.

4.2 Synthesis and Characterisation of Metal-Silsesquioxane Complexes Al-Sils1 and Ti-Sils1

Al-Sils1 was prepared using isobutyl silsesquioxane *a*7*b*3, which was reacted 1:1 with $Al(Me)_3$ in dry THF (**Figure 4.2.1**).

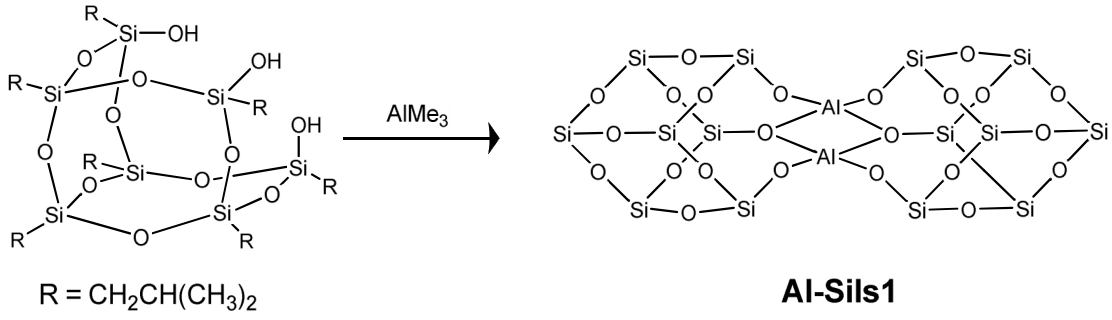

Figure 4.2.1: Reaction scheme for the formation of **Al-Sils1**

Crystals of suitable quality for single crystal X-ray diffraction were grown from a hexane solution. **Al-Sils1** is a dimeric species that crystallises in the triclinic space group *P*-1, with one molecule in the asymmetric unit that is related by the –x, y+1, -z+1 symmetry operation (**Figure 4.2.2**).

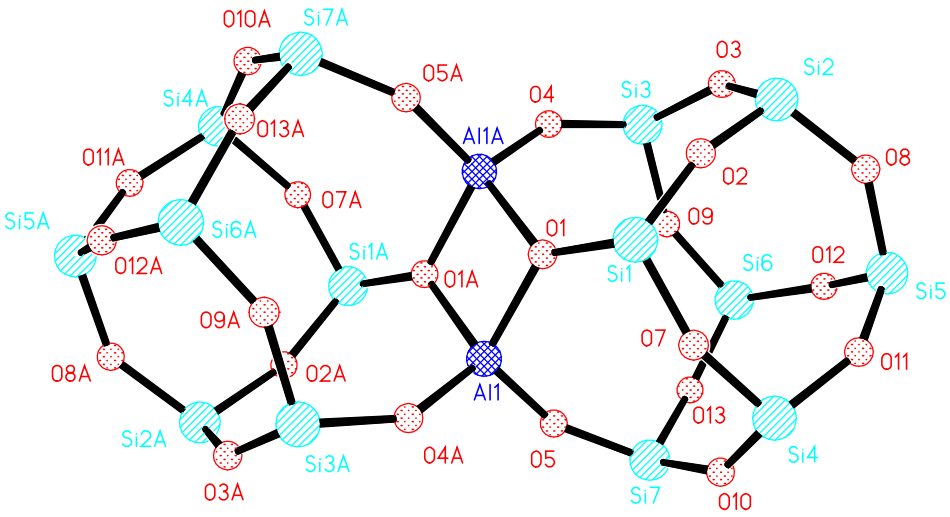

Figure 4.2.2: Molecular structure of **Al-Sils1**. Isobutyl groups have been omitted for clarity. Labels with suffix **A** relate to those in the asymmetric unit by –x, y+1, -z+1 symmetry operation

The two aluminium centres are pseudo-tetrahedral, and this is exemplified by the O(1)-Al(1)-O(5) angle of 113.95(13) °. Each Al atom is bound to two terminal silanol groups, one from each ligand, and two bridging silanols, O(1) and O(1A). The bond length for Al(1)-O(1) is 1.838(3) Å, which is significantly longer than that of Al(1)-O(4A) and Al(1)-O(5) which are 1.687(3) Å and 1.685(3) Å. A bridging silanol will have longer bond lengths than a terminal species as the electron density on the oxygen is shared over two bonds. A similar complex was previously reported by Feher *et al*, using a cyclohexyl silsesquioxane, and the bond lengths and angles seem to be in agreement.[7] **Table 4.2.1** contains summarises key bond lengths (Å) and angles (°) for complex **Al-Sils1**.

	Al-Sils1
Al(1)-O(1)	1.838(3)
Al(1)-O(5)	1.685(3)
Al(1)-O(4A)	1.687(3)
Al(1)-O(1A)	1.830(3)
O(1)-Al(1)-O(5)	113.95(13)
O(1)-Al(1)-O(4A)	113.59(13)
O(4A)-Al(1)-O(5)	116.64(13)

Table 4.2.1: Selected bond lengths (Å) and angles (°) for **Al-Sils1**

The complex was further characterised by multiple nuclei solution NMR spectroscopy. The solution structure is in agreement with the solid-state structure shown above. The ^{29}Si NMR spectrum, shows five singlets in the approximate ratio 1:2:2:1:1 at -63.0, -64.0., -66.5, -67.0, and -70.5 ppm respectively, which is again in agreement with the analogous complex prepared by Feher *et al.*[7]

The titanium complex **Ti-Sils1**, formed from the reaction of Ti(^{i}Opr)$_4$ and the isobutyl silsesquioxane, is also a dimeric species (**Figure 4.2.3**). However the structure is somewhat different as the two Ti metal centres are bridged by isopropoxide - 115 -ligands. Each Ti is bound to three terminal silanol groups of one silsesquioxane unit, and two μ-2 isopropoxide - 115 -ligands which bridge the Ti atoms.

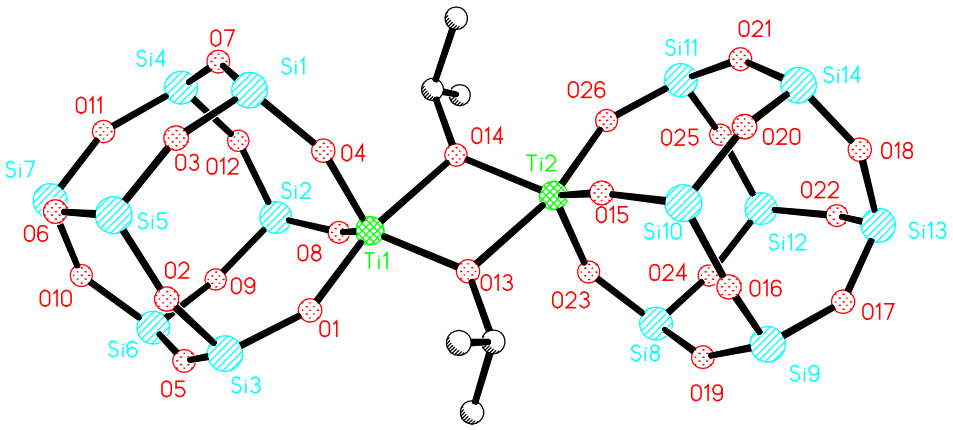

Figure 4.2.3: The molecular structure of **Ti-Sils1**. The isobutyl groups have been omitted for clarity.

A similar structure has been reported by Maschmeyer *et al* using cyclopentane and cyclohexane silsesquioxanes.[8] Selected bond lengths and angles are given below (**Table 4.2.2**).

	Ti-Sils1
Ti(1)-O(4)	1.7949(18)
Ti(1)-O(1)	1.8206(18)
Ti(1)-O(8)	1.8118(17)
Ti(1)-O(13)	1.9227(17)
Ti(1)-O(14)	2.1261(16)
O(1)-Ti(1)-O(14)	167.90(8)
O(1)-Ti(1)-O(13)	96.01(8)
O(1)-Ti(1)-O(4)	98.64(9)

Table 4.2.2: Selected bond lengths (Å) and angles (°) for **Ti-Sils1**

The solution NMR spectrum shows that the complex is mostly monomeric, although weak signals were detected for the dimeric species in the ^{29}Si NMR, with the two structures being in equilibrium, as has previously been reported by Crocker for the analogous cyclohexane silsesquioxane compound.[9] The ^{1}H NMR spectroscopy shows only one isopropoxide methane resonance indicative of the monomeric species shown in **Figure 4.2.4.**

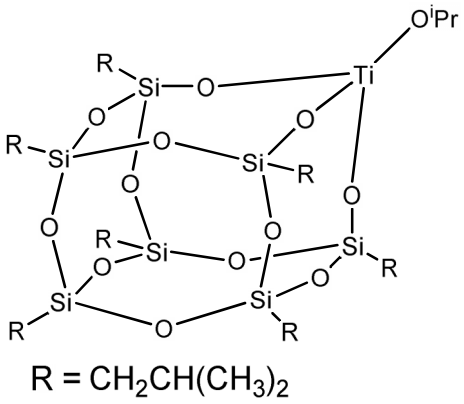

Figure 4.2.4 : Structure of the monomeric species

^{29}Si NMR shows three main peaks for the silsesquioxane Si atoms in a 3:1:3 ratio, which is consistent with the C_{3v} symmetry expected of such a monomeric complex, as well as previous literature.[9] Five distinct Si environments in a 2:2:1:1:1 ratio corresponds to the presence of small amounts of the dimer.

4.3 Synthesis and Characterisation of Two Distinct Zinc-Silsesquioxane Complexes

Isobutyl silsesquioxane *a*7*b*3 was reacted with two equivalents of $ZnMe_2$ in both toluene and THF solvents (**Figure 4.3.1**). Both reactions produced distinct, isolatable Zn(II) complexes which were characterised by single crystal X-ray diffraction as well as ^{1}H, ^{13}C and ^{29}Si{^{1}H} NMR spectroscopy. A search of the literature reveals that only one other Zn(II) silsesquioxane has been crystallographically characterised, though an analogous Mg(II) complex has been reported where an *a*7*b*3 silsesquioxane was reacted with an organometallic magnesium source.[10,11]

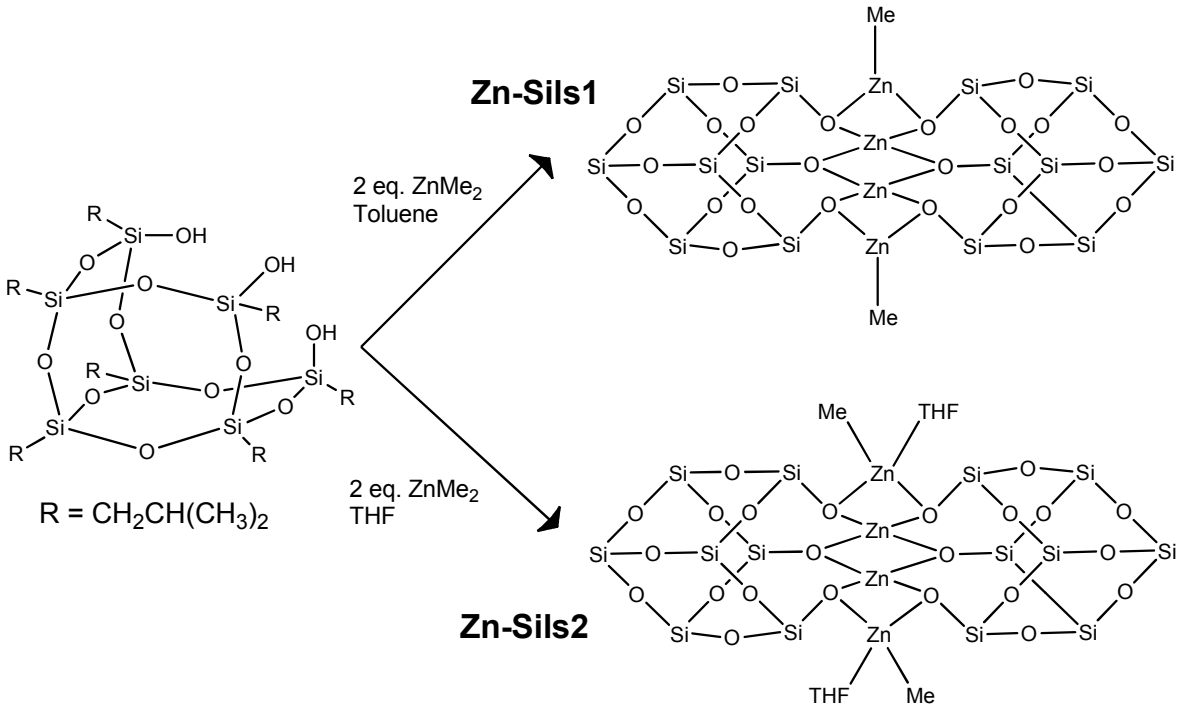

Figure 4.3.1: The two Zn(II) silsesquioxane complexes prepared

Reaction of the parent silsesquioxane with two equivalents of $ZnMe_2$ in toluene gave **Zn-Sils1**. Recrystallisation was from hexane, and crystals suitable for single crystal X-ray diffraction were produced after standing a number of days at ambient temperature. The complex features a tetrameric zinc component, which is capped by two silsesquioxane units (**Figure 4.3.2**).

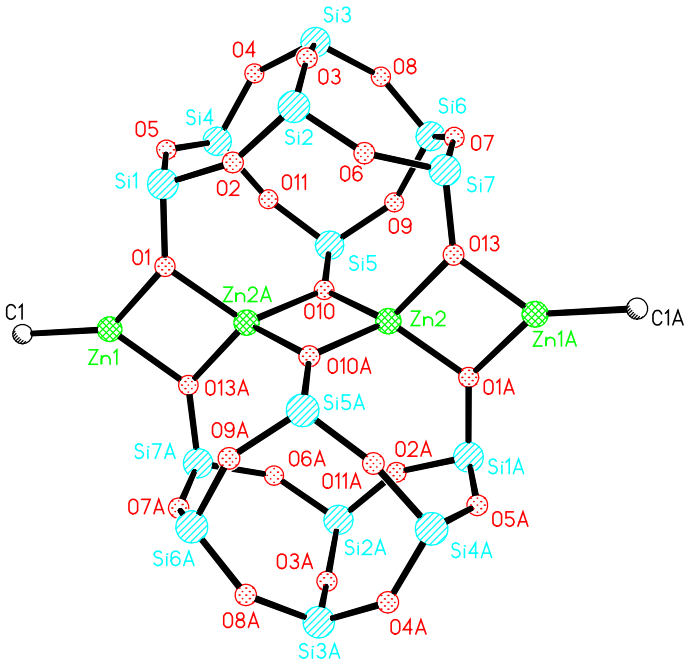

Figure 4.3.2: Molecular structure of **Zn-Sils1**. *Iso*-butyl groups and hydrogen atoms have been removed for clarity. Labels with suffix **A** relate to those in the asymmetric unit by the –x, y+1,-z+1 symmetry operation.

The complex crystallises in the triclinic space group *P*-1, and there exists two distinct Zn environments within the structure. The two core zN atoms form part of a four-membered ring and are related by a centre of inversion within the structure. The central unit of the structure consists of three planar four-membered rings, each made up of two zinc and two oxygen atoms. The inner ring {Zn(2), O(13A), Zn(2A), O(13)}, appears to be almost perpendicular to the two outer rings, and the angle between the planes formed by the inner ring and {Zn(1), O(5A), Zn(2),O(2)} is 87°. Zn(1) is bound to two oxygen atoms and a methyl group, and is in a highly distorted trigonal planar environment. The ring structure imposes a tight O(2)-Zn(1)-O(5A) angle of 84.64(11) °, which results in the other bond angles being much greater than

the ideal, 139.70(18) ° and 135.60(18) ° for O(2)-Zn(1)-C(1) and O(5A)-Zn(1)-O(5) respectively. These are similar to those reported by Duchateau *et al* for the only other previously reported Zn(II) silsesquioxane.[10] Zn(1)-C(1) bond distance is 1.922(5) Å and again is in agreement with the literature.[12]

The Zn atoms in the central unit are in a distorted tetrahedral environment, bound to four oxygen atoms. This is where the structure most significantly differs from that of Duchateau *et al*.[10] The parent silsesquioxane used by Duchateau has a methyldiphenylsilyl group in place of a silanol unit, leaving only two silanols capable of binding to a metal per silsesquioxane molecule. As a result an open cage structure is produced, where one of the oxygen moieties is bound to three Zn(II) atoms, all four of which retain a methyl group.[10] The central metallic core in **Zn-Sils1** is analogous to that of the Mg(II) silsesquioxane reported in the literature.[11] The distorted tetrahedral geometry is supported by the bond angles O(13)-Zn(2)-O(2) 120.70(10) ° and O(13)-Zn(2)-O(13A) 87.71(11) °.

The solid state structure is retained in solution, as confirmed by ^{29}Si NMR spectroscopy which exhibited five peaks in a 2:1:1:2:1 ratio expected for the solid state structure in solution. Proton and carbon NMR spectra also confirmed the presence of a Zn-CH_3 bond with singlets at -0.12 (^{1}H) and -15.7 (^{13}C{^{1}H}) ppm respectively, consistent with what has been reported.[12]

The reaction was also carried out using THF as the solvent, which resulted in the isolation **Zn-Sils2**. The composition of this complex is identical to that of the previous with the exception of a molecule of THF coordinated to each of the two outer Zn(II) atoms, resulting in a different structure (**Figure 4.3.3**).

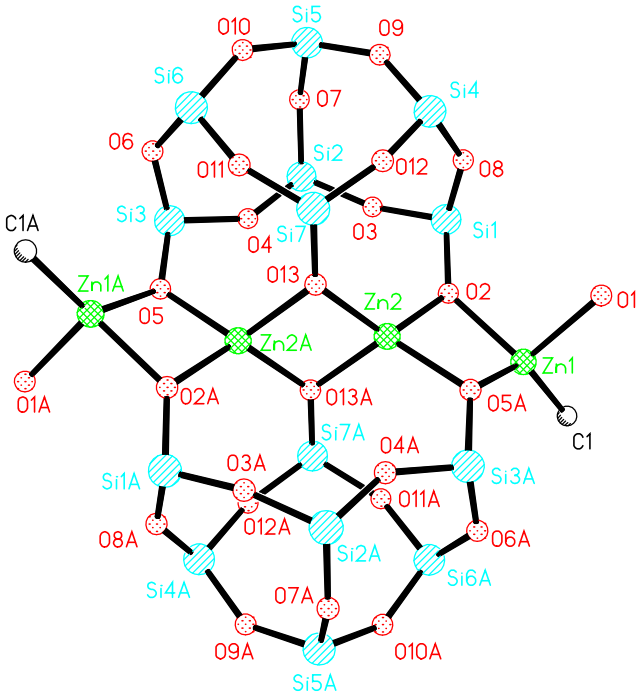

Figure 4.3.3: The molecular structure of **Zn-Sils2.** The *iso*-butyl groups, hydrogen atoms and the carbons of the THF have been omitted for clarity. Labels with suffix **A** relate to those in the asymmetric unit by the -x,-y+1,-z+1 symmetry operation.

Once again recrystallisation was from the minimum of hexane, however in this instance it took several weeks at -20°C for crystals of suitable quality to form. The outer two four-membered rings are more puckered than those in **Zn-Sils1**, as illustrated by the angle between the two planes created by Zn(2)-O(5A)-O(2) and O(2)-Zn(1)-O(5A), which is 161 ° compared to 177 ° in **Zn-Sils1**. The coordination of a molecule of THF solvent means that the outer metal atoms Zn(1) and Zn(1A) are now in a distorted tetrahedral geometry, which is supported by bond angles given in the table below (**Table 4.3.1**). The bond lengths between the outer Zn(II) and the oxygen atoms of the silsesquioxane units are also considerably longer in **Zn-Sils2** compared to **Zn-Sils1**. As with **Zn-Sils1**, ^{29}Si NMR spectroscopy gave five resonances (2:1:1:2:1) confirming that the solid structure was retained in solution, and the Zn-Me linkage was again observed in the ^{1}H and ^{13}C spectra with singlet peaks at -0.18 (^{1}H) and -15.6 (^{13}C{^{1}H}) ppm respectively.[12]

	Zn-Sils1	Zn-Sils2
Zn(1)-O(1)	-	2.127(3)
Zn(1)-C(1)	1.923(5)	1.951(4)
Zn(1)-O(2)	1.954(3)	2.015(2)
Zn(1)-O(5A)	1.959(3)	2.021(2)
Zn(2)-O(2)	1.956(3)	1.949(2)
Zn(2)-O(13)	1.959(3)	1.946(2)
Zn(2)-O(13A)	1.951(3)	1.984(2)
Zn(2)-O(5A)	1.946(3)	1.961(2)
O(1)-Zn(1)-C(1)	-	107.42(14)
O(2)-Zn(1)-C(1)	139.71(18)	131.17(14)
O(2)-Zn(1)-O(5A)	84.65(11)	83.06(8)
O(1)-Zn(1)-O(2)	-	97.76(10)
O(13)-Zn(2)-O(2)	120.69(10)	123.43(8)
O(13)-Zn(2)-O(5A)	119.41(12)	129.48(9)

Table 4.3.1: Selected bond lengths (Å) and angles (°) for **Zn-Sils1** and **Zn-Sils2**

4.4 Conclusions

Reaction of an incompletely condensed silsesquioxane with titanium, aluminium, and zinc yielded the complexes **Ti-Sils1**, **Al-Sils1, Zn-Sils1,** and **Zn-Sils2** respectively. All were characterised by single crystal X-ray diffraction. The latter two are dimers in the solid-state, and are suitable homogenous models of heterogeneous catalysts in which Ti or Al are grafted to silica. Zn-Sils1 and Zn-Sils2 both feature a tetrameric zinc core. To date, only one other Zn(II) silsesquioxane complex has been crystallographically characterised and reported in the literature.[10]

4.5 Experimental

General Experimental Procedures

All procedures involved standard air sensitive techniques, and all products were synthesised under an atmosphere of argon. Isobutyl silsesquioxane *a*7*b*3, $AlMe_3$ (2.0M in hexane), $Ti(^iOPr)_4$ and $ZnMe_2$ (2.0M in toluene) were purchased from Aldrich and used without further purification. ^1H and $^{13}C\{^1H\}$ NMR spectra were recorded on a Bruker 300 MHz spectrometer. Chemical shifts are reported in ppm and referenced to residual solvent peaks. Coupling constants are given in Hertz. ^{29}Si NMR spectra were recorded by Dr John Lowe at the University of Bath on a Bruker 500 MHz spectrometer, and spectral referencing is with respect to tetramethylsilane. Elemental analysis was performed by Mr A. K. Carver at the University of Bath. Crystallographic data was collected on a Nonius Kappa CCD area detector diffractometer using Mo-Kα radiation (λ = 0.71073 Å) at a temperature of 150 K. Structures were solved by direct methods and refined on all F^2 data using the SHELXL-97 program suite. Hydrogen atoms were included in idealised positions and refined using the riding model.

Al-Sils1 [(*iso*-C_4H_9)$_7$$Si_7O_{12}$]$_2$$Al_2$

Isobutyl silsesquioxane *a*7*b*3 (1.76 g, 2.22 mmol) was reacted with 2.0 M $AlMe_3$ solution in hexane (1.11 ml, 2.22 mmol) in 15 ml of THF. The reaction was stirred under argon for one hour, the solvent removed under reduced pressure, the product dissolved in 10 ml of hot hexane, and left to recrystallise at room temperature. After 2 days crystals had formed suitable for a single-crystal X-ray diffraction. ^1H NMR (300 MHz, $CDCl_3$) : δ = 0.54 (d J = 7.0 Hz, 12H, $SiCH_2$), 0.60 (d J = 7.0 Hz, 12H, $SiCH_2$), 0.75 (d J = 7.0 Hz, 4H, $SiCH_2$), 0.96 (m, 84H CH_3), 1.84 (sept J = 7.0 Hz, 12H, CH), 2.01 (sept J = 7.0 Hz, 2H, CH).^{13}C NMR (300 MHz, $CDCl_3$) : δ = 22.4, 22.5, 22.9, 23.2 (CH_2), 23.2 (CH), 23.4 (CH_2), 23.9, 24.0, 24.1 (CH), 25.6, 25.6, 25.7, 25.7, 25.9, 25.9, 26.0 (CH_3). ^{29}Si ($CDCl_3$) : δ = -63.0, -64.0, -66.5, -67.0, -70.5 in a 1:2:2:1:1 ratio. Elemental analysis: Calc. for $C_{56}H_{126}Al_2O_{24}Si_{14}$ C, 41.24; H 7.79. Found C, 40.7; H, 7.78.

Ti-Sils1 [(*iso*-C_4H_9)$_7Si_7O_{12}$]$_2Ti_2$(O^iPr)$_2$

Isobutyl silsesquioxane *a*7b*3* (1.00 g, 1.26 mmol) was dissolved in 40 ml of toluene. Ti(^{i}OPr)$_4$ (0.36 g, 1.26 mmol) was then added and the reaction stirred vigorously for 26 hours. The solvent was then removed *in vacuo* and the product recrystallised from 12 ml of hot hexane, after 2 days in a -20 °C freezer. ^{1}H NMR (300 MHz, $CDCl_3$): δ = 0.50 (m, 14H, $SiCH_2$), 0.98 (m, 42H, CH_3 silses), 1.30 (d J = 6 Hz, 6H, CH_3 isopropoxide), 1.85 (m, 7H, CH silses), 4.56 (sept J = 6 Hz, 1H, CH isopropoxide). ^{13}C{^{1}H} (300 MHz, $CDCl_3$) : δ = 22.3 (CH_2), 22.6 (CH_2), 23.9, 25.7, 25.7, 25.8, 79.5 (CH/CH_3). ^{29}Si{^{1}H} ($CDCl_3$) : δ = -65.5, -67.9, -68.8 (in a 3:1:3 ratio). Calc. for $C_{31}H_{70}O_{13}Si_7Ti_1$ C, 41.59; H, 7.88. Found C, 41.2; H, 7.75.

Zn-Sils1 [(*iso*-C_4H_9)$_7Si_7O_{12}$]$_2Zn_4Me_2$

Isobutyl silsesquioxane (1.57g, 2.00 mmol) was dissolved in 30 ml of toluene. To this $ZnMe_2$ (2.00 ml, 2M in hexane, 4.00 mmol) was added and vigorous effervescence was noted. The reaction was stirred at room temperature for 1 hour, after which the solvent was removed *in vacuo* and the product recrystallised from the minimum amount of hexane. Suitable crystals for X-ray diffraction were removed after 24 hours at ambient temperature. ^{1}H NMR (300 MHz, C_6D_6): δ = 0.12 (s, 6H, Zn-CH_3), 0.77 – 0.99 (m, 28H, $SiCH_2$), 1.02 – 1.34 (m, 84H, CH_3), 2.02 – 2.30 (m, 14H, CH). ^{13}C{^{1}H} (300 MHz, C_6D_6): δ = – 15.7 (Zn-CH_3), 22.9, 23.2 (CH_2), 24.4 (CH_2), 24.4, 24.5, 24.6 (CH), 24.7 (CH_2), 24.8 (CH), 24.9 (CH_2), 25.9, 26.1, 26.2, 26.2, 26.4, 26.6, 26.7 (CH_3). ^{29}Si{^{1}H} ($CDCl_3$): δ = – 57.7, – 62.5, – 64.9, – 65.3, – 70.3 (2:1:1:2:1 ratio). Calc. for $C_{58}H_{132}Zn_4O_{24}Si_{14}$ C, 37.28; H, 7.12. Found C, 37.3; H, 6.94.

Zn-Sils2 [(*iso*-C_4H_9)$_7Si_7O_{12}$]$_2Zn_4Me_2THF_2$

Isobutyl silsesquioxane (1.57g, 2.00 mmol) was dissolved in 30 ml of THF. To this $ZnMe_2$ (2.00 ml, 2M in hexane, 4.00 mmol) was added and vigorous effervescence was noted. The reaction was stirred at room temperature for 1 hour, after which the solvent was removed *in vacuo* and the white solid product recrystallised from the minimum amount of hexane. Suitable crystals for X-ray diffraction were removed after 3 weeks at -20 °C. ^{1}H NMR (300 MHz, C_6D_6): δ = 0.18 (s, 6H, Zn-CH_3), 0.76 –

0.98 (m, 28H, $SiCH_2$), 1.05 – 1.40 (m, 84H, CH_3), 1.53 (br m, 8H, CH_2 THF), 2.03 – 2.30 (m, 14H, CH), 3.82 (br m, 8H, CH_2 THF). $^{13}C\{^1H\}$ (300 MHz, C_6D_6): δ = – 15.6 (Zn-CH_3), 23.0, 23.5 (CH_2), 24.5, 24.5, 24.6 (CH), 24.6 (CH_2), 24.7 (CH_2), 24.8 (CH), 25.1 (CH_2), 25.5 (CH_2 THF), 26.0, 26.2, 26.2, 26.3, 26.5, 26.7, 26.8 (CH_3), 68.8 (O-CH_2 THF). $^{29}Si\{^1H\}$ ($CDCl_3$): δ = – 58.1, – 62.9, – 64.9, – 65.1, – 70.4 (2:1:1:2:1 ratio). Calc. for $C_{66}H_{148}Zn_4O_{26}Si_{14}$ C, 39.39; H, 7.41. Found C, 38.9; H, 7.01.

References

1. R. Duchateau, *Chem. Rev.*, 2002, **102**, 3525-3542.
2. R. Duchateau, H. C. L. Abbenhuis, R. A. van Santen, S. K. H. Thiele and M. F. H. van Tol, *Organometallics*, 1998, **17**, 5222-5224.
3. R. Duchateau, W. J. van Meerendonkt, S. Huijser, B. B. P. Staal, M. A. van Schilt, G. Gerritsen, A. Meetsma, C. E. Koning, M. F. Kemmere and J. T. F. Keurentjes, *Organometallics*, 2007, **26**, 4204-4211.
4. G. Gerritsen, R. Duchateau, R. A. van Santen and G. P. A. Yap, *Organometallics*, 2003, **22**, 100-110.
5. R. Duchateau, T. W. Dijkstra, J. R. Severn, R. A. van Santen and I. V. Korobkov, *Dalton Transactions*, 2004, 2677-2682.
6. P. P. Pescarmona, A. F. Masters, J. C. van der Waal and T. Maschmeyer, *J. Mol. Catal. A-Chem.*, 2004, **220**, 37-42.
7. F. J. Feher, T. A. Budzichowski and K. J. Weller, *J. Am. Chem. Soc.*, 1989, **111**, 7288-7289.
8. T. Maschmeyer, M. C. Klunduk, C. M. Martin, D. S. Shephard, J. M. Thomas and B. F. G. Johnson, *Chem. Commun.*, 1997, 1847-1848.
9. M. Crocker, R. H. M. Herold and A. G. Orpen, *Chem. Commun.*, 1997, 2411-2412.
10. R. Duchateau, W. J. van Meerendonkt, S. Huijser, B. B. P. Staal, M. A. van Schilt, G. Gerritsen, A. Meetsma, C. E. Koning, M. F. Kemmere and J. T. F. Keurentjes, *Organometallics*, 2007, **26**, 4204-4211.
11. R. Hanssen, A. Meetsma, R. A. van Santen and H. C. L. Abbenhuis, *Inorg. Chem.*, 2001, **40**, 4049-4052.
12. K. Merz, H. M. Hu, S. Rell and M. Driess, *Eur. J. Inorg. Chem.*, 2003, 51-53.

Chapter 5: Appendix

Crystal data and structure refinement for **$Zn_3(L1)_2(CH_3CO_2)_4$**

Identification code	k07mdj02
Empirical formula	C34 H32 N2 O10 Zn3
Formula weight	824.73
Temperature	150(2) K
Wavelength	0.71073 A
Crystal system, space group	Triclinic, P-1
Unit cell dimensions	a = 7.5650(3) A alpha = 93.511(2) deg. b = 9.7100(4) A beta = 98.233(2) deg. c = 11.5100(5) A gamma = 100.016(2) deg.
Volume	820.79(6) A^3
Z, Calculated density	1, 1.669 Mg/m^3
Absorption coefficient	2.236 mm^-1
F(000)	420
Crystal size	0.20 x 0.15 x 0.10 mm
Theta range for data collection	3.52 to 25.12 deg.
Limiting indices	-8<=h<=8, -11<=k<=11, -13<=l<=13
Reflections collected / unique	8284 / 2885 [R(int) = 0.0552]
Completeness to theta = 25.12	98.1 %
Absorption correction	Semi-empirical from equivalents
Max. and min. transmission	0.8073 and 0.6633
Refinement method	Full-matrix least-squares on F^2
Data / restraints / parameters	2885 / 0 / 224
Goodness-of-fit on F^2	1.040
Final R indices [I>2sigma(I)]	R1 = 0.0364, wR2 = 0.0857
R indices (all data)	R1 = 0.0521, wR2 = 0.0941
Extinction coefficient	0.009(2)
Largest diff. peak and hole	0.555 and -0.691 e.A^

Crystal data and structure refinement for **$Zn_3(L2)_2(CH_3CO_2)_4$**

Identification code	k07mdj08
Empirical formula	C23 H28 N O5 Zn1.50
Formula weight	496.52
Temperature	150(2) K
Wavelength	0.71073 A
Crystal system, space group	Triclinic, P-1
Unit cell dimensions	a = 8.4590(2) A alpha = 82.833(2) deg. b = 9.3100(3) A beta = 77.882(2) deg. c = 16.3850(6) A gamma = 64.206(1) deg.
Volume	1135.10(6) A^3
Z, Calculated density	2, 1.453 Mg/m^3
Absorption coefficient	1.631 mm^-1
F(000)	516
Crystal size	0.30 x 0.20 x 0.10 mm
Theta range for data collection	3.59 to 25.10 deg.
Limiting indices	-10<=h<=10, -11<=k<=11, -19<=l<=19
Reflections collected / unique	12453 / 3993 [R(int) = 0.0515]
Completeness to theta = 25.10	98.9 %
Absorption correction	Multi scan
Max. and min. transmission	0.8539 and 0.6405
Refinement method	Full-matrix least-squares on F^2
Data / restraints / parameters	3993 / 0 / 283
Goodness-of-fit on F^2	1.169
Final R indices [I>2sigma(I)]	R1 = 0.0474, wR2 = 0.1063
R indices (all data)	R1 = 0.0618, wR2 = 0.1118
Largest diff. peak and hole	0.644 and -0.464 e.A^-3

Crystal data and structure refinement for **$Zn(L3)_2$**

Identification code	h07mdj03
Empirical formula	C16 H16 N O Zn0.50
Formula weight	270.98
Temperature	150(2) K
Wavelength	0.71073 A
Crystal system, space group	Orthorhombic, Pcab
Unit cell dimensions	a = 16.1880(2) A alpha = 90 deg. b = 16.7170(2) A beta = 90 deg. c = 20.0650(2) A gamma = 90 deg.
Volume	5429.89(11) A^3
Z, Calculated density	16, 1.326 Mg/m^3
Absorption coefficient	0.936 mm^-1
F(000)	2272
Crystal size	0.20 x 0.15 x 0.10 mm
Theta range for data collection	3.65 to 27.47 deg.
Limiting indices	-18<=h<=20, -21<=k<=21, -26<=l<=26
Reflections collected / unique	72317 / 6189 [R(int) = 0.0754]
Completeness to theta = 27.47	99.6 %
Absorption correction	Multi scan
Max. and min. transmission	0.9122 and 0.8349
Refinement method	Full-matrix least-squares on F^2
Data / restraints / parameters	6189 / 0 / 348
Goodness-of-fit on F^2	1.054
Final R indices [I>2sigma(I)]	R1 = 0.0366, wR2 = 0.0876
R indices (all data)	R1 = 0.0722, wR2 = 0.0996
Largest diff. peak and hole	0.398 and -0.495 e.A^-3

Crystal data and structure refinement for **$Zn(L4)_2$**

Identification code	k07mdj03
Empirical formula	C26 H16 Cl4 N2 O2 Zn
Formula weight	595.58
Temperature	150(2) K
Wavelength	0.71073 A
Crystal system, space group	monoclinic, C2/c
Unit cell dimensions	a = 23.9480(6) A alpha = 90 deg. b = 9.1820(2) A beta = 110.131(10) deg. c = 11.7830(3) A gamma = 90 deg.
Volume	2432.68(10) A^3
Z, Calculated density	4, 1.626 Mg/m^3
Absorption coefficient	1.477 mm^-1
F(000)	1200
Crystal size	0.20 x 0.15 x 0.12 mm
Theta range for data collection	3.62 to 27.49 deg.
Limiting indices	-30<=h<=30, -11<=k<=11, -15<=l<=15
Reflections collected / unique	20007 / 2783 [R(int) = 0.0433]
Completeness to theta = 27.49	99.7 %
Absorption correction	None
Max. and min. transmission	0.8426 and 0.7565
Refinement method	Full-matrix least-squares on F^2
Data / restraints / parameters	2783 / 0 / 155
Goodness-of-fit on F^2	1.077
Final R indices [I>2sigma(I)]	R1 = 0.0347, wR2 = 0.0837
R indices (all data)	R1 = 0.0457, wR2 = 0.0896
Largest diff. peak and hole	0.679 and -0.536 e.A^-3

Crystal data and structure refinement for **$Zn(L5)_2$**

Identification code	k07mdj04
Empirical formula	C17 H16 Cl4 N O Zn0.50
Formula weight	424.79
Temperature	150(2) K
Wavelength	0.71073 A
Crystal system, space group	Monoclinic, P2/c
Unit cell dimensions	a = 11.600(2) A alpha = 90 deg. b = 8.3470(1) A beta = 105.174(1) deg. c = 18.4130(3) A gamma = 90 deg.
Volume	1720.68(5) A^3
Z, Calculated density	4, 1.640 Mg/m^3
Absorption coefficient	1.371 mm^-1
F(000)	864
Crystal size	0.30 x 0.15 x 0.15 mm
Theta range for data collection	3.64 to 27.51 deg.
Limiting indices	-15<=h<=15, -10<=k<=10, -23<=l<=23
Reflections collected / unique	27921 / 3938 [R(int) = 0.0397]
Completeness to theta = 27.51	99.5 %
Absorption correction	Semi-empirical from equivalents
Max. and min. transmission	0.8207 and 0.6838
Refinement method	Full-matrix least-squares on F^2
Data / restraints / parameters	3938 / 18 / 235
Goodness-of-fit on F^2	1.071
Final R indices [I>2sigma(I)]	R1 = 0.0650, wR2 = 0.1771
R indices (all data)	R1 = 0.0736, wR2 = 0.1862
Extinction coefficient	0.010(2)
Largest diff. peak and hole	0.850 and -1.620 e.A^-3

Crystal data and structure refinement for **$Zn(L6)_2(MeOH)_2$**

Identification code	k07mdj06
Empirical formula	C20 H24 Cl2 N O2 Zn0.50
Formula weight	413.99
Temperature	150(2) K
Wavelength	0.71073 A
Crystal system, space group	Monoclinic, $P2_1/c$
Unit cell dimensions	a = 13.5150(1) A alpha = 90 deg. b = 13.9170(1) A beta = 97.040(1) deg. c = 22.0440(2) A gamma = 90 deg.
Volume	4114.96(6) A^3
Z, Calculated density	8, 1.336 Mg/m^3
Absorption coefficient	0.897 mm^-1
F(000)	1728
Crystal size	0.30 x 0.25 x 0.25 mm
Theta range for data collection	3.60 to 27.51 deg.
Limiting indices	-17<=h<=17, -18<=k<=18, -28<=l<=28
Reflections collected / unique	75865 / 9428 [R(int) = 0.0433]
Completeness to theta = 27.51	99.6 %
Absorption correction	None
Refinement method	Full-matrix least-squares on F^2
Data / restraints / parameters	9428 / 0 / 478
Goodness-of-fit on F^2	1.030
Final R indices [I>2sigma(I)]	R1 = 0.0322, wR2 = 0.0759
R indices (all data)	R1 = 0.0441, wR2 = 0.0826
Largest diff. peak and hole	0.335 and -0.484 e.A^-3

Crystal data and structure refinement for **Zn(L7)$_2$**

Identification code	k07mdj05
Empirical formula	C28 H24 N2 O2 Zn
Formula weight	485.86
Temperature	150(2) K
Wavelength	0.71073 A
Crystal system, space group	Monoclinic, $P2_1/c$
Unit cell dimensions	a = 9.4060(1) A alpha = 90 deg. b = 18.582(3) A beta = 106.277(1) deg. c = 13.5230(2) A gamma = 90 deg.
Volume	2268.84(6) A^3
Z, Calculated density	4, 1.422 Mg/m^3
Absorption coefficient	1.111 mm^-1
F(000)	1008
Crystal size	0.20 x 0.15 x 0.15 mm
Theta range for data collection	3.14 to 27.49 deg.
Limiting indices	-12<=h<=12, -24<=k<=24, -17<=l<=17
Reflections collected / unique	43347 / 5192 [R(int) = 0.0636]
Completeness to theta = 27.49	99.9 %
Absorption correction	None
Max. and min. transmission	0.8511 and 0.8084
Refinement method	Full-matrix least-squares on F^2
Data / restraints / parameters	5192 / 0 / 308
Goodness-of-fit on F^2	1.004
Final R indices [I>2sigma(I)]	R1 = 0.0357, wR2 = 0.0883
R indices (all data)	R1 = 0.0553, wR2 = 0.0992
Largest diff. peak and hole	0.620 and -0.674 e.A^-3

Crystal data and structure refinement for **$Zn_3(L12)_2(CH_3CO_2)_4$**

Identification code	k08mdj07
Empirical formula	C25 H23 N2 O5 Zn1.50
Formula weight	529.51
Temperature	150(2) K
Wavelength	0.71073 A
Crystal system, space group	Monoclinic, P21/c
Unit cell dimensions	a = 13.65100(10) A alpha = 90 deg. b = 21.1730(2) A beta = 103.14 deg. c = 17.0070(2) A gamma = 90 deg.
Volume	4786.82(8) A^3
Z, Calculated density	8, 1.469 Mg/m^3
Absorption coefficient	1.553 mm^-1
F(000)	2176
Crystal size	0.20 x 0.20 x 0.15 mm
Theta range for data collection	3.06 to 27.47 deg.
Limiting indices	-17<=h<=17, -27<=k<=27, -22<=l<=22
Reflections collected / unique	88622 / 10940 [R(int) = 0.0480]
Completeness to theta = 27.47	99.8 %
Absorption correction	Semi-empirical from equivalents
Max. and min. transmission	0.8004 and 0.7464
Refinement method	Full-matrix least-squares on F^2
Data / restraints / parameters	10940 / 0 / 627
Goodness-of-fit on F^2	0.984
Final R indices [I>2sigma(I)]	R1 = 0.0360, wR2 = 0.0887
R indices (all data)	R1 = 0.0470, wR2 = 0.0961
Largest diff. peak and hole	1.154 and -0.828 e.A^-3

Crystal data and structure refinement for **Al-Sils1**

Empirical formula	C28 H63 Al O12 Si7
Formula weight	815.39
Temperature	150(2) K
Wavelength	0.71073 A
Crystal system, space group	Triclinic, P-1
Unit cell dimensions	a = 11.843(5) A alpha = 112.420(2) deg. b = 14.223(6) A beta = 90.025(2) deg. c = 15.343(7) A gamma = 112.209(2) deg.
Volume	2180.03(16) A^3
Z, Calculated density	2, 1.242 Mg/m^3
Absorption coefficient	0.289 mm^-1
F(000)	876
Crystal size	0.15 x 0.10 x 0.10 mm
Theta range for data collection	3.72 to 25.08 deg.
Limiting indices	-14<=h<=13, -16<=k<=16, -18<=l<=18
Reflections collected / unique	19937 / 7624 [R(int) = 0.0429]
Completeness to theta = 25.08	98.5 %
Absorption correction	None
Max. and min. transmission	0.9717 and 0.9579
Refinement method	Full-matrix least-squares on F^2
Data / restraints / parameters	7624 / 0 / 606
Goodness-of-fit on F^2	1.059
Final R indices [I>2sigma(I)]	R1 = 0.0534, wR2 = 0.1349
R indices (all data)	R1 = 0.0739, wR2 = 0.1476
Largest diff. peak and hole	0.347 and -0.368 e.A^-3

Crystal data and structure refinement for **Ti-Sils1**

Identification code	ck08mdj01
Empirical formula	C31 H70 O13 Si7 Ti
Formula weight	895.29
Temperature	150(2) K
Wavelength	0.71073 A
Crystal system, space group	Triclinic, P-1
Unit cell dimensions	a = 15.7700(2) A alpha = 112.887(1) deg. b = 17.3220 (1) A beta = 91.38(1) deg. c = 18.9630(2) A gamma = 90.60(1) deg.
Volume	4769.78(8) A^3
Z, Calculated density	4, 1.247 Mg/m^3
Absorption coefficient	0.407 mm^-1
F(000)	1920
Crystal size	0.25 x 0.25 x 0.20 mm
Theta range for data collection	3.54 to 27.52 deg.
Limiting indices	-20<=h<=20, -22<=k<=22, -24<=l<=24
Reflections collected / unique	97428 / 21879 [R(int) = 0.0457]
Completeness to theta = 27.52	99.5 %
Absorption correction	None
Refinement method	Full-matrix least-squares on F^2
Data / restraints / parameters	21879 / 0 / 1076
Goodness-of-fit on F^2	1.005
Final R indices [I>2sigma(I)]	R1 = 0.0523, wR2 = 0.1400
R indices (all data)	R1 = 0.0832, wR2 = 0.1663
Largest diff. peak and hole	0.815 and -0.666 e.A^-3

Crystal data and structure refinement for **Zn-Sils1**

Identification code	k08mdj09
Empirical formula	C29 H66 O12 Si7 Zn2
Formula weight	934.19
Temperature	150(2) K
Wavelength	0.71073 A
Crystal system, space group	Triclinic, P-1
Unit cell dimensions	a = 13.7070(5) A alpha = 71.362(2) deg. b = 14.1560(7) A beta = 68.977(2) deg. c = 14.3980(8) A gamma = 62.959(3) deg.
Volume	2281.18(19) A^3
Z, Calculated density	2, 1.360 Mg/m^3
Absorption coefficient	1.285 mm^-1
F(000)	988
Crystal size	0.20 x 0.15 x 0.10 mm
Theta range for data collection	3.53 to 25.15 deg.
Limiting indices	-16<=h<=16, -16<=k<=16, -17<=l<=17
Reflections collected / unique	21134 / 7987 [R(int) = 0.0664]
Completeness to theta = 25.15	97.7 %
Absorption correction	Semi-empirical from equivalents
Max. and min. transmission	0.8823 and 0.7832
Refinement method	Full-matrix least-squares on F^2
Data / restraints / parameters	7987 / 0 / 640
Goodness-of-fit on F^2	1.042
Final R indices [I>2sigma(I)]	R1 = 0.0483, wR2 = 0.0977
R indices (all data)	R1 = 0.0894, wR2 = 0.1165
Largest diff. peak and hole	0.384 and -0.479 e.A^-3

Crystal data and structure refinement for **Zn-Sils2**

Identification code	h08mdj02
Empirical formula	C33 H74 O13 Si7 Zn2
Formula weight	1006.29
Temperature	150(2) K
Wavelength	0.71073 A
Crystal system, space group	Triclinic, P-1
Unit cell dimensions	a = 12.0510(2) A alpha = 64.0860(10) deg. b = 15.3660(3) A beta = 70.2020(10) deg. c = 16.2700(3) A gamma = 70.6720(10) deg.
Volume	2489.41(8) A^3
Z, Calculated density	2, 1.342 Mg/m^3
Absorption coefficient	1.184 mm^-1
F(000)	1068
Crystal size	0.20 x 0.10 x 0.10 mm
Theta range for data collection	3.69 to 27.51 deg.
Limiting indices	-15<=h<=15, -19<=k<=19, -21<=l<=21
Reflections collected / unique	49676 / 11359 [R(int) = 0.0961]
Completeness to theta = 27.51	99.3 %
Absorption correction	None
Refinement method	Full-matrix least-squares on F^2
Data / restraints / parameters	11359 / 0 / 616
Goodness-of-fit on F^2	1.012
Final R indices [I>2sigma(I)]	R1 = 0.0468, wR2 = 0.1035
R indices (all data)	R1 = 0.0901, wR2 = 0.1213
Largest diff. peak and hole	0.948 and -0.650 e.A^-3

Example Workup of 1,3-Butadiene Catalysis Data

Mass Balance, Conversion and Selectivity Worksheet for **CuZnZrSi-60** *(3 hour run)*

Date		11/06/2009				**Gas Comp**.		**Mw**		**No moles**	**Weight**
Catalyst Description		Zr(1%)/Cu(1%)Zn(1%)/SiO2			**Ethylene**	2.8	vol%	28	g/mol	0.013894696	0.389051478
Mass Charged		1.06	g		**1-Butene**	0.25	vol%	56	g/mol	0.001240598	0.069473478
Volume of Catalyst		3.2	ml		**Et2O**	0.55	vol%	74	g/mol	0.002729315	0.201969326
Temperature		375	°C		**Acetaldehyde**	3.45	vol%	44	g/mol	0.01712025	0.753291
Time		180	min		**1,3-Butadiene**	3.47	vol%	54	g/mol	0.017219498	0.929852883
EtOH flow rate		0.1	ml/min								
Initial Mass EtOH flask		210	g		**Sum**	10.52			**Sum**	0.052204357	2.343638165
Final Mass EtOH flask		211.7	g								
EtOH over catalyst		12.502	g								
Mass of EtOH added		14.202	g		**Selectivity**	%				**Mass C accounted for**	**1.760588252**
Mass of EtOH used		12.502	g							**Total Mass of C used**	**2.3591274**
Moles of EtOH added		0.30873913			**Ethylene**	26.61596958				**Mass of H acounted for**	**0.272684792**
Volume of EtOH added		7409.73913	ml		**1-Butene**	2.376425856				**Total Mass of H used**	**0.5896688**
Ar flow rate		25	ml/min		**Et2O**	5.228136882				**Mass of O accounted for**	**0.317521982**
Total gas flow Ar		4500	ml		**Acetaldehyde**	32.79467681				**Total Mass of O used**	**1.5727516**
		4.5	litres		**1,3-Butadiene**	32.98479087				**Carbon in**	6.5222934
Total volume into catalyst		11909.7391	ml							**Carbon GC**	1.760588252
Total volume into catalyst		11.9097391	litres							**Carbon in EtOH in Acetone**	4.163166
Mass of EtOH in Bubblers		7.98	g							**C in**	6.5222934
LHSV		1.65055978	h-1							**C out**	5.923754252
										C balance	**90.82317964**
%C in EtOH		52.17								**Conversion on C**	**26.99339241**
%O in EtOH		34.78									
%H in EtOH		13.04		**Run Time** (hrs)		**Peak Area from GC**				**% vol**	
					Ethylene	*1-Butene*	*1,3-BD*		*Ethylene*	*1-Butene*	*1,3-BD*
				0.5	375.5	126.6	1179.8		3.41364	0.562666667	5.129565217
				1	303.3	55	823.1		2.75727	0.244444444	3.578695652
				2	310.8	40.8	720.1		2.82545	0.181333333	3.130869565
				3	279.5	35.1	677.5		2.54091	0.156	2.945652174
								Average	2.81727	0.246962963	3.476884058

Determining Acetone Bubbler Contents by ^{1}H NMR Spectroscopy for **CuZnZr-60** *(3 hour run)*

Integrals:										
Acetone	**EtOH**	**Et2O**	**Acetaldehyde**	**1,3-Butadiene**	**%Acetone**	**%EtOH**	**%Et2O**	**%Acetaldehyde**	**%1,3-BD**	
19.5	3	0.1	0.095	0.1	0.74229159	0.228397411	0.0038066	0.021697754	0.003807	**B1**
775	3	0	0.7	3.04	0.98320309	0.007611895	0	0.005328326	0.003857	**B2**
Average Molecular Weight of Solution:			55.00114199		**B1**					
			57.81863392		**B2**					
Mass of the acetone+EtOH+Et2O			38.5079		**B1**					
			21.4661		**B2**					
Number of moles of solution			0.700129099		**B1**					
			0.371266122		**B2**					
Number of moles of each constituent:										
Acetone	**EtOH**	**Et2O**	**Acetaldehyde**	**1,3-Butadiene**						
0.51969994	0.159907674	0.002665128	0.015191229	0.002665128	**B1**					
0.365029997	0.002826039	0	0.001978227	0.00143186	**B2**					
Mass of each constituent:										
Acetone	**EtOH**	**Et2O**	**Acetaldehyde**	**1,3-Butadiene**						
30.14259655	7.355753004	0.197219465	0.668414077	0.143916907	**B1**					
21.17173981	0.129997779	0	0.087041991	0.077320418	**B2**					
51.31433636	7.485750783	0.197219465	0.755456069	0.221237325	**Total**					

Raw 0.5 hour GC Data for **CuZnZrSi-60** *(3 hour run)*

Peak	Name	Type	RT(Mins)	Height	Area	Base	Conc
1	Ethylene	BB	E 2.054	90.302	375.239	0.008	3.283
2		VV	S 2.463	15.094	64.973	0.07	0
3	1-Butene	BB	3.521	16.843	126.602	0.009	0.545
4		BB	E 4.158	0.158	2.219	0.014	0
5		VT	S 4.308	6.177	40.667	0.096	0
6		BB	E 6.100	0.666	40.538	0.006	0
7	1,3-Butadiene	VT	S 6.221	25.214	1179.873	0.601	0
8		VV	S 8.408	0.138	0.867	0.031	0
9		VB	S 8.658	0.336	1.626	0.034	0
10		BB	E 9.125	0.139	2.668	0.017	0
11		VV	S 9.317	0.165	0.514	0.042	0
12		VV	S 9.438	0.531	3.255	0.04	0
13		VV	S 9.563	0.192	0.758	0.036	0
14		VV	S 9.683	0.427	2.367	0.033	0
15		VV	S 9.958	0.11	0.665	0.027	0
16		VV	S 10.233	0.247	1.278	0.02	0
17		VV	S 10.463	0.38	2.091	0.015	0
18		VV	S 11.058	2.109	11.466	0.01	0
19		VV	S 11.292	1.007	5.199	0.012	0
20		VV	S 11.571	0.222	1.712	0.014	0
21		VV	S 12.154	0.746	3.976	0.024	0
22		VV	S 12.338	0.517	3.215	0.027	0
23		VV	S 12.688	0.996	6.302	0.034	0
24		VV	S 12.913	0.655	3.926	0.039	0
25		VV	S 13.096	0.277	2.058	0.042	0
26		VV	S 13.342	1.297	7.111	0.047	0
27		VB	S 13.642	0.958	4.692	0.063	0
28		BT	E 13.988	1.154	5.341	0.069	0
29		BB	E 15.350	0.061	0.408	0.05	0
30		VV	S 15.675	0.108	0.816	0.05	0
31		VB	S 16.104	0.144	0.771	0.069	0
32		BB	16.4	0.151	0.754	0.08	0
33		BB	E 17.038	0.212	20.41	0.09	0
34		VV	S 17.404	0.313	3.011	0.268	0
35		VV	S 17.575	0.19	1.99	0.258	0
36	Diethylether	VV	S 17.921	11.359	333.363	0.237	1.958
37	Acetaldehyde	VV	S 18.704	3.103	98.618	0.189	1.57

0.5 hour Gas Chromatograph for **CuZnZrSi-60** *(3 hour run)*

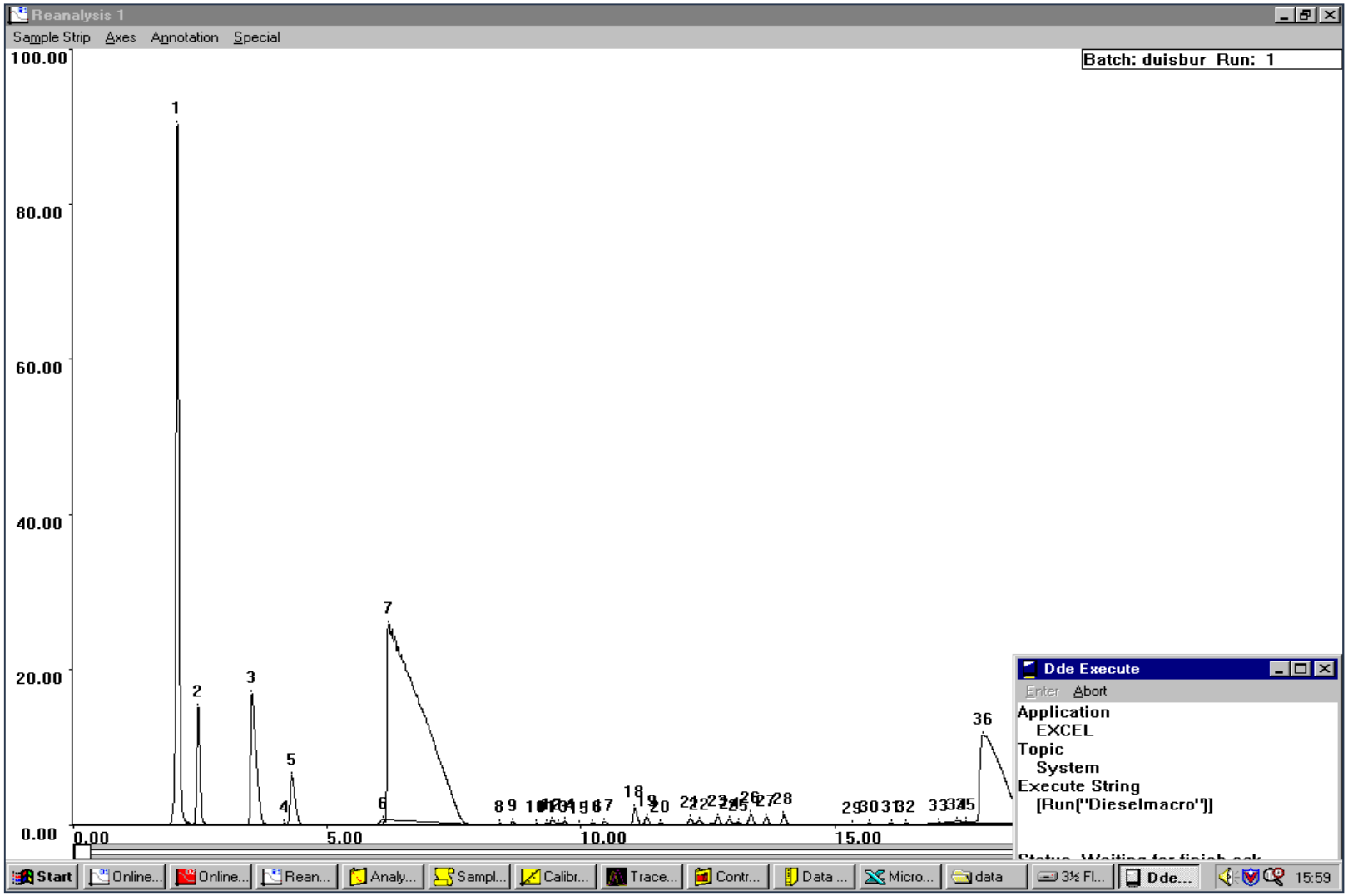

Raw 1 hour GC Data for **CuZnZrSi-60** *(3 hour run)*

Peak	Name	Type	RT(Mins)	Height	Area	Base	Conc
1	Ethylene	BB	E 2.021	75.926	303.317	0.008	2.654
2		VV	S 2.425	9.021	36.418	0.046	0
3	1-Butene	BB	3.504	7.81	55.059	0.012	0.237
4		BT	E 4.088	0.088	0.801	0.018	0
5		VT	S 4.271	2.937	17.928	0.032	0
6		BB	E 6.154	0.239	2.077	0.012	0
7	1,3-Butadiene	VB	S 6.358	21.553	823.139	0.023	0
8		BT	E 8.354	0.063	0.326	0.043	0
9		VB	S 8.600	0.114	0.576	0.036	0
10		BB	E 9.071	0.076	0.93	0.033	0
11		VV	S 9.396	0.206	1.204	0.035	0
12		VB	S 9.633	0.148	0.644	0.043	0
13		BT	E 9.883	0.056	0.349	0.038	0
14		VV	S 10.192	0.115	0.537	0.024	0
15		VB	S 10.417	0.113	0.58	0.022	0
16		BB	E 11.021	1.036	5.24	0.025	0
17		VV	S 11.246	0.398	1.942	0.025	0
18		BB	E 11.958	0.037	0.015	0.034	0
19		VV	S 12.108	0.444	2.202	0.04	0
20		VV	S 12.283	0.323	1.699	0.039	0
21		VV	S 12.638	0.508	3.334	0.038	0
22		VV	S 12.850	0.354	2.162	0.038	0
23		VV	S 13.033	0.141	0.839	0.038	0
24		VV	S 13.275	0.708	3.636	0.037	0
25		VB	S 13.571	0.483	2.321	0.044	0
26		BT	13.904	0.548	2.7	0.044	0
27		BB	15.954	0.236	1.173	0.053	0
28		BB	16.229	1.268	7.117	0.067	0
29		BB	E 17.233	0.391	41.444	0.204	0
30		VV	S 17.692	12.52	519.275	0.591	0
31	Diethylether	VV	S 19.075	1.505	30.33	0.667	0.483
32	Acetaldehyde	VB	S 19.654	0.738	18.504	0.699	0

1 hour Gas Chromatograph for **CuZnZrSi-60** *(3 hour run)*

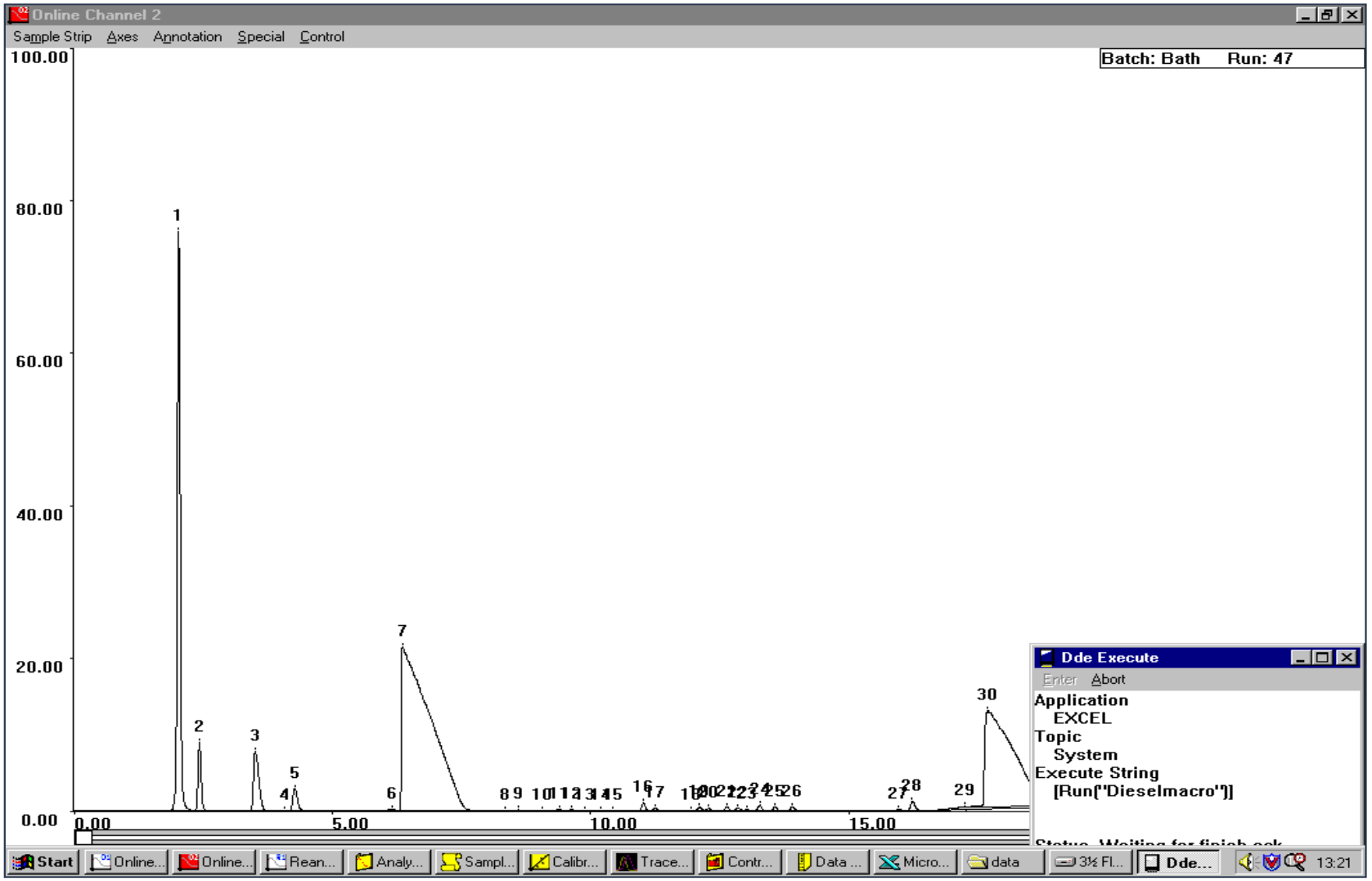

Raw 2 hour GC Data for **CuZnZrSi-60** *(3 hour run)*

Peak	Name	Type	RT(Mins)	Height	Area	Base	Conc
1	Ethylene	BT	E 1.983	79.545	310.869	0.007	2.72
2		VV	S 2.371	8.201	33.286	0.048	0
3	1-Butene	BB	3.425	5.804	40.845	0.022	0.176
4		BB	E 3.971	0.085	0.535	0.017	0
5		VB	S 4.158	2.399	14.157	0.028	0
6		BB	E 6.058	0.198	1.659	0.013	0
7	1,3-Butadiene	VB	S 6.267	19.737	720.086	0.017	0
8		BB	E 8.958	0.071	0.698	0.028	0
9		VV	S 9.288	0.178	1.056	0.024	0
10		VB	S 9.533	0.128	0.563	0.037	0
11		BT	E 9.767	0.04	1.265	0.04	0
12		BB	E 10.925	0.933	4.544	0.02	0
13		VV	S 11.154	0.35	1.744	0.018	0
14		BB	E 11.879	0.026	0.671	0.029	0
15		VV	S 12.021	0.358	1.769	0.034	0
16		VV	S 12.204	0.289	1.504	0.037	0
17		VV	S 12.558	0.402	2.484	0.042	0
18		VV	S 12.767	0.263	1.481	0.045	0
19		BT	13.192	0.582	2.896	0.043	0
20		BB	13.483	0.362	1.652	0.05	0
21		BT	13.821	0.394	1.915	0.047	0
22		BB	15.85	0.209	0.991	0.069	0
23		BB	16.117	1.267	6.986	0.077	0
24		BB	E 17.621	13.78	710.837	0.326	0
25	Diethylether	VT	S 18.588	0.659	15.406	3.927	0.09
26	Acetaldehyde	BB	21.529	0.13	2.365	0.657	0

2 hour Gas Chromatograph for **CuZnZrSi-60** *(3 hour run)*

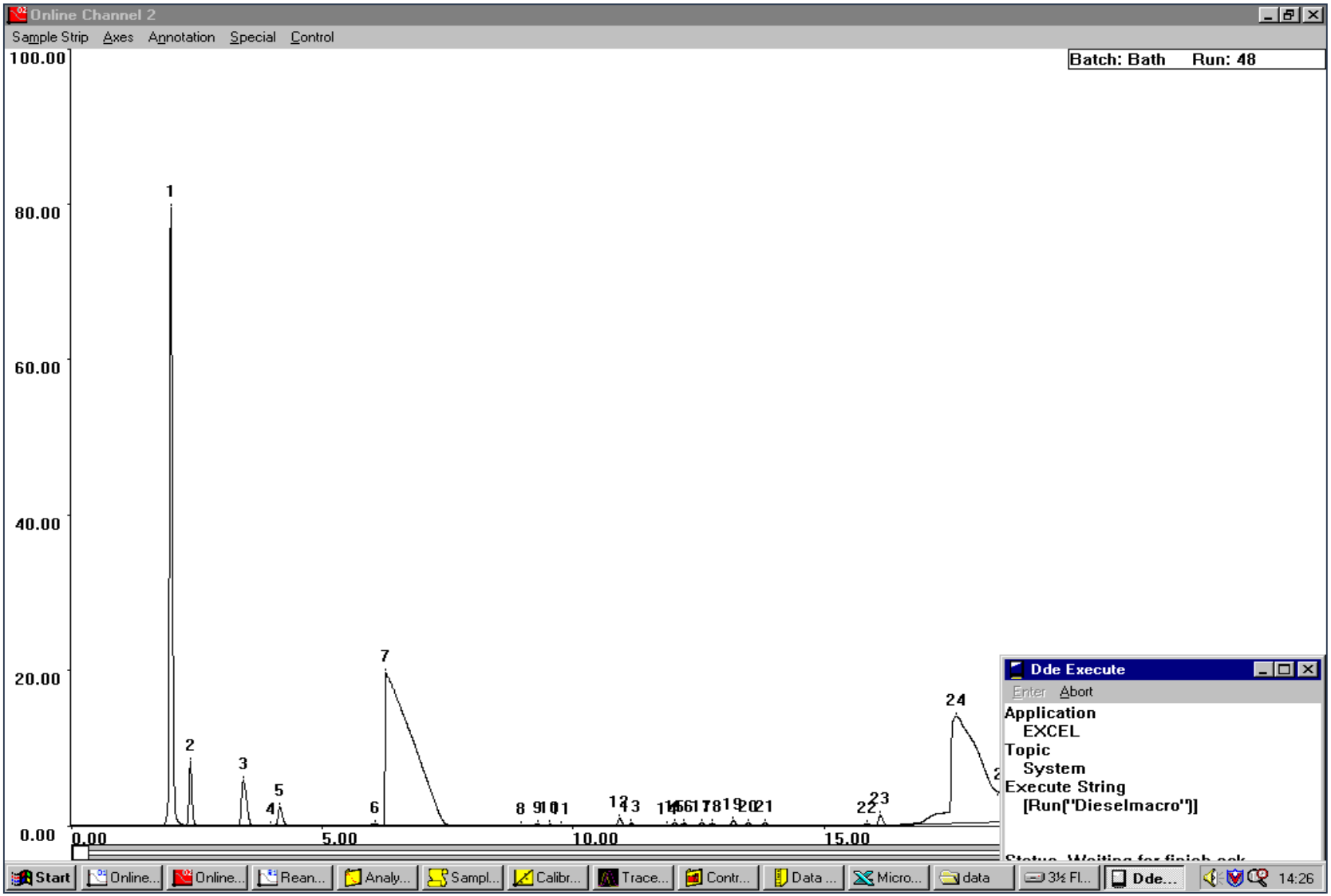

Raw 3 hour GC Data for **CuZnZrSi-60** *(3 hour run)*

Peak	Name	Type	RT(Mins)	Height	Area	Base	Conc
1	Ethylene	BB	E 1.950	72.814	279.54	0.01	2.446
2		VV	S 2.329	7.843	31.665	0.051	0
3	1-Butene	BB	3.358	4.993	35.167	0.012	0.151
4		BB	E 3.883	0.095	0.823	0.008	0
5		VT	S 4.067	2.209	12.698	0.025	0
6		BB	5.958	0.184	1.736	0.019	0
7	1,3-Butadiene	BB	6.171	18.769	677.505	0.017	0
8		BB	E 9.075	0.076	0.954	0.026	0
9		VV	S 9.196	0.146	0.708	0.062	0
10		VT	S 9.446	0.13	0.528	0.047	0
11		BT	E 9.846	0.043	0.935	0.034	0
12		BB	E 10.838	0.9	4.491	0.028	0
13		VB	S 11.067	0.334	1.578	0.049	0
14		BB	E 11.942	0.365	2.121	0.154	0
15		VV	S 12.129	0.28	1.309	0.194	0
16		VV	S 12.488	0.403	2.121	0.235	0
17		VB	S 12.696	0.229	1.078	0.264	0
18		BB	13.129	0.621	2.954	0.261	0
19		BB	13.429	0.347	1.581	0.294	0
20		BB	13.767	0.382	1.83	0.341	0
21		BB	E 16.088	0.744	4.859	0.807	0
22		VT	E 17.633	12.404	634.367	1.023	0
23	Diethylether	VV	S 18.388	0.885	13.263	4.131	0.078
24	Acetaldehyde	VT	S 18.829	0.533	5.322	3.035	0.085
25		VT	S 20.988	0.225	5.056	0.756	0
26		BB	24.146	0.567	4.35	1.846	0

3 hour Gas Chromatograph for **CuZnZrSi-60** *(3 hour run)*